ANALYSIS OF THE MOLECULAR MECHANISM OF AUTOPHAGOSOME FORMATION IN THE YEAST *SACCHAROMYCES CEREVISIAE*

by

Jiefei Geng

A dissertation submitted in partial fulfillment
of the requirements for the degree of
Doctor of Philosophy
(Molecular Cellular and Developmental Biology)
in The University of Michigan
2010

Doctoral Committee:

Professor Daniel J. Klionsky, Chair
Associate Professor Laura J. Olsen
Associate Professor Anuj Kumar
Assistant Professor John Kim

Dedication

This dissertation is dedicated to my family, for their endless love and support.

Acknowledgements

First, I would like to thank my graduate mentor, Dr Daniel J. Klionsky, for his invaluable guidance and training throughout my graduate studies. I have learned a lot from his expertise in research and am always inspired by his passion toward science. I should never forget his patience and encouragement as I struggled with my work. He is one of the rare advisors that students dream that they will find. I also want to thank my thesis committee members, Dr. Laura Olsen, Dr. Anuj Kumar and Dr. John Kim, for their perceptive suggestion on my research. Without their support, I could not have done what I was able to do.

I am indebted to many current and previous members of the Klionsky lab. This dissertation would not have been the same without their generous help and collaborations. My gratitude goes to Dr. Julie E. Legakis and Dr. Ju Huang for the training they gave me when I was new to the lab. I want to thank Dr. Usha Nair, with whom I collaborated on several different projects including the two presented in Chapters III and IV. I also had a pleasant experience in the collaboration with Dr. Iryna Monastyrska, Dr. Heesun Cheong, Dr. Zhiping Xie, Dr. Wei-Lien Yen and Dr. Zhifen Yang.

My graduate studies began with the rotation work with Dr. John Kuwada and Dr. Robert Denver, and I really appreciate their guidance. I am thankful to the staff members in the MCDB Department, especially Ms. Mary Carr, for making my study at the

University of Michigan a wonderful experience. I also want to thank my advisor, Dr. Hong-Wei Xue, at the Institute of Plant Physiology and Ecology, Chinese Academy of Sciences, for showing me what scientific research is and how fascinating it could be.

Special thanks are due to my parents and wife for their everlasting love and care. Grateful words would never be enough. I dedicate this dissertation to them.

Chapter II is reprinted from *EMBO Reports*, Volume 9, Jiefei Geng and Daniel J. Klionsky. The Atg8 and Atg12 ubiquitin-like conjugation systems in macroautophagy, pg. 859-64, Copyright (2008), with minor modifications.

Chapter III is reprinted from *Journal of Cell Biology*, Volume 182, Jiefei Geng, Misuzu Baba, Usha Nair and Daniel J. Klionsky. Quantitative analysis of autophagy-related protein stoichiometry by fluorescence microscopy, pg. 129-40, Copyright (2008), with minor modifications; and from *Autophagy*, Volume 4, Jiefei Geng and Daniel J. Klionsky. Quantitative regulation of vesicle formation in yeast nonspecific autophagy, pg. 955-7, Copyright (2008), with minor modifications. Dr. Usha Nair and Dr. Misuzu Baba performed the transmission electron microscopy and immunoelectron microscopy in Figure 3.2. I contributed the rest of the data and wrote the paper.

Chapter IV is reprinted from *Molecular Biology of the Cell*, Volume 21, Jiefei Geng, Usha Nair, Kyoko Yasumura-Yorimitsu and Daniel J. Klionsky. Two post-Golgi Sec proteins are required for autophagy in *Saccharomyces cerevisiae*, pg. 2257-69, Copyright (2010), with minor modifications. Dr. Kyoko Yasumura-Yorimitsu did the initial screening and identified an autophagic defect in the *sec2-41* strain. Dr. Usha Nair

performed the transmission electron microscopy in Figure 4.2 and Figure 4.8. I contributed the rest of the data and wrote the paper.

Appendix A is reprinted from *Autophagy*, Volume 6, Jiefei Geng and Daniel J. Klionsky. Determining Atg protein stoichiometry at the phagophore assembly site by fluorescence microscopy, pg. 144-7, Copyright (2010), with minor modifications.

Table of Contents

Dedication ii

Acknowledgements iii

List of Figures vii

List of Tables ix

Chapter

I. Introduction 1

II. The Atg8 and Atg12 ubiquitin-like conjugation systems in macroautophagy 16

III. Quantitative analysis of autophagy-related protein stoichiometry by fluorescence microscopy 29

IV. Post-Golgi Sec proteins are required for autophagy in *Saccharomyces cerevisiae* 76

V. Conclusion 123

Appendix

A. Determining Atg protein stoichiometry at the PAS by fluorescence microscopy 133

References 144

List of Figures

Figure:

1.1 Schematic representation of different types of autophagy 3

2.1 Structural comparisons of ubiquitin, LC3 and *At*Atg12 18

2.2 Conjugation processes in yeast 22

2.3 Atg12 and Atg8 conjugation systems in vesicle formation 25

3.1 The amount of Atg11 affects the capacity of the Cvt pathway 34

3.2 More Cvt vesicles were formed in Atg11-overexpressing cells 37

3.S1 Examination of the relationship between GFP-tagged protein amount and fluorescence intensity 41

3.3 Linear relationship between GFP-tagged protein amount and fluorescence intensity 44

3.S2 Chromosomally tagged Atg proteins had a more consistent expression level than proteins expressed from centromeric plasmids 45

3.S3 Reliability of the standard curve 46

3.4 Localization does not affect the linearity of the fluorescent signal 48

3.5 Effect of Atg11 overexpression on the PAS intensity of Atg8 and Atg9 50

3.6 Amount of Atg proteins at the PAS during either the Cvt pathway or autophagy....54

3.7 Kinetics of Atg proteins at the PAS during autophagy....56

3.8 Schematic relationship between the Atg8 and Atg9 PAS population and vesicle formation....71

4.1 Sec2 is involved in both autophagy and the Cvt pathway....87

4.2 A 58-amino acid domain on Sec2 is essential for its role in autophagy....90

4.3 Sec2 mutation results in a reduced number of autophagic bodies, but has no effect on their size....94

4.4 Recruitment of Atg8 to the PAS is affected in the *sec2-59* mutant....97

4.S1 In the *vam3*^{ts} background *sec2-59* cells accumulate fewer GFP-Atg8 dots in the cytosol even after longer starvation....98

4.5 Atg9 anterograde movement is less efficient in the *sec2* mutant....100

4.6 The *sec4* mutant displays an autophagic defect....103

4.7 Protein secretion is down-regulated during starvation conditions....107

4.S2 Cycloheximide blocked protein synthesis....108

4.S3 *ypt31/32*^{ts} mutant affects Atg8 localization....111

4.8 Autophagy defect and abnormal Atg8 localization in the *ypt31/32*^{ts} mutant....112

4.S4 Protein secretion is not regulated by rapamycin treatment....115

5.1 Working model of Sec2 and Sec4 in autophagy....130

List of Tables

Table

1.1. Proteins essential for autophagy in yeast 13

2.1. In need of answers 28

3.1 Local and global amount of Atg proteins in growing conditions 53

3.2 Yeast strains used in this study 67

4.1 Yeast strains used in this study 120

Chapter I. Introduction

Autophagy is a ubiquitous degradation pathway in eukaryotes, which is used for the turnover of cytoplasmic components in response to stress conditions. By transporting cargos to the degradative organelle, the lysosome (or the analogous yeast vacuole), autophagy mediates the recycling of unnecessary macromolecules and the disposal of excess/defective organelles. During the past two decades, a tremendous amount of work has been done to elucidate the molecular mechanism of the autophagy pathway and its diverse physiological roles in various organisms.

Autophagy: an old field just coming into the spotlight

There is a long history of autophagy research in mammalian cells. The concept of "autophagy" was first introduced in the 1960s to describe a "self-eating" process [1]. The double-membrane vesicle responsible for packing the cytoplasm is referred to as the autophagosome. The knowledge of autophagy had been limited to morphological descriptions for decades, until the identification of this pathway in the budding yeast *Saccharomyces cerevisiae* [2]. Thereafter, the powerful tool of yeast genetics led to a burst of research activity and the discovery of multiple genes essential for autophagy. In 2003, researchers adopted a unified nomenclature to name AuTophaGy-related genes by the acronym *ATG* [3]. To date, 33 *ATG* genes have been characterized in *S. cerevisiae* and other fungi. Following the breakthrough in yeast, the first mammalian *ATG* gene was

identified [4] and, afterward, more evidence demonstrating the conservation of the autophagy mechanism between yeast and higher eukaryotes. Although the molecular era of autophagy study was initiated with the genetically facile yeast system, the identification of mammalian *ATG* genes strengthened our understanding of autophagy. For example, by tagging Atg proteins with fluorophores, researchers did time-lapse experiments to trace the process of autophagosome formation in mammalian cells and showed it occurs in a step-wise manner [5]. This type of analysis can be barely done in yeast because of the relatively smaller size of yeast autophagosomes. More importantly, autophagy studies in the mammalian system have changed the awareness of the significance of autophagy in higher eukaryotes. Initially thought of as a "garbage disposal" system, the autophagy pathway now has been shown to play critical physiological roles in various species, and the dysfunction of autophagy may result in severe diseases, including cancer, neurodegeneration and cardiovascular disorders [6-8].

Different types of autophagy

There are different forms of autophagy and they can be grouped into several categories. Based on the way that cargo is delivered to the vacuole/lysosome, there are macroautophagy, microautophagy and chaperone-mediated autophagy. Depending on the substrate-specificity, autophagy can be nonspecific or specific; according to the cargo, subcategories of specific autophagy include the cytoplasm-to-vacuole targeting pathway, mitophagy, pexophagy and piecemeal microautophagy of the nucleus/micronucleophagy (Figure 1.1).

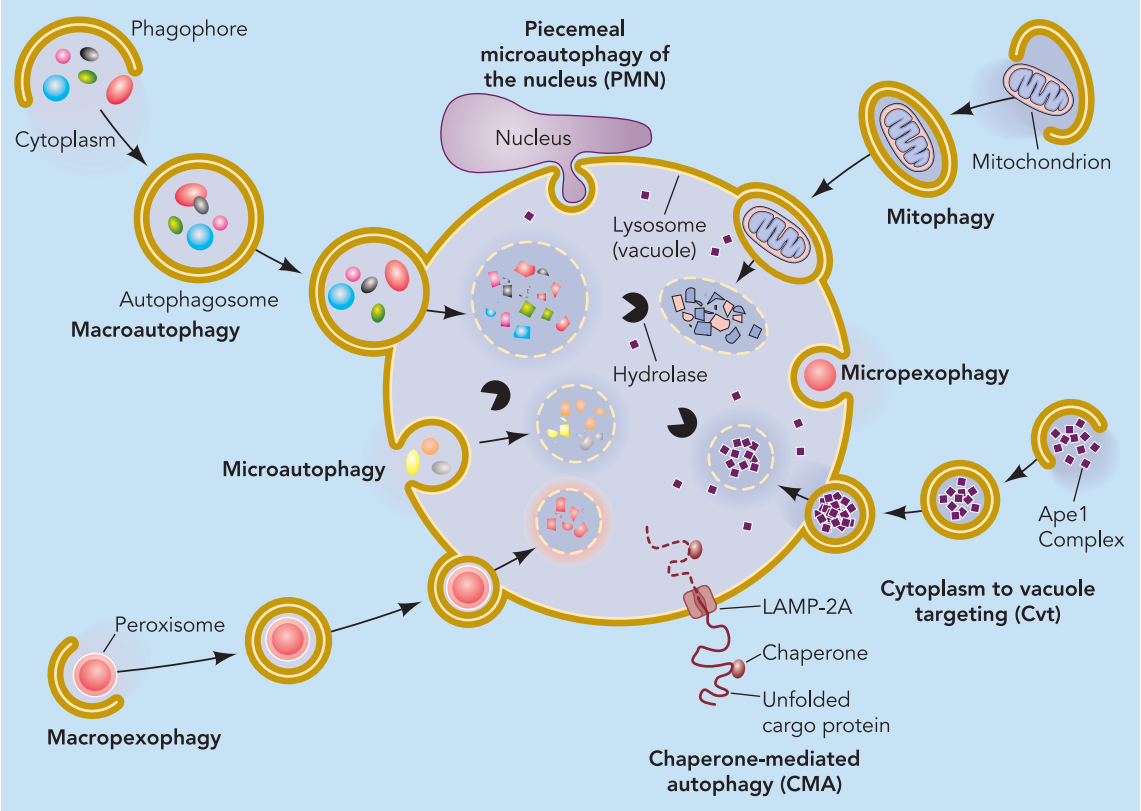

Figure 1.1 Schematic representation of different types of autophagy [9].

1. Macroautophagy

In macroautophagy, cytosolic components are randomly sequestered into the autophagosome. Autophagosome formation initiates with a crescent-shaped phagophore, which expands probably through vesicular addition and enwraps portions of the cytoplasm. The expanding phagophore matures into the completed autophagosome, which is a double-membrane vesicle. The outer membrane of the autophagosome fuses with the vacuolar/lysosomal membrane to release the inner vesicles, termed autophagic bodies, which are ultimately degraded. Macroautophagy is the best-characterized type of autophagy. The whole process can be divided into four steps: 1) Induction of autophagy;

2) autophagosome formation; 3) docking and fusion between the autophagosomes and vacuole/lysosome; and 4) degradation of autophagic bodies together with their contents followed by releasing of the degradation products back to the cytoplasm for reuse [10]. Compared to other types of autophagy, the most prominent feature of macroautophagy is the *de novo* formation of the autophagosome; this process is referred to as being *de novo* because the sequestering vesicle does not form in a single step from a pre-existing organelle. Most identified Atg proteins act during the autophagosome formation step. Great efforts have been applied in studying this process, and so far its molecular mechanism (see below) has been revealed piece-by-piece, although many questions remain unsolved. In *S. cerevisiae*, macroautophagy is an inducible process; nitrogen starvation and rapamycin treatment—inhibitors of the TOR signaling pathway [11]—are the most commonly used conditions to stimulate the occurrence of autophagy [2,12].

2. Microautophagy

Microautophagy refers to the direct uptake of cytosolic components via the invagination and/or protrusion/septation of the vacuolar/lysosomal membrane. This phenomenon has been observed in both mammals and yeast. In *S. cerevisiae*, the invagination of the vacuolar membrane results in a structure called an autophagic tube that contains a small proportion of the cytoplasm. The tip of the autophagic tube pinches off to form an autophagic body that is subsequently degraded in the vacuolar lumen. Different from macroautophagy, the membrane of autophagic bodies in microautophagy directly originates from the vacuolar membrane. Microautophagy can be reconstituted *in vitro*, in which purified vacuoles uptake a fluorescent dye or biochemical substrate in an

ATP- and cytosol-dependent manner [13]. Studies using chemical inhibitors indicate that microautophagy can be dissected into four sequential stages including the initial invagination of the vacuolar membrane and the last scission step [14]. Microautophagy can be induced by starvation conditions and requires some Atg proteins essential for macroautophagy, although the role of Atg proteins in microautophagy may not be direct [13,15]. Invagination of the vacuolar membrane during microautophagy may balance the membrane influx to the limiting membrane of this organelle caused by macroautophagy, thus contributing to the maintenance of vacuole size and membrane composition. Overall, the molecular mechanism of microautophagy is less characterized.

3. Chaperone-mediated autophagy (CMA)

CMA is a specific type of autophagy that does not involve membrane engulfment as seen in macroautophagy and microautophagy. In CMA, soluble cytosolic proteins can be selectively recognized by cytosolic chaperones and delivered to the lysosome surface, where substrate proteins undergo unfolding and direct translocation across the lysosomal membrane into the lysosomal lumen for degradation [16]. Both macroautophagy and CMA can be induced by nutrient-depletion, while CMA usually occurs after prolonged starvation when macroautophagy activity has already passed its peak level [17]. Although it is not clear how various types of autophagy are activated in a concerted manner, the cross-talk between autophagic pathways has been seen; block of one type of autophagy results in the activation of another [18,19].

Most identified CMA substrate proteins have a KFERQ-like motif in their amino acid sequence. This pentapeptide motif was first identified in RNase A [20], and more

examples in other substrates suggest that the motif does not rely on the exact amino acid sequence but rather on the charge of the residues [21]. When exposed, the pentapeptide motif in the CMA substrates can be recognized by the chaperone protein hsc70 [16], and this substrate-chaperone complex further interacts with a group of cochaperones [22]. LAMP-2A has been identified as a receptor protein on lysosomal membrane that interacts with the substrate-chaperone complex [23]. LAMP-2A is a single-span membrane protein with a short cytosolic tail. The binding with CMA substrates may promote the multimerization of LAMP-2A to form a 700-kDa complex across the lysosomal membrane, which mediates the translocation of substrate protein [24].

4. The cytoplasm-to-vacuole targeting (Cvt) pathway

The Cvt pathway is a biosynthetic pathway that transport at least two hydrolases, aminopeptidase I (Ape1) and α-mannosidase (Ams1), to the vacuole [25,26]. It can be regarded as a specific type of autophagy. Synthesized in the cytosol, precursor Ape1 (prApe1) rapidly forms a dodecamer, and multiple dodecamers assemble into a higher order complex, the Ape1 complex [27]. The oligomeric complex is then specifically packed into a double-membrane vesicle, the Cvt vesicle, which subsequently fuses with the vacuole and releases the inner vesicle called the Cvt body into the vacuole lumen [28,29]. In the vacuole lumen, prApe1 is processed into the mature form (mApe1) after the cleavage of its propeptide, and it functions as a resident vacuolar hydrolase [30]. The Cvt pathway is constitutively active in nutrient-rich conditions, whereas during starvation prApe1 is delivered to the vacuole as a preferential cargo of the macroautophagy pathway [29]. Genetic screening revealed that the macroautophagy mutants overlap with those

mutants defective in prApe1 maturation [31], and further analysis confirmed these two pathways share much of the same protein machinery (see below). Besides the shared components, the Cvt pathway also has its unique components that afford the specificity of the cargo recognition process. prApe1 directly binds to its receptor, Atg19, to form the Cvt complex [32,33]. Another Cvt-specific Atg protein, Atg11, interacts with Atg19 and directs the Cvt complex to the vesicle-formation machinery [34,35]. Atg19 also interacts with a lipid-conjugated protein, Atg8, which may act as an anchor point for membrane expansion during formation of Cvt vesicles, which exclude other cytosolic components [34]. The Cvt pathway has only been reported in fungi, but its well-studied molecular mechanism provides intriguing hints to investigate other types of specific autophagy observed in high eukaryotes.

5. Mitophagy

Mitophagy refers to the selective degradation of mitochondria through autophagy. For most eukaryotic cells, mitochondria are the organelle that generates energy by oxidative phosphorylation. Meanwhile, mitochondria also produce reactive oxygen species (ROS) that can cause potential oxidative damage to the cells. Thereby, it is physiologically necessary to eliminate the damaged, aged or excess mitochondria. In both yeast and mammalian cells, mitophagy is responsible for clearance of mitochondria [36,37], although the molecular mechanism is not well understood. In *S. cerevisiae*, mitophagy can be induced by starvation after pre-culturing in non-fermentable media that induce mitochondria proliferation. Yeast mitophagy can be easily monitored by the Om45-GFP processing assay [38]. With this method, we proved that the known

autophagy machinery is generally required for mitophagy [39,40], and new mitophagy-specific Atg proteins, such as Atg32 and Atg33, have been identified through genetic screening [39,41,42]. Atg32 localizes to the mitochondria outer membrane and may confer the specificity of mitophagy by interaction with Atg11. Further analysis on the physiological role and molecular mechanism of mitophagy is needed.

6. Pexophagy

In yeast and mammalian cells, the population of peroxisomes can be induced by metabolic adaption to changes in environmental or physiological conditions. After the removal of the peroxisome proliferation stimulus, excess peroxisomes can be degraded through pexophagy. In yeast models, such as *Pichia pastoris* and *Hansenula polymorpha*, peroxisome proliferation is substantially enhanced when methanol is the sole carbon source. Upon shifting to medium containing a preferred carbon source, such as glucose or ethanol, the superfluous peroxisomes are rapidly delivered to the vacuole for degradation via the pexophagy pathway [43,44]. Either macropexophagy or micropexophagy can be induced depending on the nutrient conditions. Genetic screening showed that most of the pexophagy genes overlap with the orthologues of the same genes involved in macroautophagy in *S. cerevisiae* [45].

7. Piecemeal microautophagy of the nucleus (PMN)

PMN, also referred to as micronucleophagy, occurs in *S. cerevisiae* at the nucleus-vacuole (NV) junctions. The NV junction buds into invagination of the vacuolar membrane, resulting in the sequestration and degradation of a portion of the nucleus [46].

The NV junction is formed depending on the interaction of Vac8 on the vacuolar membrane and Nvj1 on the perinuclear ER [47]. Nvj1 further recruits Osh1 to the NV junction [48,49]. When Nvj1 or Osh1 is tagged with GFP, its localization to the vacuolar lumen and subsequent processing can be used to monitor the occurrence of PMN [50]. Using this method, most known Atg proteins are shown to be essential for PMN [51].

Molecular mechanism of autophagy in yeast

In this thesis, I am focusing on the Cvt pathway and macroautophagy in *S. cerevisiae* as representatives of specific and nonspecific autophagy, respectively. Hereafter, macroautophagy will be referred to as autophagy. One feature of yeast autophagy is the phagophore assembly site (PAS; also known as the pre-autophagosomal structure) [52,53]. When tagged with fluorophore, most Atg proteins colocalize at this perivacuolar site. The PAS is proposed to be the vesicle formation site for both the Cvt pathway and autophagy and it can be defined as a hybrid of forming vesicle and autophagy machinery. The proper localization of Atg protein to the PAS is essential for autophagy, and the kinetics of Atg protein recruitment to this site is under precise regulation (see Chapter III).

Among the 33 identified *ATG* genes (Table 1.1), approximately half of them are essential for both the Cvt pathway and autophagy. This subset of *ATG* genes is usually described as the core machinery of autophagosome formation [54]. They can be classified into three major functional groups:

1. The Atg8 and Atg12 conjugation systems

Eight Atg proteins are implicated directly in Atg8 and Atg12 conjugation. Atg8 and Atg12 are two ubiquitin-like (Ubl) proteins that can be covalently attached to phosphatidylethanolamine (PE) and Atg5, respectively, in a ubiquitination-like process [55,56]. The Atg12–Atg5 conjugate has an E3-like activity on the formation of Atg8–PE, whereas Atg8 lipidation functions essentially in phagophore expansion [57]. Details of the Atg8 and Atg12 conjugation systems are discussed in Chapter II.

2. Atg9 and its cycling system

Atg9 is the only transmembrane protein indispensable for autophagosome formation [58]. Atg9 may exist in a homologous complex via self-interaction [59]. Unlike most Atg proteins that show predominant PAS localization as well as a diffuse cytosol signal under fluorescence microscopy, Atg9 is localized to multiple punctate membrane structures and shuttles between the PAS and the peripheral (non-PAS) sites [60]. The Atg9-positive peripheral structures are speculated to be the potential membrane source(s) for phagophore expansion. Atg9 may function as a membrane carrier and its transport to the PAS represents the lipid supply for autophagosome formation. In agreement with this hypothesis, disruption of Atg9 cycling results in defective autophagy [61-64]. The recruitment of Atg9 to the PAS is dependent on Atg11 or Atg17 during the Cvt pathway or autophagy, respectively [65,66]. The efficient transport of Atg9 to the PAS also involves Atg23 and Atg27 as a functional complex [61,64]. The retrieval of Atg9 from the PAS back to its peripheral sites requires the Atg1-Atg13 complex, Atg2 and Atg18; a mutation in any of these proteins restricts Atg9 at the PAS [62]. Atg1 is a serine-threonine kinase and its kinase activity is essential for autophagy but not for Atg9

retrieval, so the function of Atg1 is broader than regulating Atg9 cycling [62,67,68]. In mammalian cells, Atg9 also shuttles between different membrane structures during starvation in a ULK1 (mammalian Atg1 homolog)-dependent manner [69], suggesting the possible membrane carrier function of Atg9 is conserved across species.

3. The phosphatidylinositol (PtdIns) 3-kinase complex I

In *S. cerevisiae*, Vps34 is a class III PtdIns 3-kinase and involved in forming two functionally distinct complexes: complex I functions in the autophagy pathway, and complex II in the vacuolar protein sorting (Vps) pathway [70]. Complex I consists of Vps34, Vps14, Atg6 (Vps30) and Atg14, while Complex II contains the same set of proteins except that Atg14 is replaced by Vps38. Yeast Atg6 is involved in both autophagy and the Vps pathway, whereas its mammalian homolog, Beclin 1, is essential only for autophagy [71]. The PtdIns 3-kinase is proposed to function at the PAS by recruiting several phosphatidylinositol 3-phosphate [PtdIns(3)P]-binding proteins such as Atg18, Atg20, Atg21 and Atg24 [72-74].

There has been a breakthrough in our understanding of the molecular mechanism of autophagy during the past decade, although we are still facing many unanswered questions in this field. In this thesis, I am trying to answer two questions: 1) How is the autophagosome formation process quantitatively regulated? Upon shifting from nutrient-rich to starvation conditions, yeast cells must adapt the autophagy machinery from generating smaller, cargo-specific Cvt vesicles to the formation of bigger autophagosomes with random cargoes packed inside. Using a fluorescence microscopy-

based method, we quantified the stoichiometry of Atg proteins at the PAS in different conditions. We found that Atg8 and Atg9 are key factors that quantitatively control the vesicle formation process in the Cvt pathway and autophagy (see Chapter III); 2) What is the membrane source for autophagosome formation? The autophagosome formation process is described as the addition of small vesicles to the expanding phagophore, but it is unknown where these vesicles come from. We found that the late stage of the secretory pathway plays an important role in autophagosome formation, suggesting the Golgi apparatus in yeast may contribute to autophagy as a potential membrane source (see Chapter IV). Our conclusions and future directions are discussed in Chapter V.

Table 1.1 Proteins essential for autophagy in yeast

Protein	Description of function	Cvt	ATG
Atg1	A serine/threonine kinase involved in induction of autophagy; required for Atg9 retrieval from the PAS to peripheral sites; a component of the Atg1-Atg13-Atg17 complex [62,67,68,75]	-	-
Atg2	Required for Atg9 retrieval from PAS to peripheral sites [62,76]	-	-
Atg3	An E2-like enzyme involved in Atg8–PE conjugation [56]	-	-
Atg4	A cysteine protease that cleaves the C-terminal Arginine of Atg8 prior to its lipidation and mediates the deconjugation of Atg8–PE [77]	-	-
Atg5	A component of the Atg12–Atg5-Atg16 complex which has an E3-like function in Atg8 lipidation [55,57]	-	-
Atg6	A component of two PtdIns 3-kinase complexes involved in autophagy (Complex I) and the Vps pathway (Complex II) [70,78]	-	-
Atg7	An E1-like enzyme involved in the formation of Atg8–PE and Atg12–Atg5 conjugates [55,56]	-	-
Atg8	A ubiquitin-like protein conjugated to PE; involved in phagophore expansion; usually used as an autophagosome marker [56,79,80]	-	-
Atg9	An integral membrane protein that cycles between the PAS and multiple peripheral sites [58,60,62,63,65]	-	-
Atg10	An E2-like enzyme involved in the formation of the Atg12–Atg5 conjugate [81]	-	-
Atg11	A protein involved in cargo recognition and PAS assembly during specific autophagy; mediates Atg9 transport to the PAS during specific autophagy [34,35,65,82]	-	+
Atg12	A ubiquitin-like protein covalently conjugated to Atg5 to form the Atg12–Atg5-Atg16 complex, which has	-	-

	E3-like function in Atg8 lipidation [55,57]		
Atg13	A component of the Atg1-Atg13-Atg17 complex; dephosphorylated during starvation conditions [75,83,84]	-	-
Atg14	A component of PtdIns 3-kinase complex I involved in autophagy [70,78]		
Atg15	A vacuolar lipase required for the lysis of autophagic and Cvt bodies [85]	-	-
Atg16	A component of the Atg12–Atg5-Atg16 complex; determines the localization of the complex and the site of Atg8 lipidation [86,87]	-	-
Atg17	A scaffold protein essential for PAS assembly during starvation; a component of the Atg1-Atg13-Atg17 complex that regulates Atg1 kinase activity; a component of the Atg17-Atg29-Atg31 complex [75,88-90]	+	-
Atg18	A PtdIns(3)P binding protein essential for vesicle formation in autophagy and the Cvt pathway; required for Atg9 retrieval from the PAS to peripheral sites [62,73,91,92]	-	-
Atg19	A cargo receptor in the Cvt pathway; directs the cargo complex to the PAS by interaction with Atg11 [32,34]	-	+
Atg20	A protein with a PX domain that binds to PtdIns(3)P; interacts with Atg11 [35,72]	-	+
Atg21	A PtdIns(3)P binding protein required for the Cvt pathway [74,92-94]	-	partial
Atg22	An amino acid permease on the vacuolar membrane that releases amino acids generated by vacuolar degradation back to the cytosol [95]	+	+
Atg23	A protein partially colocalized with Atg9 and essential for its transport to the PAS [61,96]	-	partial
Atg24	A protein with a PX domain that binds to PtdIns(3)P [72]	-	+
Atg25	Not identified in *S. cerevisiae*; required for pexophagy	N.A.	N.A.

	in *H. polymorpha* [97]		
Atg26	A protein with a GRAM domain required for pexophagy in *P. pastoris*, but not in *S. cerevisiae* [98,99]	+	+
Atg27	An integral membrane protein partially colocalized with Atg9 and essential for its transport to the PAS [61,64]	-	partial
Atg28	A coiled-coil protein required for pexophagy in *P. pastoris*; not identified in *S. cerevisiae* [100]	N.A.	N.A.
Atg29	A component of the Atg17-Atg29-Atg31 complex [90,101,102]	+	-
Atg30	Not identified in *S. cerevisiae*; required for pexophagy in *P. pastoris*	N.A.	N.A.
Atg31	A component of the Atg17-Atg29-Atg31 complex [90,103]	+	-
Atg32	An integral membrane protein localized on the mitochondria outer membrane; mediates cargo recognition in mitophagy by interaction with Atg11 [39,41]	+	+
Atg33	A protein required for mitophagy [42]	+	+

Chapter II. The Atg8 and Atg12 ubiquitin-like conjugation systems in macroautophagy

Abstract

As a lysosomal/vacuolar degradative pathway that is conserved in eukaryotic organisms, autophagy mediates the turnover of long-lived proteins and excess or aberrant organelles. The main characteristic of autophagy is the formation of a double-membrane vesicle, the autophagosome, which envelops part of the cytoplasm and delivers it to the lysosome/vacuole for breakdown and eventual recycling of the degradation products. Among the approximately 30 autophagy-related (*ATG*) genes identified so far, there are two ubiquitin-like proteins, Atg12 and Atg8. Analogous to ubiquitination, Atg12 is conjugated to Atg5 by Atg7, an E1-like protein, and Atg10, an E2-like protein. Similarly, Atg7 and Atg3 are the E1-like and E2-like proteins that mediate the conjugation of Atg8 to phosphatidylethanolamine. Both Atg12–Atg5 and Atg8 localize to the developing autophagosome. The Atg12–Atg5 conjugate facilitates the lipidation of Atg8 and directs its correct subcellular localization. Atg8–phosphatidylethanolamine is probably a scaffold protein that supports membrane expansion and the amount present correlates with the size of autophagosomes.

Introduction

In eukaryotic organisms, the functional diversity of the protein repertoire can be greatly extended by post-translational modifications. These change the property of target proteins by modulating their activity, localization, degradation and interaction with other proteins. In this process, the target proteins are covalently modified with other molecules such as ubiquitin. A family of small proteins related to ubiquitin—known as the ubiquitin-like proteins (Ubls)—which can be covalently attached to other proteins has been recently characterized [104]. Among the approximately 10 Ubl family members identified so far are two autophagy-related proteins Atg8 and Atg12, which are specifically involved in this conserved degradative pathway in eukaryotic organisms. In the past decade, the molecular mechanism of autophagy has begun to be elucidated, leading to the identification of approximately 30 genes that are specifically required for this pathway [54]. These are referred to as autophagy-related (*ATG*) genes. Among them, eight are directly implicated directly in the Atg8 and Atg12 conjugation systems. Although Atg8 and Atg12 have no clear sequence homology to ubiquitin, their crystal structures reveal a conserved ubiquitin-fold region [105,106] (Figure 2.1). Furthermore, these two proteins are attached to their substrate through enzymatic pathways that are similar to the ubiquitin system. Here, we focus on the molecular mechanism of the Atg8 and Atg12 conjugation process and its regulatory network.

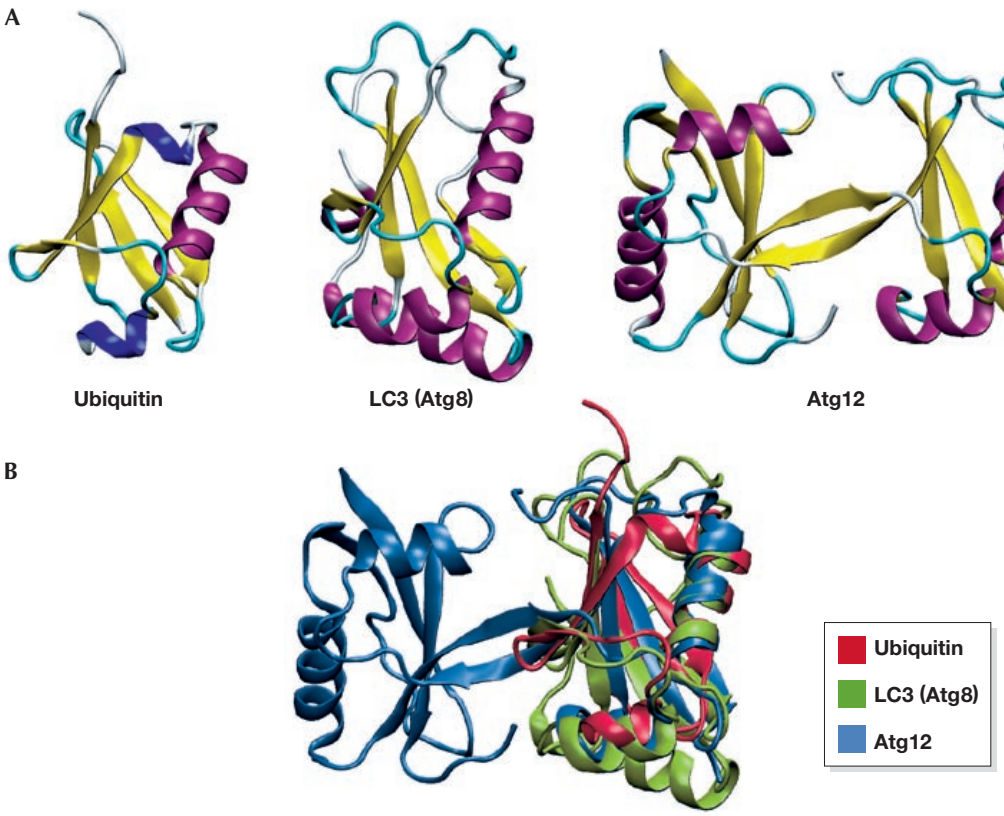

Figure 2.1 Structural comparisons of ubiquitin, LC3 and *At*Atg12. (A) Ribbon diagrams of ubiquitin [Protein Data Bank (PDB] code 1UBQ) [107], LC3 (PDB code 1UGM) [105] and *At*Atg12 (PDB code 1WZ3) [106] are shown in the same orientation; α-helices are shown in purple, 3_{10} helices in blue, β-strands in yellow, β-turns in cyan and unstructured loops in while. (B) Superimposition of ubiquitin (red), LC3 (blue) and *At*Atg12 (green). A multiple structural alignment was constructed using MAMMOTH-mult (http://ub.cbm.uam.es.mammoth/mult) [108] and the structures were visualized with the Visual Molecular Dynamics (VMD) program (http://www.ks.uiuc.edu/Research/vmd). *At*, *Arabidopsis thaliana*; Atg, autophagy related, LC3, microtubule-associated protein 1 light chain3.

An Overview of Autophagy

Autophagy mediates the lysosome-dependent turnover of macromolecules and entire organelles. Induced by environmental change, such as nutrient depletion, cytosolic components are delivered to the vacuole (the lysosome analog in yeast) through the autophagy pathway and are degraded by resident hydrolases. Degradation products are recycled to allow the synthesis of new macromolecules. Autophagy also has an important

role in various cellular processes and is associated with many human diseases [109,110].

There are several forms of autophagy, including macroautophagy, microautophagy and chaperone-mediated autophagy. In contrast to the other two types of autophagy, macroautophagy involves *de novo* vesicle formation that takes place separate from the lysosomal/vacuolar membrane. In this process, cytosolic components are sequestered in a double-membrane vesicle known as autophagosome. The outer membrane of autophagosome fuses with the lysosome/vacuole allowing access to the inner contents of the vesicle, which are subsequently degraded. As the mechanism of macroautophagy is better characterized than the other types of autophagy, it is hereafter referred to as autophagy for the purposes of this review. Autophagy has been studied in mammalian cells since the 1950s, and in the 1990s this degradative pathway was reported in the yeast *Saccharomyces cerevisiae*. Since then, mutant screening in fungi has led to the identification of molecular components of autophagy, the *ATG* genes [3]. Orthologues of the *ATG* genes have recently been found and functionally characterized in higher eukaryotes, implying a conserved mechanism.

Autophagosome formation can be divided into three steps: nucleation, expansion and completion. The initial sequestering compartment is called the phagophore, which expands, probably through vesicular addition, to envelop portions of the cytoplasm. The expanding phagophore eventually matures into the autophagosome. In *S. cerevisiae*, the phagophore assembly site (PAS; also known as pre-autophagosomal structure) is proposed to be the site from which the autophagosome originates [52,53]. Most Atg proteins co-localize at this site, presumably to participate in vesicle formation in a concerted manner. Accordingly, the PAS can be regarded as a hybrid of Atg proteins and

developing vesicles. In yeast, the PAS appears to be perivacuolar and, in most cases, there is one per cell. In mammalian cells, the co-localization of Atg proteins has been observed at multiple loci [5,69,111], probably corresponding to multiple vesicle-formation sites.

Primarily identified as a non-selective degradative pathway, autophagy can also mediate specific cargo delivery. The best studied example is a biosynthetic pathway called the cytoplasm-to-vacuole targeting (Cvt) pathway, which transports the resident vacuolar hydrolase aminopeptidase I (Ape1) into the vacuole [112]. Autophagy also plays a role in homeostatic control of unwanted organelles, such as excess peroxisomes and mitochondria, which are specifically delivered to the vacuole for degradation through pexophagy and mitophagy, respectively [36,113].

Atg12 conjugation system

Atg12 was the first ubiquitin-like Atg protein to be identified. In the canonical system, ubiquitin is synthesized as a precursor and is processed by a specific protease to expose the carboxy-terminal glycine residue. Activated by an E1 enzyme, ubiquitin is then transferred to an E2 enzyme, forming a thioester bond. An E3 ubiquitin ligase recognizes the target protein and transfers ubiquitin from the E2 to a lysine residue on the target (Figure 2.2 A).

The amino-acid sequence of Atg12 ends with a glycine residue and there is no protease involved in Atg12 conjugation. Analogous to ubiquitination, there is a E1-like enzyme, Atg7, and Atg12 is activated by forming a thioester bond between the C-terminal Gly186 of Atg12 and the Cys507 of Atg7 [114]. After activation, Atg12 is

transferred to Atg10, which is an E2 enzyme [81], and is eventually conjugated to the target protein Atg5 at Lys149 through an isopeptide bond [55] (Figure 2.2 B). There is no typical E3 enzyme involved in Atg12–Atg5 conjugation. Atg5 interacts further with a small coiled-coil protein, Atg16, and Atg12–Atg5-Atg16 forms a multimeric complex through the homo-oligomerization of Atg16 [86]. The molecular weight of this multimeric complex is approximately 350 kDa and it probably represents a tetramer of Atg12–Atg5-Atg16 [115].

Although the overall sequence of Atg7 shows little similarity to E1 enzymes in yeast, and so far only Atg7 has been shown to function in the form of a homodimer [116], Atg7 shares a conserved metal-binding motif and downstream active-site cysteine residue with other E1 enzymes such as Uba2, Uba3, Uba4 and Uba5. The ATP-binding domain of Atg7 is also homologous to the corresponding region in other E1 enzymes and is essential for the formation of the Atg12–Atg5 conjugate. In contrast to ubiquitin, which is conjugated to multiple targets in an inducible and reversible manner, Atg5 seems to be the only target of Atg12 and the conjugation of Atg12–Atg5 occurs constitutively [55]. In addition, no processing enzyme has been identified that cleaves the isopeptide bond between Atg12 and Atg5, suggesting that this conjugation is irreversible.

Orthologues of each component of the Atg12 system has been found in mice and humans, and they function similarly to their yeast counterparts [4,117,118]. There is also a mammalian Atg16-like protein (Atg16L) that mediates the formation of an Atg12–Atg5-Atg16L complex of approximately 800 kDa [111].

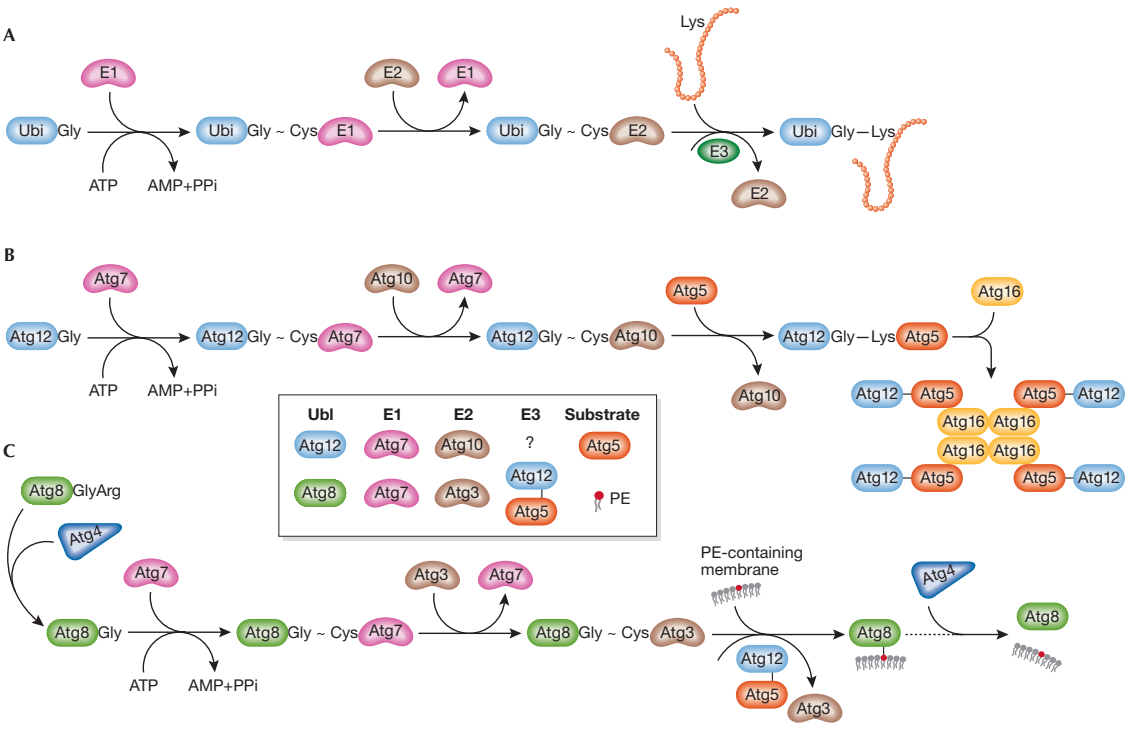

Figure 2.2 Conjugation processes in yeast. (A) Ubiquitin, (B) Atg12. (C) Atg8. See text for details.

Atg8 conjugation system

Rather than conjugating to another protein, the Ubl protein Atg8 is attached to phosphatidylethanolamine (PE). The C-terminal Arg117 residue of Atg8 is initially proteolytically removed by a cysteine protease, Atg4, to expose Gly116 [77]. This exposed Gly forms a thioester bond with Cys507 of Atg7, which is also the site participating in the Atg12–Atg5 conjugation [56]. This feature differentiates Atg7 from most other E1 enzymes, which activate single Ubl. Activated Atg8 is then transferred to the E2-like enzyme Atg3, also through a thioester bond [56]. In the final step of Atg8 lipidation, Gly116 of Atg8 is conjugated to PE through an amide bond [56] (Figure 2.2 C). Atg8–PE exists in a tightly membrane-associated form.

Although Atg3 shares little sequence homology with other E2 enzymes, structural

comparison shows the mead moiety of Atg3 is similar to that of canonical E2 enzymes [119]. The amino-acid sequence around the active-site cysteine residue of Atg3 (Cys234) is also homologous to the corresponding region (Cys133) in Atg10. Unlike Atg12–Atg5 conjugation, lipidation of Atg8 is reversible; Atg8–PE can be cleaved by Atg4 to release free Atg8 [77]. The Atg8 conjugation cycle, including the second cleavage by Atg4, is important for autophagy; when the processed form Atg8ΔR—which bypasses the need for the initial processing by Atg4—is expressed in an *atg4*Δ mutant, the efficiency of autophagy is low although Atg8–PE can still be formed. Another difference between the Atg8 and Atg12 systems is the regulation of Atg8–PE formation. In yeast, most Atg8 exists in the unconjugated form under nutrient-rich conditions. When autophagy is induced, most Atg8 is converted to the PE-conjugated form [120].

In mammalian cells, several homologues of yeast Atg8 have been identified: microtubule-associated protein 1 light chain 3 (LC3), Golgi-associated ATPase enhancer of 16 kDa (GATE16), γ-aminobutyric-acid-type-A-receptor-associated protein (GABARAP) and Atg8L. All of these undergo a modification process similar to that of their yeast counterpart, which is also catalyzed by Atg4, Atg3 and Atg7 [117,121-124]. Among them, LC3 has been best characterized as an autophagosome marker in mammalian cells. LC3 is synthesized as proLC3, and Atg4B processes this precursor into LC3-I with an exposed C-terminal glycine [121]. Catalyzed by Atg7 and Atg3, cytosolic LC3-I is transformed to a membrane-bound form, LC3-II, which corresponds to Atg8–PE in yeast. Further analysis shows that LC3 is also attached to PE, and the conjugate can be cleaved by Atg4B. In mammalian cells, the formation of LC3-II can be induced by nutrient depletion or in response to hormone [125], although the induction level is usually

cell line-dependent and tissue-dependent [126].

Crosstalk between two conjugation systems

Until recently, E3 activity did not seem to be required for Atg8 lipidation; however, it has now been reported that the Atg12–Atg5 conjugate has an E3-like activity for Atg8 lipidation [57,87]. Canonical E3 enzyme binds with both the substrate and E2 enzyme, and, most importantly, the E3 enzyme stimulates the transfer of ubiquitin from the E2-ubiquitin intermediate to the final target. Corresponding to these criteria, Atg12 interacts with Atg3 in both yeast and mammals [57,123]; Atg12–Atg5 also associates with PE-containing liposome [57]; Atg12–Atg5 accelerate the transfer of Atg8 from Atg3 to PE [57]; and few Atg8–PE/LC3-II molecules can be detected by Western blot in mutants affecting the Atg12–Atg5-Atg16 complex [5,52]. However, although Atg12–Atg5 fits well with E3 criteria, it lacks the domains that are conserved in other known E3 ligases such as HECT-type and RING- types E3 ligases.

Atg12–Atg5-Atg16 is also required for the correct localization of Atg8/LC3. In yeast, GFP-tagged Atg5, Atg16 and Atg8 have a specific localization at the PAS, as well as a cytosolic pool, as shown by fluorescence microscopy [52]. In mammalian cells, Atg12–Atg5-Atg16 also partly co-localizes with LC3 [5,111]. In yeast Atg8 does not localize to the PAS in the absence of Atg12–Atg5-Atg16 [89] and, in mammalian cells, ectopic expression of a plasma membrane-targeted Atg16L directs Atg12–Atg5, as well as LC3, to the plasma membrane [87].

Function of conjugation systems in autophagy

The formation of the Atg12–Atg5 complex and Atg8–PE is essential for autophagy. Mutation of any member of the conjugates, or of other components required for their formation, results in a defect in autophagosome formation [54]. Electron-microscopy analysis shows that defects in the recruitment of Atg12–Atg5 or Atg8 to the expanding phagophore do not affect its initiation, suggesting that the two conjugation systems participate in the membrane-expansion step [5]. In yeast, Atg8 is localized to the PAS in an Atg12–Atg5-Atg16-dependent manner, whereas Atg12–Atg5-Atg16 appears at the PAS normally in an *atg8*Δ mutant [89], implying that the Atg12–Atg5-Atg16 complex functions epistatically with respect to Atg8 in terms of PAS organization.

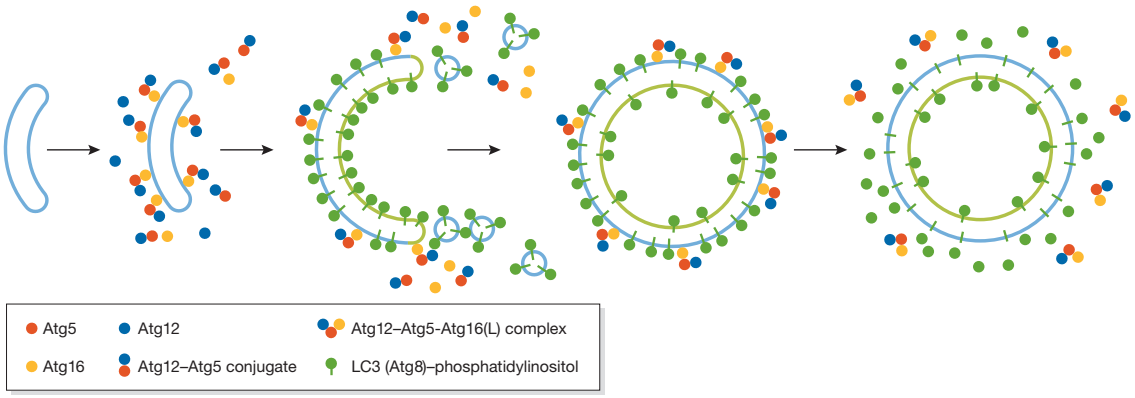

Figure 2.3 Atg12 and Atg8 conjugation systems in vesicle formation. The initiation of the early-stage phagophore occurs independent of the presence of the Atg12–Atg5 conjugate, and the Atg12–Atg5-Atg16 complex is subsequently recruited to this structure. Atg12–Atg5-Atg16 somehow redistributes mostly to the outer surface of the phagophore and directs additional Atg8 to this site. The presence of Atg8 on the phagophore supports its expansion. Upon the completion of the autophagosome, the Atg12–Atg5-Atg16 complex dissociates from the vesicle and Atg8 on the external surface is proteolytically released by Atg4.

Atg12–Atg5-Atg16 is localized on the expanding phagophore—mostly on the outer surface—and dissociates from the membrane immediately before or after autophagosome

completion [5,111]. On the basis of these phenomena, Atg12–Atg5-Atg16 was proposed as a candidate for a coatomer involved in autophagosome formation. However, a recent quantitative study shows that the number of Atg12–Atg5-Atg16 molecules at the PAS is not sufficient to coat the forming vesicle [127]. Therefore, promoting Atg8 lipidation and correct localization [87] is the only function identified so far for Atg12–Atg5-Atg16.

As Atg12–Atg5-Atg16 might not be directly involved in membrane expansion, Atg8–PE is the only candidate scaffold for membrane expansion in the two conjugation systems. The amount of Atg8 at the PAS is almost one order of magnitude higher than that of Atg16 [127]. In contrast to Atg5, Atg8/LC3 is distributed symmetrically on both sides of the phagophore, and part of the population of Atg8/LC3 on the concave surface remains inside the completed vesicle following delivery to the vacuole/lysosome [80,120,125]. Accumulating evidence indicates a quantitative relationship between the amount of Atg8 and the vesicle size. In yeast, the induction of autophagy results in the upregulation of Atg8 expression [120] and the formation of larger autophagosomes [79]. In mammals, Group A *Streptococcus* invasion results in the formation of bacteria-containing autophagosomes that are bigger than those induced by starvation and the LC3 expression level is also higher [128]. These results suggest a possible role of Atg8 as a component of the scaffold that supports the expanding membrane (Figure 2.3).

In some specific types of autophagy, Atg8 also functions in cargo selection by interacting with receptors. For example, in the Cvt pathway, Atg8 interacts with Atg19, which is the receptor for precursor Ape1 [32,34]. In autophagic degradation of ubiquitinated protein aggregates in mammalian cells, LC3 interacts with p62, which is a ubiquitin-binding protein [129]. These interactions might contribute to the specificity of

these processes, so that the vesicle contains only its cargo and excludes other cytosolic components or organelles. Recently, Nakatogawa and colleagues reported that Atg8–PE can mediate membrane tethering and hemifusion *in vitro* [130], although it is unclear how membrane fusion *in vivo* only occurs on the edge of expanding phagophore if Atg8 is distributed evenly on the membrane surface.

Although we have some knowledge regarding the role of Ubls in autophagy, many questions remain to be answered (Table 2.1). Further studies on the mechanism of sequestering vesicle formation are needed to answer them and to elucidate the functions of post-translational modifications in the regulation of this process.

Acknowledgements

This work was supported by National Institutes of Health Public Health Service grant GM53396 to D.J.K.

Table 2.1 In need of answers

1. What is the function of Atg8/LC3 and what role does it have in phagophore expansion?
2. Do coat elements participate in sequestering vesicle formation?
3. How are the different sizes and curvatures of the sequestering vesicles determined?
4. What regulates the activity of Atg4 and controls the cleavage of Atg8/LC3–PE?
5. What is the nature and purpose of the interaction between Atg8 and the Atg19 cytoplasm-to-vacuole targeting pathway cargo receptor?
6. What controls the timing of Atg12–Atg5-Atg16 association with, or dissociation from, the phagophore or autophagosome?
7. What are the roles of the mammalian Atg8 homologues?

Chapter III. Quantitative analysis of autophagy-related protein stoichiometry by fluorescence microscopy

Abstract

In yeast, ~ 31 autophagy-related (Atg) proteins have been identified. Most of them reside at the phagophore assembly site (PAS), although the function of the PAS mostly remains unclear. One reason for the latter is the lack of stoichiometric information regarding the Atg proteins at this site. We report the application of fluorescence microscopy to study the amount of Atg proteins at the PAS. We find that an increase in the amount of Atg11 at the PAS enhances the recruitment of Atg8 and Atg9 to this site and facilitates the formation of more cytoplasm-to-vacuole targeting vesicles. In response to autophagy induction, the amount of most Atg proteins remains unchanged at the PAS whereas we see an enhanced recruitment of Atg8 and 9 at this site. During autophagy, the amount of Atg8 at the PAS showed a periodic change, indicating the formation of autophagosomes. Application of this method and further analysis will provide more insight into the functions of Atg proteins.

Introduction

Autophagy is an intralysosomal degradation pathway conserved in various eukaryotic organisms. Increasing evidence has pointed out the connection between autophagy and various physiological processes in higher eukaryotes [109,110]. One of the areas that have lagged, however, is a mechanistic understanding of autophagy, and the function of the Atg proteins. This problem is exacerbated by the fact that only 7 of the 30 currently identified Atg proteins have clear functional motifs [131]. An additional issue is that there is essentially no quantitative information on the stoichiometries of the Atg proteins. In this study, we report a method using fluorescence microscopy to study the quantitative behavior of Atg proteins during autophagy.

There are different types of autophagy, but the best characterized is macroautophagy, hereafter referred to as autophagy. During autophagy, a portion of the cytoplasm is sequestered, randomly in most cases, by an expanding membrane sac (called the phagophore). Upon completion, the phagophore generates a double-membrane vesicle termed an autophagosome. The autophagosome then fuses with the vacuole (lysosome analog in yeast), releasing the inner vesicle, the autophagic body, into the lumen. The autophagic body, along with its cargo, is then degraded by vacuolar hydrolases, and the resulting macromolecules are released back into the cytosol for reuse.

Although originally identified as a nonselective degradative pathway, autophagy in yeast can also mediate a selective biosynthetic pathway called the cytoplasm-to-vacuole targeting (Cvt) pathway, which uses much of the same protein machinery to transport the resident vacuolar hydrolase aminopeptidase I (Ape1) [25,26,30]. The Cvt pathway has

only been described in fungi; however, there are many examples of selective types of autophagy in higher eukaryotes [45,110,132,133].

For both autophagy and the Cvt pathway, the phagophore assembly site (PAS) is thought to be the organization center for the formation of the Cvt vesicle and autophagosome during growing and starvation conditions, respectively [52,53,72]. As detected by fluorescence microscopy, most Atg proteins show a specific localization at this punctate perivacuolar structure. Although the function of the PAS is still not fully understood, it is known that the correct targeting of Atg proteins to this site is essential for their normal function. In the Cvt pathway, Atg11 is reported to play a predominant role in PAS formation because the absence of this protein results in no detectable PAS under vegetative conditions [34]. According to our current model, Atg11 acts as a scaffold protein and participates in several steps of the Cvt pathway. For example, Atg11 plays a role in cargo recognition by binding Atg19, the receptor of precursor Ape1 (prApe1) [32,34]. Atg19 also interacts with Atg8, which is normally localized at the PAS [34,53]. In an *atg11*Δ mutant, however, the Atg19 and prApe1 proteins interact and form a complex, but this complex localizes away from the PAS. Similarly, Atg8 primarily shows a diffuse cytosolic localization in this mutant strain. Another interaction partner of Atg11 is Atg9, and the interaction between them mediates the movement of Atg9 from peripheral pools (potential membrane sources) to the PAS [65].

Although these studies have provided substantial information about the temporal order of action of components involved in cargo recognition and packaging, we are hampered in our attempt to understand the process at a molecular level because none of these data deal with quantitative properties. For example, the capacity of the Cvt pathway

can be overwhelmed by overexpression of the cargo, prApe1 [25,29,30]. In contrast, the elevated level of prApe1 can be accommodated by nonspecific autophagy [31]. What are the alterations that provide the increased capacity for the autophagic machinery under starvation conditions? This question pertains to similar issues in higher eukaryotes, such as the sequestration of damaged organelles or invasive microbes within autophagosomes of the appropriate size [110].

We used the Cvt pathway as a model to investigate the stoichiometric changes in Atg proteins that allow adaptations to specific intracellular demands. Recently, a new method was reported to measure protein concentrations directly in living cells of the yeast *Schizosaccharomyces pombe* using fluorescence microscopy [134]. A linear relationship was observed between the protein amount and fluorescence intensity, which means within a certain range, no matter what protein is tagged by the fluorophore or where the tagged protein is localized, the fluorescence intensity is determined only by the protein amount. In this paper, we used a similar strategy, measuring the amounts of various Atg proteins at the PAS in different conditions and examined the levels of proteins involved in specific cargo delivery.

Results

Overexpressed prApe1 exceeds the capacity of the Cvt pathway

In wild-type cells, most of the Ape1 is detected as mApe1 (the mature form) under steady-state conditions. In contrast, prApe1 accumulates when the protein is overexpressed [25,30]. The accumulated prApe1 is rapidly matured when cells are shifted to starvation conditions [31], and further precursor accumulation does not occur. The machinery of specific autophagy clearly has a limited capacity for cargo delivery, and import via this pathway is saturated if the cargo amount exceeds this capacity. The nonspecific autophagy pathway utilizes sequestering vesicles with a much larger volume and thus delivers more cargo into the vacuole. We decided to determine whether the altered expression of particular Atg proteins that occurs during autophagy could account for the enhanced capacity of the nonspecific pathway with regard to the import of prApe1.

First, we replicated the accumulation of prApe1 induced by overexpression. In wild-type cells, the expression level of Ape1 could be induced upon starvation (Figure 3.1 A, lanes 1 and 2). As expected, no prApe1 was detected under these conditions. In a prApe1 overexpression strain in which the *CUP1* promoter drove prApe1 synthesis, the level of the protein was dramatically enhanced and >50% accumulated as the precursor form (Figure 3.1 A, lane 3). When the cells were shifted to starvation conditions to induce nonspecific autophagy, the accumulated prApe1 was completely matured (Figure 3.1 A, lane 4).

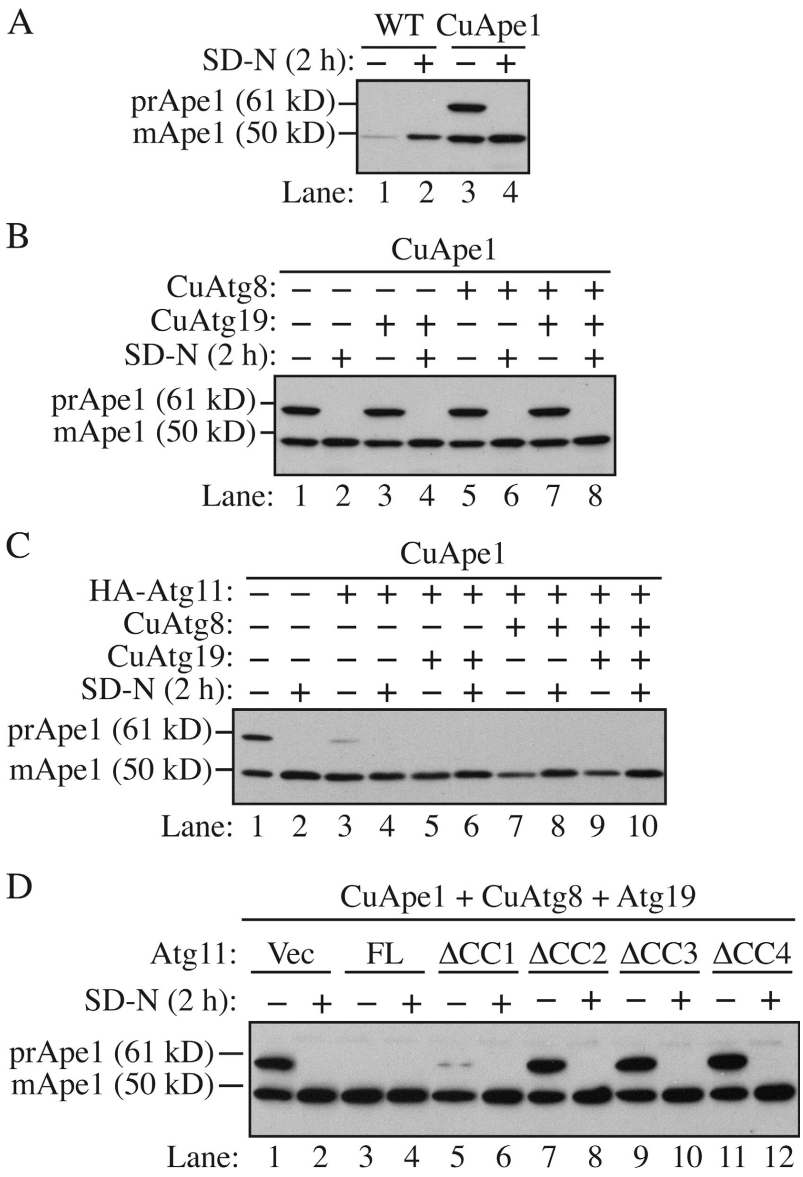

Figure 3.1 The amount of Atg11 affects the capacity of the Cvt pathway. Strains were cultured in SMD and then starved for 2 h. Cells were harvested before or after starvation and analyzed by Western blotting with anti-Ape1 antiserum. (A) Overexpression of prApe1 overwhelms the Cvt pathway. The wild-type (SEY6210) or prApe1 overexpression (JGY069) strain was analyzed. (B) Overexpression of Atg8 and 19 could not restore the maturation of overexpressed prApe1. The prApe1 overexpression strain harboring pCuAtg19, pCuAtg8, or both were analyzed. (C) A higher level of Atg11 enhanced the processing of overexpressed prApe1. Cells expressing a combination of pHA-Atg11, pCuAtg8, and pCuAtg19 were examined. (D) The CC domains (CC2, CC3, and CC4 but not CC1) were required for the effect of Atg11 on Cvt pathway capacity. Besides Atg19 and 8, full-length (FL) or truncations of Atg11 were expressed in the prApe1 overexpressing strain and the maturation of prApe1 was examined.

Next, we compared the expression level of Atg proteins between growing and starvation conditions. Among those required for prApe1 import, Atg8 and 19 show an increased expression level during starvation [32,80]. Atg19 is a specific receptor protein for prApe1, whereas Atg8 is involved in the expansion of the autophagosomal membrane [130], and the amount of Atg8 is correlated with the size of the autophagosome [79]. We hypothesized that the basal level of Atg19 and 8 under growing conditions is not abundant enough to transport excess prApe1. Therefore, we tested whether it was possible to restore the maturation of excess prApe1 by overexpressing these two proteins. Cells were transformed with plasmids expressing Atg8, 19, or both, driven by the *CUP1* promoter. When Atg19 was overexpressed along with prApe1, the precursor form of Ape1 still accumulated in rich medium conditions (Figure 3.1 B). Induction of autophagy by starvation rescued the precursor accumulation phenotype, so the overexpressed Atg19 did not act in a dominant-negative manner. Similarly, overexpression of Atg8 did not prevent accumulation of prApe1 and did not interfere with maturation via nonspecific autophagy. Finally, overexpression of both Atg8 and 19 was also ineffective in allowing maturation of the elevated level of prApe1. This suggested the existence of other limiting factors besides Atg8 and 19 that can determine the capacity of cargo delivery in the Cvt pathway.

A higher level of Atg11 facilitates the import of excess prApe1 by the Cvt pathway

Because Atg11 is the key component involved in the recruitment of Atg8, 19 and other Atg proteins to the PAS [34,35,82], we tested whether the Atg11 amount has an effect on Cvt pathway capacity. The Cvt pathway is sensitive to the dosage of Atg11. When

expressed from a multicopy plasmid, Atg11 displays a dominant-negative phenotype, which results in ~40-50% of prApe1 remaining in the unprocessed form [82]. To avoid the dominant-negative effect of excess Atg11, we decided to express the *ATG11* gene under the control of the endogenous promoter on a centromeric (CEN) plasmid in addition to the chromosomal copy of *ATG11*, which resulted in a modulated increase of Atg11 amount (approximately three- to fourfold; unpublished data). With this level of Atg11, only a small amount of prApe1 accumulated in growing conditions (Figure 3.1 C, lane 3). When Atg8 and/or 19 were coexpressed with Atg11, prApe1 was fully processed and no precursor could be detected (Figure 3.1 C, lanes 5, 7, and 9). The maturation of prApe1 under starvation conditions was not affected in these overexpression strains (Figure 3.1 C, lanes 4, 6, 8, and 10). It is known that Atg11 interacts with other Atg proteins via its coiled-coil (CC) domains [35]. When cells expressed a plasmid encoding Atg11ΔCC2, ΔCC3, or ΔCC4 in which the corresponding CC domain was deleted, there was no effect on prApe1 maturation, whereas full-length Atg11 expression reduced the accumulation of prApe1 (Figure 3.1 D, lanes 3, 7, 9, and 11). The expression of Atg11ΔCC1, however, substantially facilitated the maturation of prApe1 although with a little bit less efficiency than the full-length protein (Figure 3.1 D, lane 5). This observation is consistent with previous results that CC1 of Atg11 is not required for the Cvt pathway [35]. Therefore, the ability of Atg11 to rescue the prApe1 accumulation phenotype depends on its interaction with other Atg proteins.

More Cvt vesicles were synthesized in cells overexpressing Atg11

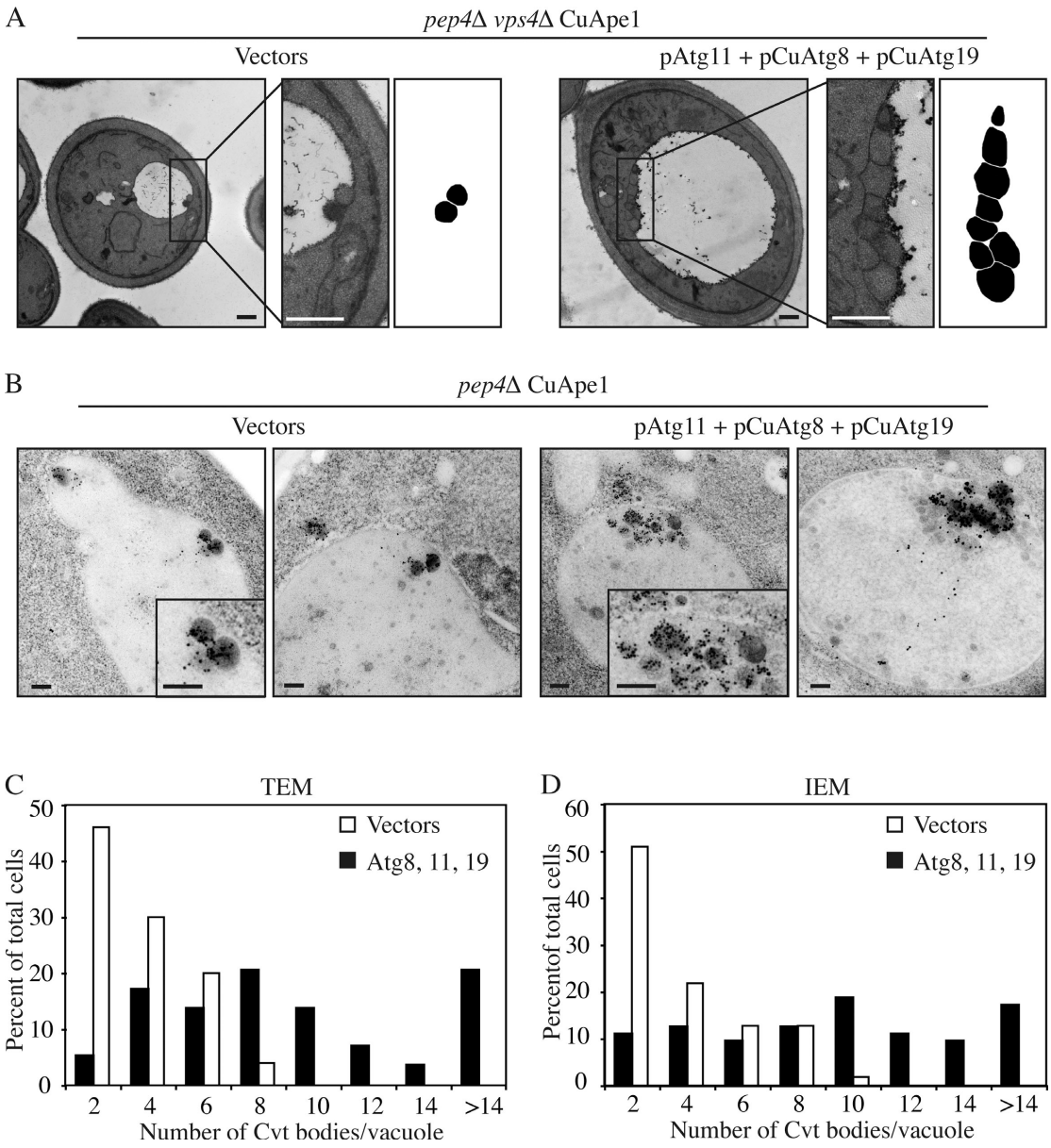

Figure 3.2 More Cvt vesicles were formed in Atg11-overexpressing cells. Cells (*pep4*Δ *vps4*Δ CuApe1; JGY089) expressing either pAtg11, pCuAtg8, and pCuAtg19 or empty vectors were cultured in SMD medium to mid-log phase. Cells were harvested and prepared for EM as described in Materials and methods. Representative images of TEM and IEM are shown in A and B, respectively. Areas with typical Cvt vesicles are shown with higher magnification at the right. In A, the Cvt vesicles were drawn in black in the far right. Scale bar: (A) 500 nm; (B) 200 nm. (C and D) Quantification of Cvt body accumulation. The number was determined from cells with clearly defined Cvt bodies inside the vacuole.

To address whether the higher amount of mApe1 in Atg11 overexpressing cells is caused by elevated vesicle formation or increased vesicle size, we performed a morphological analysis by transmission EM (TEM). During the Cvt pathway, the outer membrane of the Cvt vesicle fuses with the vacuolar membrane, releasing the single-membrane Cvt body. Within the vacuolar lumen, the Cvt body is broken down in a Pep4-dependent manner. Pep4 is a vacuolar protease required for the maturation of other vacuolar enzymes [135]. In a *pep4*Δ strain, intact Cvt bodies accumulate in the vacuole and can be visualized by EM. In addition, we knocked out Vps4 to eliminate vesicles generated from the multivesicular body pathway [136,137]. In *pep4*Δ *vps4*Δ CuApe1 (JGY089) cells harboring empty vectors as controls, Cvt bodies were observed inside the vacuole. The mean number was 3 ± 0.2 vesicles per vacuole (mean ± SEM, standard error of mean; n = 50) (Figure 3.2 A and C). In *pep4*Δ *vps4*Δ CuApe1 cells simultaneously overexpressing Atg8, 11, and 19, numerous Cvt bodies appeared and the mean was 9.1 ± 0.8 per vacuole (mean ± SEM; n = 59), which was significantly higher than the number observed in the control ($P < 0.01$; Figure 3.2 A and C). To determine whether overexpression of Atg8, 11, and 19 affected the size of the Cvt bodies, we quantified their diameter. In cells overexpressing these three proteins, the mean diameter was 252 ± 3.5 nm (mean ± SEM; n = 538), whereas that of control cells was 209 ± 5.4 nm (mean ± SEM; n = 151). This difference was also statistically significant ($P < 0.01$).

In addition to TEM, we also performed immuno-EM (IEM) with Ape1 antibody to analyze the formation and verify the identity of Cvt vesicles in cells overexpressing Atg11. Cvt vesicles and Cvt bodies labeled with gold particles were detected outside and inside the vacuoles, respectively, in *pep4*Δ CuApe1 (JGY088) cells harboring pAtg11,

pCuAtg8, and pCuAtg19 or empty vectors (Figure 3.2 B). Occasionally, multiple Ape1 complexes were present within a single larger membrane in cells overexpressing Atg8, 11, and 19 (unpublished data) and we also counted them in the quantification. The mean number of Cvt bodies in cells overexpressing Atg8, 11, and 19 was 9.5 ± 0.7 (mean ± SEM; n = 65), while the number in control cells was 3.3 ± 0.3 (mean ± SEM; n = 55; $P < 0.01$). This result was consistent with our observation by TEM. However, the small increase in Cvt body diameter seen by TEM with Atg8, 11, and 19 overexpression was not observed by IEM ($P = 0.39$), which may be explained by the different sample preparation procedures needed for TEM versus IEM. Therefore, with the overexpression of Atg11, as well as Atg8 and 19, the number of Cvt bodies increased substantially by approximately threefold, resulting in the formation of more mApe1, which was detected by western blot (Figure 3.1). The size of Cvt vesicles may also be affected, but was apparently less significant than the change in vesicle number.

What is the mechanism through which the Atg11 level can affect the efficiency of Cvt vesicle formation? Given the function of Atg11 in recruiting the prApe1 complex to the PAS via Atg11-Atg19 interaction, we speculated that the higher amount of Atg11 resulted in a higher efficiency of cargo recruitment. Another aspect of Atg11 function, however, is in the anterograde movement of Atg9 (from peripheral sites to the PAS). Recently it was reported that defective anterograde movement of Atg9 in the *atg27*Δ mutant results in fewer but normal-sized autophagosomes produced in starvation conditions [64]. In contrast, Atg9 localization is restricted to the PAS when Atg11 is overexpressed, which blocks prApe1 maturation [65], although the levels of Atg9 and 11 were not quantified. This suggests a relationship between cargo delivery and the proper

targeting of Atg9 to the PAS. Accordingly it is also possible that the intermediate increase in Atg11 expression used in the present analysis caused an increase in the flux of Atg9 from the putative membrane source to the PAS, supplying extra lipid for the formation of more Cvt vesicles. Thus, to gain specific quantitative information on whether the increase in Atg11 affected the functional pool of other proteins that are bound to prApe1 or present at the PAS, we needed to establish a method to study the stoichiometry of the Atg proteins at the PAS.

A fluorescence-based method can be used to determine the stoichiometry of the Atg proteins

Recently, a method was established in *S. pombe* that demonstrates that within a certain range the fluorescence intensity of fusion proteins is proportional to the number of protein molecules [134]. This method has a clear utility for an analysis of the Cvt pathway and autophagy because most of the Atg proteins are partly restricted at a specific location: the PAS. If we can establish the linear relationship between protein amount and fluorescence intensity, then it will be easy to calculate the level of any Atg protein at the PAS via its PAS fluorescence intensity. Accordingly, we investigated the applicability of this strategy in *Saccharomyces cerevisiae*.

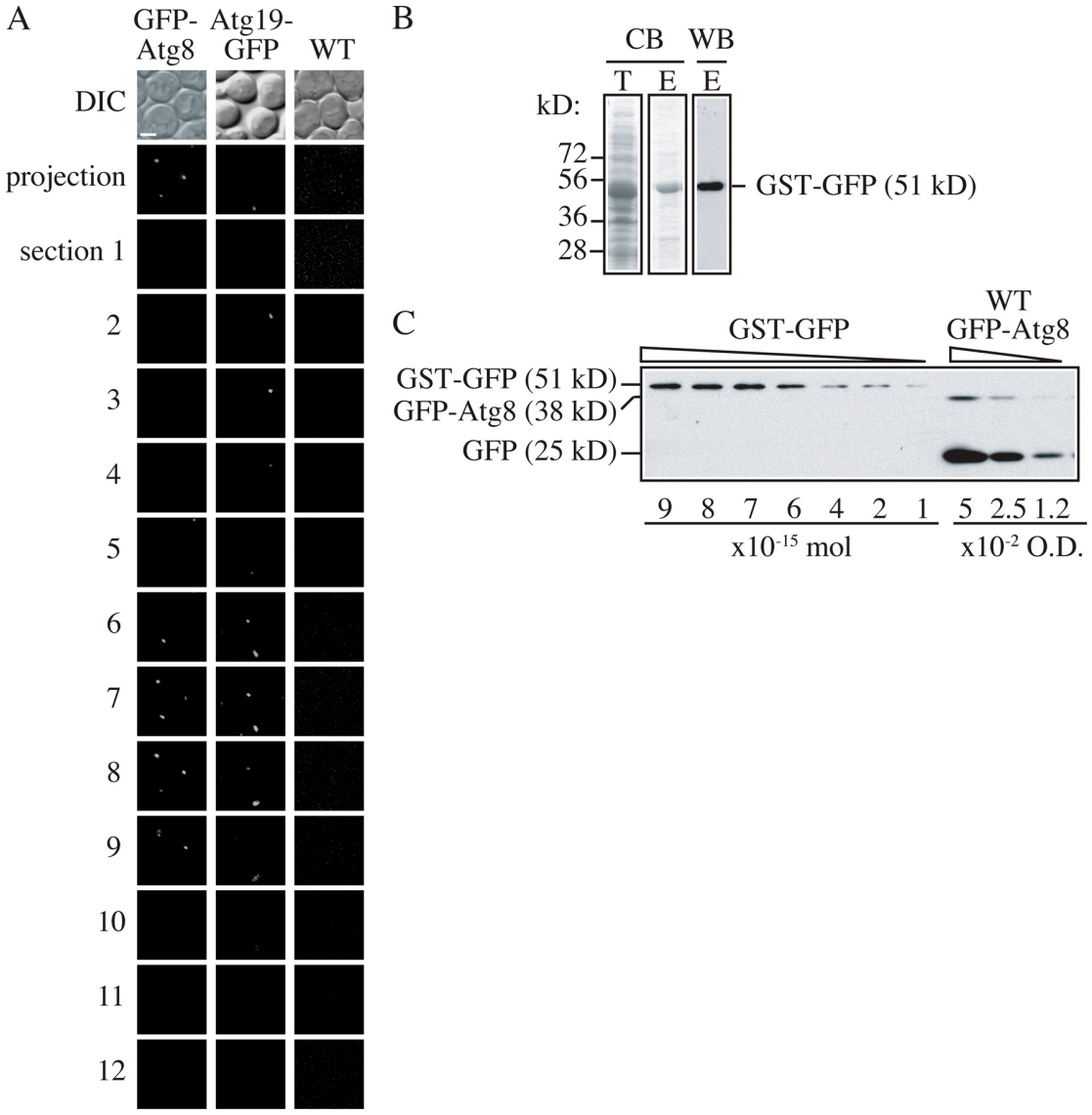

Figure 3.S1 Examination of the relationship between GFP-tagged protein amount and fluorescence intensity. (A) Wild-type (SEY6210) and Atg19-GFP (JGY018) cells cultured in nutrient-rich medium and GFP-Atg8 (YZX247) cells starved for 2 h were subjected to microscopy. A stack of 12 Z-section pictures was collected and projected into a 2D image, and the fluorescence signals per cell were quantified as described in Materials and methods. The intensity values from wild-type cells were subtracted as background. Bar, 2 μm. (B) The GST-GFP fusion protein was purified from *E. coli* BL21 cells as a protein standard as described in Materials and methods. Total cell lysate and elution of glutathione Sepharose were examined by Coomassie Blue staining. The elution was confirmed by Western blot using anti-YFP antibody. (C) Quantitative Western blot. Different amounts of purified GST-GFP were loaded as standard, and protein samples from other GFP-tagged strains (GFP-Atg8 is shown here) were tested on the same gel. Duplicate samples of GFP-Atg8 corresponding to 0.05, 0.025, and 0.0125 OD_{600} units of cells were loaded to fit both GFP-Atg8 and free GFP bands into the range of the standard protein.

We began by testing the linearity between protein concentration and fluorescence intensity. We generated a series of strains harboring GFP-tagged fusion proteins expressed at different levels. In YZX247, YZX251, and YZX257, GFP-Atg8 expression was driven by the *ATG8*, *ATG27*, or *ATG3* promoter, respectively. In YZX246, there are two copies of GFP-Atg8, which are independently expressed under the control of the *VPS30* and *ATG18* promoters. Upon starvation, GFP-Atg8 expression was induced to different levels depending on the particular promoter (unpublished data). In the wild-type background, GFP-Atg8 is delivered into the vacuole and degraded in a Pep4-dependent manner [80]. Therefore, we generated four additional strains in which the *PEP4* gene was deleted to block the degradation of GFP-Atg8. In these *pep4*Δ GFP-Atg8 strains, the amount of GFP-Atg8 was slightly higher than their counterparts in the *PEP4* GFP-Atg8 background. In this way, we constructed a total of eight strains expressing GFP-Atg8 at different levels.

Using these GFP-Atg8 strains, we measured the fluorescence intensity and protein amount of the fusion proteins after 2 h of starvation by microscopy and immunoblotting, respectively. For fluorescence intensity, each sample was imaged at 12 focal planes. The interval between two adjacent sections was set to 0.5 μm to cover the depth of a yeast cell. Then these 12 sections were additively projected in a 2D image (Figure 3.S1 A), and the fluorescence intensity of the whole cell was measure by microscopy software (as described in Materials and methods). To quantify the protein amount, because all the fusion proteins we would study were tagged with GFP, we used purified GST-GFP (Figure 3.S1 B) as a standard protein with known concentration. When GFP-Atg8 is delivered into the vacuole, the GFP moiety is relatively stable, and free GFP accumulates

within the vacuolar lumen [138]. Because the free GFP in the vacuole also contributed to the fluorescence signal of the whole cell, we quantified both the GFP-Atg8 and free GFP bands by Western blot and calculated the sum (Figure 3.S1 C). However, in the *pep4*Δ GFP-Atg8 strains, no free GFP could be formed and only the GFP-Atg8 band was quantified. After determining the fluorescence intensity and protein level of GFP-Atg8 (or free GFP) in each strain, we plotted the intensity against the protein amount. A linear relationship was shown and linear regression was done to generate a formula describing this relationship (Figure 3.3), $R^2 = 0.9765$, suggesting that our data fit the formula reasonably well. The intercept was set to zero because when the protein concentration is zero, we expect the fluorescence intensity to theoretically be zero as well.

Among Atg proteins, Atg8 is expressed at relatively higher levels of ~2,000 molecules per cell in growing conditions [139]. To add additional data points to our analysis, in particular at lower expression levels, we analyzed two more proteins. Cdc12 and Mlc2 are two critical proteins involved in cytokinesis [140,141]. Their expression levels are ~1,000 molecules per cell, which is close to the estimated values for most Atg proteins other than Atg8. Using the same methods, the fluorescence intensity and protein amount of Cdc12-GFP and Mlc2-GFP were measured. We found that these two proteins fit well into the linear relationship that we had calculated based on the various strains expressing GFP-Atg8 (Figure 3.3). Therefore, the plot in Figure 3.3 can theoretically be used as a standard curve to calculate protein amount from fluorescence intensity over a relatively wide range. To avoid the variance of fluorescence signal from experiment to experiment, we used the P_{ATG27}GFP-Atg8 and P_{ATG8}GFP-Atg8 *pep4*Δ strains (Figure 3.3, a and j) to calibrate the standard curve for the following experiments.

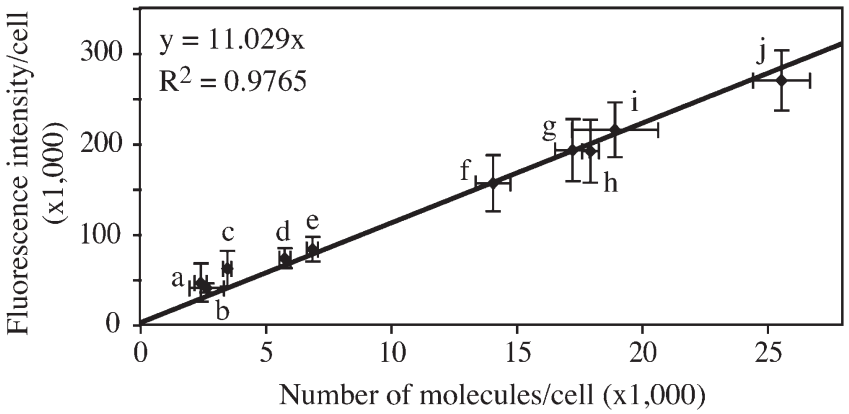

Figure 3.3 Linear relationship between GFP-tagged protein amount and fluorescence intensity. The standard curve showed the relationship between protein amount and fluorescence intensity. Fluorescence intensity and GFP-tagged protein amount were quantified in the following strains: (a) P_{ATG27}GFP-Atg8; (b) Mlc2-GFP; (c) P_{ATG27}GFP-Atg8 *pep4*Δ; (d) $P_{VPS30\text{-}ATG18}$GFP-Atg8; (e) $P_{VPS30\text{-}ATG18}$GFP-Atg8 *pep4*Δ; (f) P_{ATG3}GFP-Atg8; (g) P_{ATG3}GFP-Atg8 *pep4*Δ; (h) P_{ATG8}GFP-Atg8; (i) Cdc12-GFP; and (j) P_{ATG8}GFP-Atg8 *pep4*Δ. Error bars indicate the SD of three independent experiments. For fluorescence intensity, >200 cells of each strain were analyzed by microscopy as described in Materials and methods. Linear regression was performed to generate the formula y = 11.029x.

So far, all the GFP fusion proteins that we discussed were expressed by plasmid-based integration or chromosomal tagging, not from CEN plasmids. The reason is that we found the SD of fluorescence intensity of CEN plasmid-based fusion proteins was much higher than that of chromosomally expressed fusion proteins. For example, based on microscopy, the GFP-Atg8 (CEN) signal was extremely bright in some cells but very dim in others, whereas the intensity of chromosomally expressed GFP-Atg8 was relatively constant from cell to cell (Figure 3.S2 A). The relative SD (SD/mean) of the fluorescence signal among cells was calculated. All the chromosomally expressed proteins had a low relative SD, which was less than one-tenth of that for GFP-Atg8 expressed from a CEN plasmid (Figure 3.S2 B).

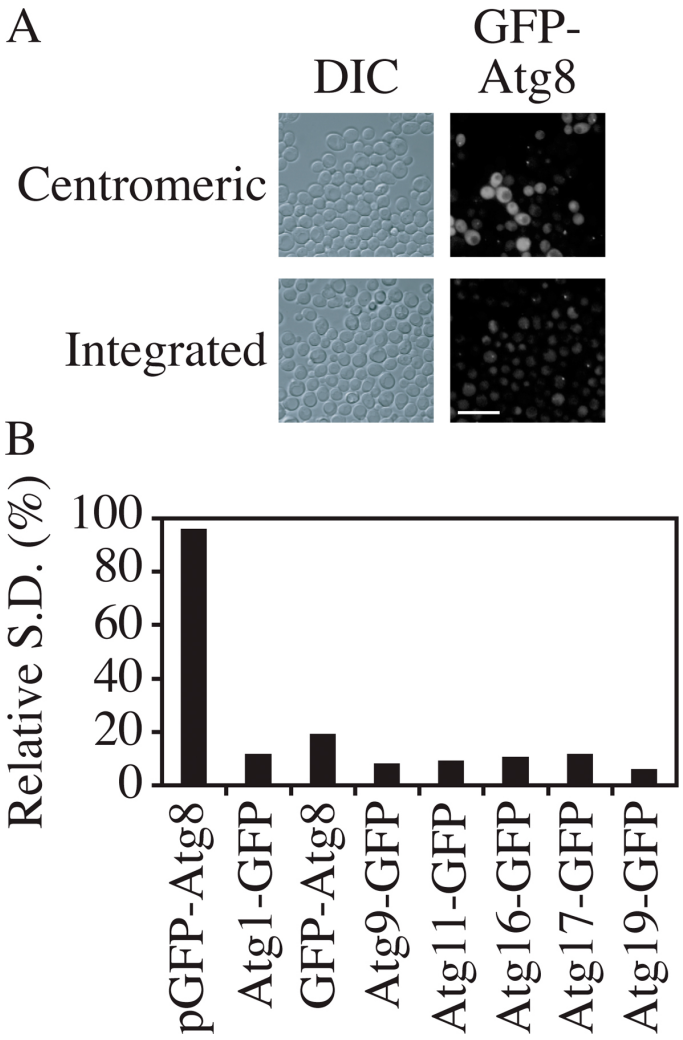

Figure 3.S2 Chromosomally tagged Atg proteins had a more consistent expression level than proteins expressed from centromeric plasmids. (A) Representative images of chromosomally expressed or plasmid-based GFP-Atg8. GFP-Atg8 cells (YZX247) or wild-type cells expressing pGFP-Atg8(416) were grown in nutrient-rich medium and imaged by microscopy. Bar, 15 μm. (B) The signal intensity per cell was quantified from 50 cells of each strain and the relative SD from cell to cell was calculated. Relative SD is equal to SD divided by the mean. All cells expressed chromosomally tagged proteins except for those shown in lane 1, which expressed GFP-Atg8 from a centromeric plasmid.

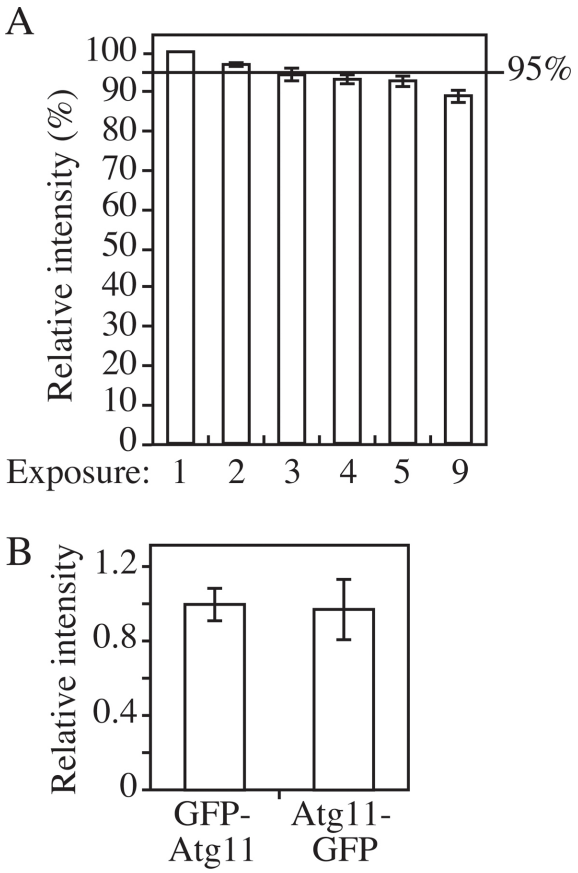

Figure 3.S3 Reliability of the standard curve. (A) Effect of photobleaching. A strain expressing GFP-Atg8 (YZX247) was starved for 2 h. Using fluorescence microscopy, nine stacks of images were taken in a row and each stack was projected and quantified (n = 60). The fluorescence intensity from the first image was normalized as 100%. After taking three stacks of pictures, the intensity decreased by 5% and after nine stacks the reduction was 11%. (B) Relative fluorescence intensity of Atg11 tagged with GFP at either the N or C terminus. GFP-Atg11 (JGY075) and Atg11-GFP (PSY101) strains were cultured in nutrient-rich medium and the fluorescence signals were quantified (n = 80). Note that because Atg8 cannot be tagged at the C terminus and remain intact as a fusion protein (except in an *atg4*Δ mutant), we compared Atg11-GFP and GFP-Atg11 strains. In both strains the endogenous *ATG11* promoter drove the expression of the fusion proteins. Error bars indicate the SEM of three independent experiments.

To test the reliability of the standard curve, we examined its accuracy under different parameters. First, a criterion was established in this study that no more than three pictures were taken on the same slide to minimize the effect of photobleaching (Figure 3.S3 A). Second, the quenching effect was examined. For most proteins, the

subcellular distribution is not uniform. Therefore, the local concentration of a certain protein may be higher at some specific locations than at others. If the local concentration at a particular site is extremely high, it is possible that the fluorescent signal at that location may be saturated. To test this possibility, the intensities of GFP-Atg8 were measured in different genetic backgrounds. When GFP-Atg8 is exposed to vacuolar hydrolases, released free GFP will be evenly diffuse in the vacuole lumen. In a hydrolase-deficient mutant such as *pep4*Δ, autophagic bodies will not be broken down and tend to cluster together in the vacuole lumen [2,80] (Figure 3.4 A). Atg5 is required for the recruitment of Atg8 to the PAS. In an *atg5*Δ mutant, GFP-Atg8 will be evenly diffuse in the cytosol but absent in the vacuole [52] (Figure 3.4 A). In contrast, in the *atg2*Δ mutant, GFP-Atg8 is constrained at the PAS, giving an extremely strong fluorescence signal at this small region [89] (Figure 3.4 A). Thus, in the background of *pep4*Δ, *atg2*Δ, or *atg5*Δ mutants, GFP-Atg8 has totally different localization patterns, ranging from diffuse to concentrated. Western blotting showed that the protein amount of GFP-Atg8 in these three strains was the same (Figure 3.4 B). If a quenching effect was significant, the intensity of concentrated GFP-Atg8 would be lower than the diffuse GFP-Atg8. However, quantification of the fluorescence microscopy indicated that the total intensity per cell was essentially the same in all three strains (Figure 3.4 C). This observation suggested that fluorescent signals that result from clustering within the vacuole or from being concentrated at the PAS will not dramatically affect the signal intensity. Because Atg8 has the highest concentration at the PAS among the Atg proteins, the lack of saturation for the Atg8 signal means that saturation should not be an issue for the other Atg proteins.

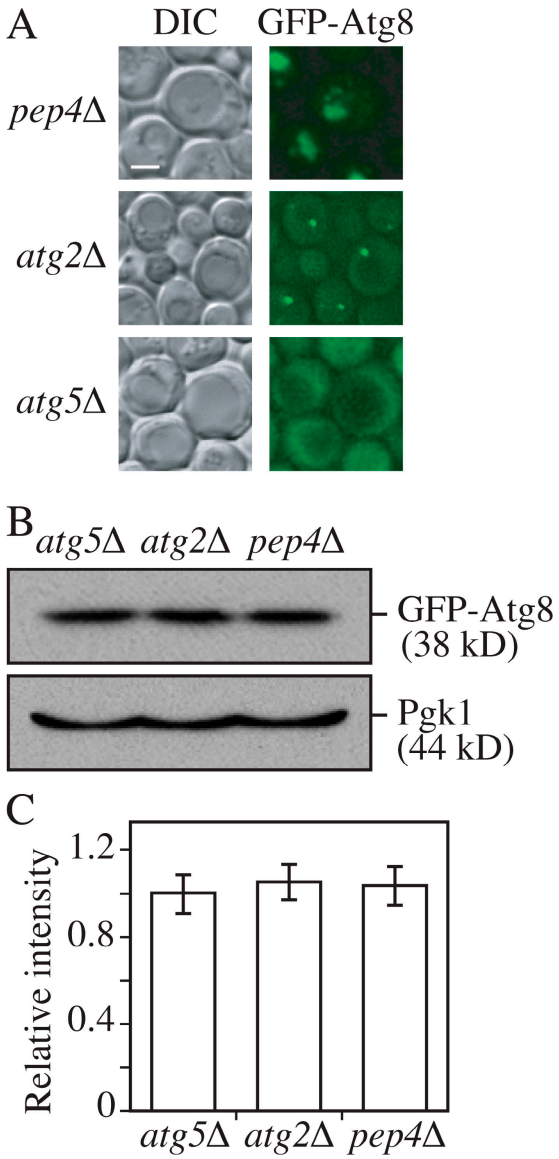

Figure 3.4 Localization does not affect the linearity of the fluorescent signal. (A) Representative images of GFP-Atg8 localization in *pep4*Δ, *atg2*Δ, and *atg5*Δ strains, which result in autophagic body, PAS, and diffuse cytosolic staining patterns, respectively. GFP-Atg8 *pep4*Δ (YZX254), GFP-Atg8 *atg2*Δ (JGY054), or GFP-Atg8 *atg5*Δ (JGY053) cells were starved for 2 h and examined by fluorescence microscopy. Bar, 2µm. (B) The protein amount of GFP-Atg8 was the same in the *pep4*Δ, *atg2*Δ, or *atg5*Δ backgrounds. The amount of Pgk1 protein in each strain was used as a loading control. (C) Relative fluorescence intensity of GFP-Atg8 per cell in *pep4*Δ, *atg2*Δ, and *atg5*Δ strains (n = 60). Images of all of these strains were quantified as described in Materials and methods. The intensity of GFP-Atg8 in the *atg5*Δ strain was normalized to 1 as a reference. Error bars indicate the SEM of three independent experiments.

Finally, we tested the difference between N- and C- terminal tagging. To establish the standard curve, we used a series of N-terminal tagged GFP-Atg8 strains, because a GFP moiety at the C terminus of Atg8 will be cleaved off in the cytosol during the formation of Atg8–phosphatidylethanolamine (PE) [56]. Most of the other Atg proteins in our analysis, however, are tagged at the C terminus because of the ease of construction via the PCR-based gene-tagging method [142]. Microscopy data showed that the difference between C- and N-terminal tagging was insignificant (Figure 3.S3 B). Therefore, the standard curve calibrated by tagging strains at the N terminus is applicable to C-terminally tagged strains.

The increased amount of Atg11 enhanced the recruitment of Atg8 and 9, but not Atg19, to the PAS

Given the linear relationship between protein amount and fluorescence intensity, we investigated the change in the local concentrations of Atg8 and 9 to test our hypothesis that higher amounts of Atg11 enhanced the recruitment of these proteins to the PAS. To measure the local protein concentration at the PAS, a small circle was drawn around the PAS dot. Another circle with the same size drawn at an adjacent cytosolic area was used as background and subtracted (Figure 3.5 A). The difference between these two was recorded as the PAS intensity.

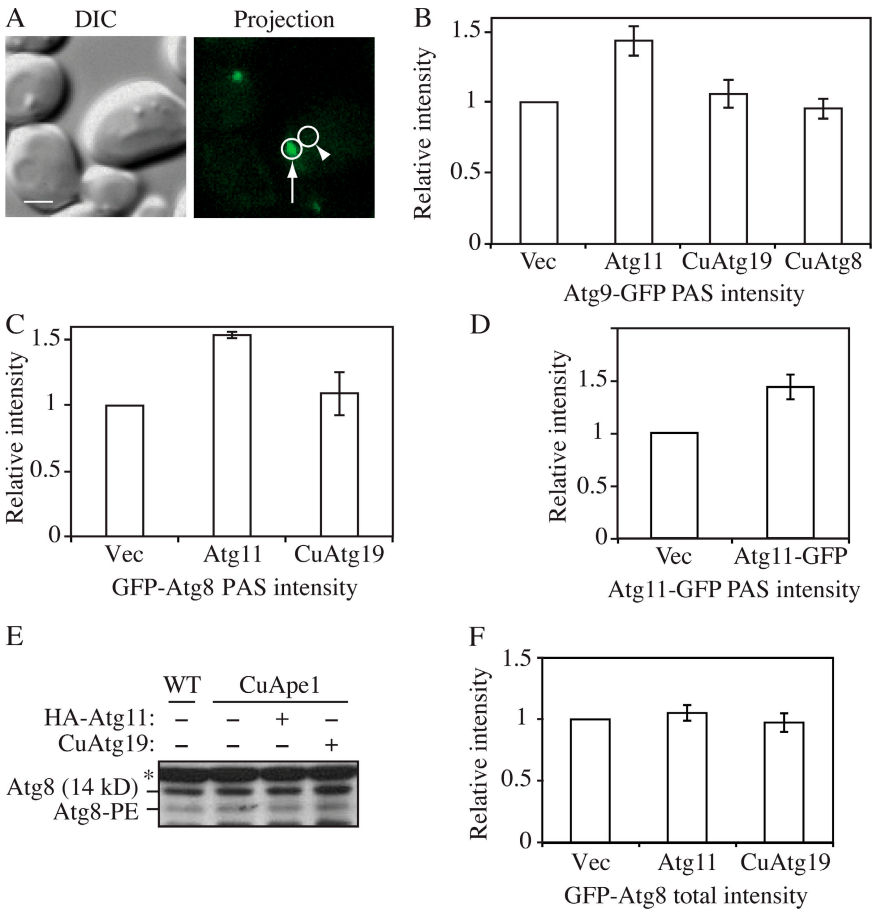

Figure 3.5 Effect of Atg11 overexpression on the PAS intensity of Atg8 and Atg9. (A) On the 2D projection image, circles were drawn around the PAS (arrow) and the adjacent cytosolic region (arrowhead) as background. The difference between these two regions was recorded as the PAS intensity. Bar, 2μm. (B) The CuApe1 Atg9-GFP strain (JGY072) expressing pHA-Atg11, pCuAtg8, or pCuAtg19 was cultured in SMD medium and examined by microscopy (n = 80). (C) CuApe1 *atg8*Δ cells (JGY071) harboring pGFP-Atg8 together with pHA-Atg11, pCuAtg19, or empty vector were cultured in SMD medium and examined by microscopy (n = 80). (D) Increase of Atg11-GFP intensity at the PAS in Atg11 overexpression cells. The CuApe1 Atg11-GFP strain (JGY087) transformed with empty vector or pAtg11-GFP was grown in SMD media and the PAS intensity of Atg11-GFP was analyzed by microscopy (n = 80). (E) Overexpression of Ape1 or Atg11 did not induce lipidation of Atg8. Wild-type (SEY6210) cells or the CuApe1 strain (JGY069) expressing pHA-Atg11 or pCuAtg19 were cultured in nutrient-rich medium, and a protein extract was resolved by SDS-PAGE and examined by Western blot with anti-Atg8 antiserum. The asterisk marks a nonspecific band. (F) The total GFP-Atg8 signal was not affect by the increase of Atg11. The same strains as in C were used, but instead of measuring the signal at the PAS, the GFP-Atg8 intensity of the whole cell was measured (n = 60). The relative intensity of cells expressing empty vector was set to 1 as reference, and error bars indicate the SEM of three independent experiments.

Atg9-GFP cells with overexpressed Atg11 were subjected to fluorescence microscopy. The PAS intensity of Atg9-GFP increased by 45% when Atg11 was overexpressed (Figure 3.5 B). However, when Atg8 or 19 were overexpressed, the intensity of Atg9-GFP was still the same as in the control strain expressing the empty vector (Figure 3.5 B). Because the intensity of the fluorescent signal indicated the amount of the corresponding protein, this result suggested that in the strain overexpressing Atg11, more Atg9 molecules were located at the PAS. This observation agrees with our previous data, which show Atg9 restricted at the PAS in the presence of dominant-negative levels of Atg11 [65]. Thus, the elevated Atg9 at the PAS in the present analysis may have resulted from an enhanced movement of Atg9 from the peripheral pool to the PAS. We also used this approach to examine the intensity of GFP-Atg8. We found that overexpression of Atg11 increased the localized amount of Atg8 at the PAS by ~50%, whereas Atg19 overexpression had essentially no effect (Figure 3.5 C). In contrast, the PAS intensity of Atg19-GFP was not significantly changed when Atg11 was overexpressed (unpublished data), which suggests that an extra amount of specific cargo receptor may not be critical at this stage.

The amount of Atg11 at the PAS when overexpressed was also evaluated. In previous experiments (Figure 3.1), chromosomal Atg11 plus another copy on a CEN plasmid were considered to provide modulated overexpression. Therefore, a chromosome-tagged Atg11-GFP strain (JGY087) expressing a pAtg11-GFP (CEN) plasmid was used here. Analyzed by our microscopy assay, the PAS intensity of Atg11 in the strain expressing pAtg11-GFP (CEN) was ~50% higher than the same strain

expressing an empty vector (Figure 3.5 D). Thus, there was a clear correlation between Atg11 PAS intensity and that of both Atg8 and 9.

We also tested whether Atg11 overexpression changed the expression level or lipidation status of Atg8. We found that the amount of Atg8 and Atg8–PE remained unchanged either when Atg11 or 19 was expressed alone or when both proteins were expressed together (Figure 3.5 E). This result was supported by our microscopy assay, which is more sensitive. The total GFP-Atg8 signal of cells expressing Atg11 did not show any substantial difference from cells expressing an empty vector or Atg19 (Figure 3.5 F). This suggested that Atg11 only changed the distribution pattern of Atg8 and not its expression or stability. Thus, it was clear that the recruitment of Atg8 and 9 to the PAS was substantially upregulated when Atg11 was overexpressed. Considering the role of the former two proteins in sequestering vesicle formation, higher levels of Atg8 and 9 at the PAS may provide the capacity to form a larger number of vesicles, which could explain the EM data (Figure 3.2) and the enhanced capacity for import of overexpressed prApe1 even under growing conditions.

Stoichiometries of Atg proteins at the PAS

After establishing a method to measure local protein amount, we extended our analysis to additional components involved in either the Cvt or autophagy pathway. Altogether, we analyzed Atg1, 8, 9, 11, 16, 17, and 19. We chromosomally fused the GFP tag at either the N (Atg8) or C (others) terminus and used the corresponding strains to investigate the respective stoichiometries.

Table 3.1 Local and global amount of Atg proteins in growing conditions

Protein	Number of molecules/cell (database)[a]	Number of molecules/cell (present study) (mean ± SEM; n = 80)	Number of molecules at the PAS (mean ± SEM; n = 100)
Atg1	1070	1780 ± 144	49 ± 7
Atg8	2010	2244 ± 156[b]	116 ± 7
Atg9	ND	906 ± 88	70 ± 3
Atg11	ND	1162 ± 121	40 ± 2
Atg16	573	421 ± 31	34 ± 2
Atg17	358	469 ± 41	56 ± 6
Atg19	1250	1290 ± 137	110 ± 4

ND, not determined;
[a], [139].
[b], n = 200

We first fit the whole cell fluorescence intensity of these strains into the standard curve established previously. The total fluorescence intensity per cell in each strain was measured in nutrient-rich conditions, and then for each Atg protein the molecular number per cell was calculated via the standard curve. The expression levels of GFP-Atg proteins range from ~400 to 2,000 molecules per cell (Table 3.1). Recently, a large-scale analysis of protein expression was carried out in yeast [139]. Comparison between our fluorescence-based molecular number and the previous Western-based number showed a good correlation between these two groups of data (Table 3.1), which again confirmed the correlation between the fluorescent signal and the protein concentration.

Next, we examined the PAS intensity of these GFP-tagged Atg proteins in growing conditions. For all the Atg proteins we tested, only a small portion of the protein pool was located at the PAS. Atg8 had the highest concentration at the PAS, whereas Atg16 had

the lowest (Table 3.1 and Figure 3.6 A). For Atg1, 8, 11, 16, and 17, the non-PAS population was evenly diffuse in the cytosol, whereas the integral membrane protein Atg9 showed multiple punctate non-PAS structures as reported previously [60].

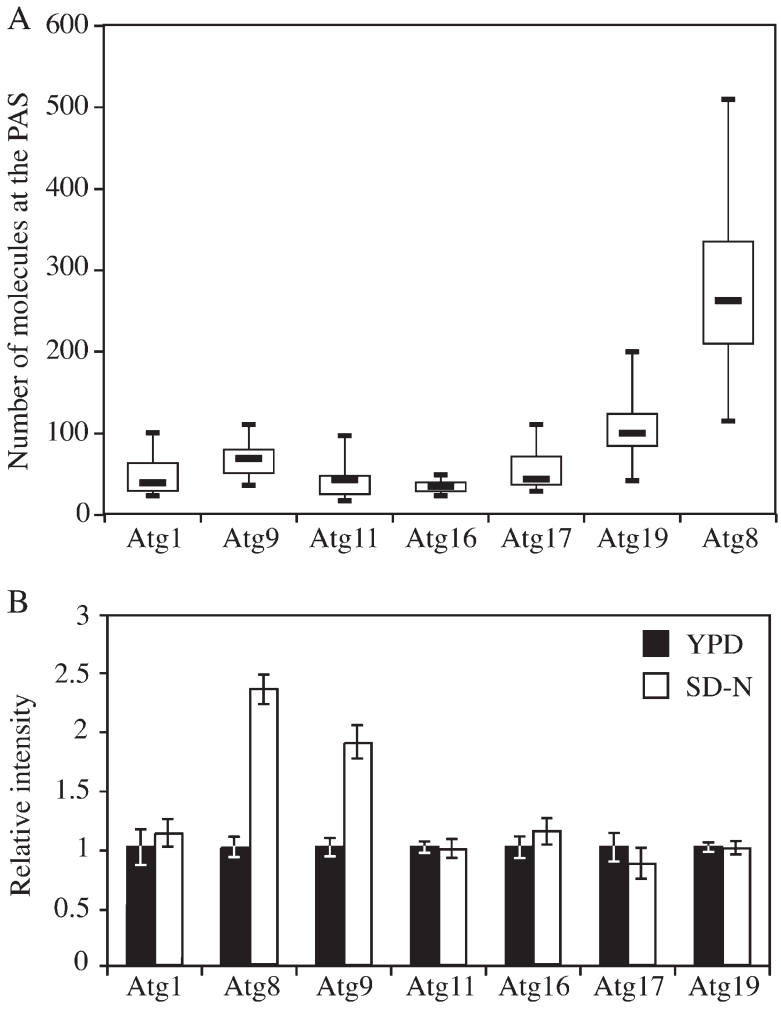

Figure 3.6 Amount of Atg proteins at the PAS during either the Cvt pathway or autophagy. (A) Boxplot of the amount of Atg proteins at the PAS in growing conditions (except Atg8 in starvation conditions). The local protein amount was calculated as described in Materials and methods and graphed into a boxplot (n = 100). (B) Difference in the PAS intensity between the Cvt pathway and autophagy. GFP-tagged strains were cultured in nutrient-rich conditions (YPD medium; n = 100) and then shifted to starvation conditions (SD-N medium; n = 60) for 2 h. Microscopy was done before and after starvation. Error bars indicate the SEM of three independent experiments.

The ability to rapidly switch from the Cvt pathway to bulk autophagy is necessary for yeast cells to respond to the stress of starvation. The Atg1 complex is critical for the switch between these two pathways [68], but it is still unclear as to how this transition occurs. In addition, even for those Atg proteins required for both autophagy and the Cvt pathway, their quantitative behavior at the PAS is unknown. To understand more about the mechanism involved in converting cells from the vegetative Cvt pathway to nonspecific autophagy, we measured the PAS fluorescence intensity of GFP-tagged Atg proteins in either growing or starvation conditions (Figure 3.6 B). In Atg1-, Atg11-, Atg16-, Atg17-, and Atg19-GFP strains, the PAS intensity did not change after cells were starved for 2 h. In contrast, the PAS intensity of GFP-Atg8 increased by 130% and that of Atg9 by 90%. Similar to the change of Atg8 and Atg9 PAS intensity seen in Atg11 overexpression conditions, an increase in the amount of Atg8 and Atg9 at the PAS correlated with the delivery capacity of either the Cvt pathway or nonspecific autophagy.

Kinetics of Atg proteins at the PAS

Most Atg proteins involved in vesicle formation are primarily detected at the PAS [52]. Our current understanding is that the PAS plays a role in the initiation and expansion of the phagophore by concentrating Atg proteins to this confined small region. Thus, this structure can be considered as a hybrid of autophagy machinery and forming vesicles. Most Atg proteins recruited to the forming vesicle will dissociate from this structure prior to or upon completion of the vesicle. However, the relationship between the PAS and the forming vesicle is still not clear. Therefore, we decided to investigate the kinetics of Atg proteins at the PAS during the process of autophagy.

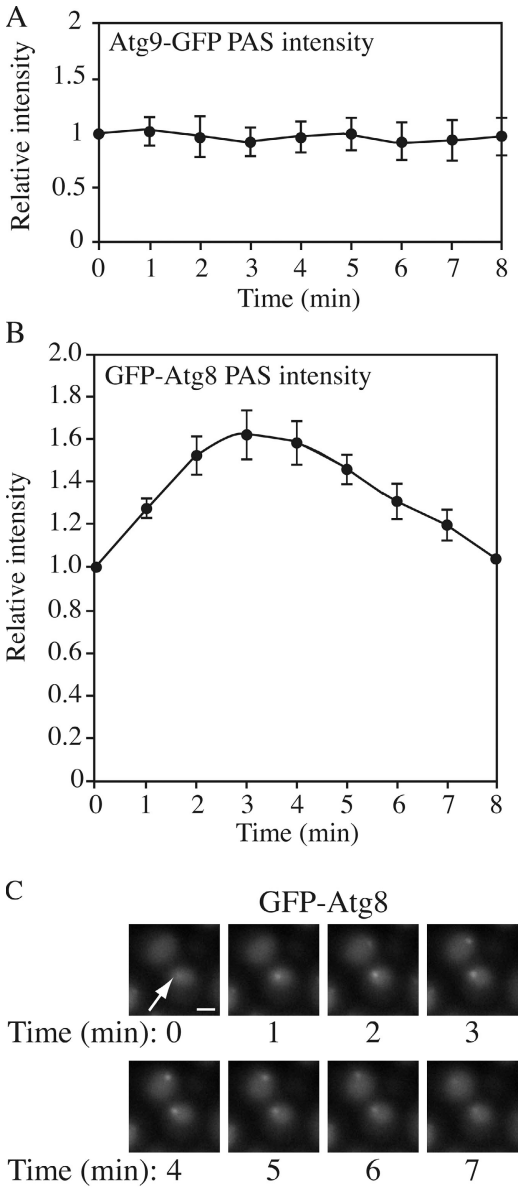

Figure 3.7 Kinetics of Atg proteins at the PAS during autophagy. GFP-tagged strains were starved for 2 h and analyzed by microscopy. (A) For Atg9-GFP, the PAS intensity remained as a relative constant for 30 min, but only nine time-points are shown. Fluorescence intensity at time 0 was normalized to 1 (n = 9). Essentially the same results were seen for Atg1-, Atg11-, Atg16-, Atg17-, and Atg19-GFP. (B) For GFP-Atg8, the PAS intensity changed over time. The time point at which the punctate structure could first be seen was set as time 0 and fluorescence intensity at this time point was set to 1 (n = 11). In (A) and (B), all data points came from three independent experiments and error bars indicate the SEM. (C) Representative images of GFP-Atg8 showing the change of PAS (arrow) intensity. Bar, 2μm.

To address this issue, we examined the amount of Atg proteins at the PAS over time during autophagy. Cells expressing different GFP-tagged Atg proteins were incubated in SD-N medium for 2 h to induce autophagy and subjected to microscopy. Among the Atg proteins we tested (Atg1, 8, 9, 11, 16, 17, and 19), all of them except Atg8 showed a relatively constant PAS intensity over a 30-min time course (Figure 3.7 A). Atg8, however, showed a periodic change of PAS intensity (Figure 3.7, B and C). This observation agrees with recent published results on Atg8 kinetics at the PAS [75]. After 2 h in starvation conditions, a substantial amount of free GFP had accumulated in the vacuole so that the vacuolar region was much brighter than the cytosolic region when viewed by fluorescence microscopy (Figure 3.7 C); however, we could detect a GFP-Atg8 punctate structure germinating adjacent to the vacuole. The GFP-Atg8 dot became brighter over 4-5 min (Figure 3.7 B). After reaching its peak intensity, the dot became dimmer and finally disappeared. With an interval of 0-4 min, another cycle started and each cycle lasted for ~7-9 min (Figure 3.7 C). In some cells, a new cycle started before the initial cycle was completely finished, so that we saw two GFP-Atg8 dots in one cell at a particular time point.

Discussion

In this study, we used the strategy established by the Pollard lab to determine protein concentration by fluorescence microscopy and applied this method to the analysis of autophagy. This approach provided information that is inaccessible by traditional methods. In this paper, we succeeded in using fluorescence microscopy to show that overexpression of Atg11 increased the amount of Atg8 and 9 at the PAS, which enhanced vesicle formation, and to study the stoichiometry of Atg proteins under different conditions.

Several lines of evidence have suggested that a proper control of the amounts of Atg8 and 9, or the kinetics of their transport, is essential for nonspecific autophagy [64,79]. Our observation that an increased amount of Atg8 and 9 at the PAS led to the formation of more Cvt vesicles in growing conditions suggested that the quantity control of these two proteins is also critical for specific autophagy, and represents a nontranscriptional means of regulation. For Atg9, although we did not directly quantify its anterograde flux, the increased Atg9 PAS amount at steady state may reflect an increased amount of lipid transported from the membrane source to the vesicle formation site, which is necessary for synthesizing more vesicles. When Atg11 overexpression exceeds a certain limit, such as *CUP1*-driven expression [65], the balance between anterograde and retrograde movement of Atg9 is completely disrupted. This results in a dominant-negative phenotype. Atg8 is hypothesized to be a scaffold protein that supports the expansion of the phagophore membrane. Therefore more Atg8 recruited to the PAS may facilitate the formation of a bigger scaffold or allow the assembly of the same-sized scaffold in a more efficient manner. Interestingly, in starvation conditions an attenuated

amount of Atg8 reduced the size of the autophagosome and thus limited the magnitude of nonspecific autophagy [79]. However, in our assay of specific autophagy, the increased amount of Atg8 affected primarily the number of vesicles instead of the size. One explanation is that in specific autophagy the cargo determines the size of the vesicle. Given the unchanged concentration of the cargo receptor Atg19 at the PAS, it is possible that cargo recruitment is not significantly increased by Atg11 overexpression.

Atg11 and 17 are believed to play critical roles at the organization center during either the Cvt pathway or autophagy, respectively, but neither is required for the other pathway [35,82,88,89]. However, our data showed that the amounts of these two proteins at the PAS remained constant during either the Cvt pathway or nonspecific autophagy. This observation suggested that these two proteins do not leave the PAS structure even when their functionality is not required. This stable PAS localization of Atg11 and 17 may contribute to the cell's ability to quickly switch between specific and nonspecific autophagy. Upon environmental change, such as a shift in the nutrient conditions, the Cvt or autophagy machinery is physically ready at the functional site, the PAS, and rapid changes in phosphorylation status and/or protein-protein interaction can be done within a relatively short period of time to complete the switch from one pathway to another.

In vesicle-trafficking pathways in eukaryotic cells, a coat protein complex is required to initiate the budding process. However, coat proteins in the autophagy pathway have not been clearly identified. Among the known Atg proteins, the Atg12–Atg5-Atg16 complex has been suggested as a candidate for coatomer-type proteins that cover the forming autophagosomes or Cvt vesicles and dissociate from the completed vesicle [115], although direct evidence in support of this hypothesis is missing. Our analysis of Atg

protein stoichiometry casts some doubt upon this hypothesis. In the microscopy conditions we used, the PAS signal of Atg5- and Atg12-GFP could hardly be detected. The GFP-Atg16 signal was also weak compared to other Atg proteins. Translated into a molecular number, the amount of Atg16-GFP at the PAS is 34 ± 2 molecules. A recent study showed that the mean radius of an autophagosome was ~162 nm [79]. Assuming that all the Atg16-GFP molecules at the PAS are distributed evenly on the outer surface of a forming autophagosome, then 34 molecules per PAS can be translated into one Atg16-GFP molecule per 9.7×10^3 nm^2 of surface area. This calculation suggests the amount of Atg16 at the PAS is too low to allow the Atg12–Atg5-Atg16 complexes to cover the entire surface of an autophagosome. It is possible that the main function of the Atg12–Atg5-Atg16 complex is to facilitate the formation of Atg8–PE and recruit it to the PAS [87] rather than to act as a conventional coatomer complex.

The microscopy method described in this paper makes it possible to quantitatively elucidate the kinetics of Atg proteins during the progression of autophagy. Interestingly, our real-time data on Atg8 fluorescence intensity changes suggested a possibility to explain the function of Atg8 in a temporal manner. Combined with our previous understanding of Atg8, one cycle of Atg8 fluorescence at the PAS can be translated into the formation of one autophagosome [79]. That is, the number of GFP-Atg8 signal peaks can indicate the number of autophagosomes formed. Compared with conventional methods, which rely on EM to count the number of autophagic bodies accumulated in the vacuole in a *pep4*Δ background, this new method can measure the autophagosome number in a real-time manner. Furthermore, this approach may even be more sensitive

when the smaller size of abnormal autophagosomes makes the conventional method problematic.

Materials and methods

Media and growth conditions

Yeast cells were grown in YPD (rich [1% yeast extract, 2% peptone, and 2% glucose]) or SMD (synthetic minimal [0.67% yeast nitrogen base, 2% glucose, and auxotrophic amino acids and vitamins as needed]) media. For starvation condition, SD-N medium (0.17% yeast nitrogen base, without ammonium sulfate or amino acids, and 2% glucose) was used.

Plasmids

pGFP-Atg11(414) and plasmids lacking the Atg11 CC domains, pCuAtg8(416), pHA-Atg11(313), pGFP-Atg11(414), pGFP-Atg8(416), and pCuGFP-Atg8(416) have been described previously [35,82,120,143]. The plasmid pGFP-Atg11(404) was made by cloning the GFP-Atg11 fragment together with the endogenous promoter of *ATG11* from pGFP-Atg11(416) [65] into pRS404. Plasmid pCuApe1(405) was made by cloning the CuApe1 fragment from pCuApe1(414) [144] into pRS405. For Atg19 overexpression, the ORF of *ATG19* was amplified from yeast genomic DNA, digested with XmaI-XhoI, and cloned into pCu(414) [145] to generate the pCuAtg19(414) plasmid. To make the pGEX-GST-GFP construct for protein purification, the ORF of GFP was amplified from pKT128 [146] by PCR. The PCR product was digested with EcoRI and XhoI and cloned into the pGEX-4T-1 plasmid (GE Healthcare).

Strains

The yeast strains used in this study are listed in Table 3.2. The prApe1 overexpression strain (JGY069) was made by digesting the pCuApe1(405) plasmid with AflII and integrating the fragment into the genome of strain SEY6210 at the *LEU2* locus. Tagging of genes by integration of GFP at the corresponding chromosomal loci was performed by a PCR-based procedure [142]. The functionality of each tagged protein was confirmed by examining prApe1 maturation. For gene disruption, the entire coding region was replaced with the *Escherichia coli kan*^{r}, *S. cerevisiae TRP1*, *S. pombe HIS*5, *Kluyveromyces lactis URA3, Saccharomyces. kluyveri HIS3*, or *S. cerevisiae TRP1*, *LEU2*, or *URA3* gene using PCR primers containing ~40 bases of identity to the regions flanking the open reading frame. Western blotting, PCR, or both verified putative gene knockout and tagged strains. The GFP-Atg11 strain (JGY075) was constructed by integrating pGFP-Atg11(404) into the genome of the *atg11*Δ mutant [82].

Protein purification

To express GST-GFP, *E. coli* strain BL-21 harboring pGEX-GST-GFP was cultured to OD_{600} = 0.6 at 37°C and induced with 1 mM IPTG at 18°C for 12 h. The protein was purified on glutathione-Sepharose beads (GE Healthcare). The purification was confirmed by Coomassie Blue staining and Western blotting. The concentration of the purified protein was measured by the bicinchoninic acid assay.

Western blot and quantitative immunoblotting

Protein samples for immunoblotting were extracted by trichloroacetic acid precipitation, and Western blotting was performed as described previously [88]. For quantitative

immunoblotting, purified GST-GFP was used as the standard sample with known concentration (in mol). The cell lysates corresponding to a certain amount of GFP-tagged cells (based on OD_{600}) were loaded on the same gel with the standard protein and detected with anti-YFP antibody (Clontech Laboratories, Inc.), which recognizes GFP with a high specificity. The intensity of the band was quantified with ImageJ software (National Institute of Health), and the concentrations of GFP-tagged proteins (mol per OD_{600}) were calculated. Then the numbers in mol per OD_{600} were converted into molecules per cell by multiplying by Avogadro's number and dividing by the number of cells per OD_{600}. In *PEP4* GFP-Atg8 strains, we quantified both the GFP-Atg8 and free GFP bands and calculated the sum. However, in the *pep4*Δ GFP-Atg8 strains, no free GFP band could be detected and only the GFP-Atg8 band was quantified.

Fluorescence microscopy

Cells were cultured in YPD or SMD without auxotrophic amino acids to mid-log phase. For experiments under growing conditions, cells were pelleted and resuspended in fresh SMD without vitamins. For starvation experiments, cells were shifted to SD-N, incubated for 2 h and pelleted, then resuspended in SD-N. The samples were then examined with a microscope (DeltaVision Spectris; Applied Precision, LLC) and pictures were captured with a camera (CoolSnap HQ; Photometrics). For each microscopy image at a certain region, 12 Z-section images were collected and stacked into one 2D image by sum projection. The interval between each Z-section was 0.5 μm and the depth of each stack was 5.5 μm, which is the approximate diameter of a normal yeast cell. Projections were analyzed and quantified using softWoRx® software (Applied Precision, LLC).

Electron microscopy

Transmission electron microscopy was performed as described previously [75]. Images of vacuoles with visible vesicles were collected. The number and area of vesicles with clear membrane boundary was measured. Then the area was converted into diameter. The preparation of samples for IEM was done according to the procedures described previously [29] with slight modification. The Cvt body number was quantified as for TEM images. The size of the Cvt body was defined as the average of the long and short axes of the Cvt body.

Acknowledgments

We thank Dr. Noriko Nagata (Japan Women's University) for the use of the electron microscopy facilities and Dr. Tom Pollard for helpful advice. . This work was supported by National Institutes of Health Public Health Service grant GM53396 to D.J. Klionsky.

Abbreviations

Ape1, aminopeptidase I; Atg, autophagy-related; CC, coiled coil; CEN, centromeric; Cvt, cytoplasm-to-vacuole targeting; IEM, immuno-EM; PAS, phagophore assembly site; prApe1, precursor Ape1; TEM, transmission EM.

Table 3.2 Yeast strains used in this study

Name	Genotype	Reference
CWY241	SEY6210 *ATG17-GFP::HIS3*	[88]
JGY018	SEY6210 *ATG19-GFP::TRP1*	This study
JGY053	TN124 *atg8Δ::KAN* P_{ATG8}*GFP-ATG8::URA3 atg5Δ::TRP1*	This study
JGY054	TN124 *atg8Δ::KAN* P_{ATG8}*GFP-ATG8::URA3 atg2Δ::TRP1*	This study
JGY056	TN124 *atg8Δ::KAN* P_{ATG3}*GFP-ATG8::URA3 pep4Δ::TRP1*	This study
JGY057	TN124 *atg8Δ::KAN* $P_{VPS30\text{-}ATG18}$*GFP-ATG8::URA3 pep4Δ::TRP1*	This study
JGY058	TN124 *atg8Δ::KAN* P_{ATG27}*GFP-ATG8::URA3 pep4Δ::TRP1*	This study
JGY059	SEY6210 *MLC2-GFP::TRP1*	This study
JGY060	SEY6210 *CDC12-GFP::TRP1*	This study
JGY069	SEY6210 P_{CUP1}*APE1::LEU2*	This study
JGY070	JGY069 *ATG19-GFP::KAN*	This study
JGY071	JGY069 *atg8Δ::KAN*	This study
JGY072	JGY069 *ATG9-GFP::KAN*	This study
JGY075	SEY6210 *atg11Δ::HIS3 GFP-ATG11::TRP1*	This study
JGY087	JGY069 *Atg11-GFP::KAN*	This study
JGY088	JGY069 *pep4Δ:: KAN*	This study
JGY089	JGY088 *vps4Δ::ble*	This study
KTY97	SEY6210 *ATG9-GFP::TRP1*	[79]
KTY148	SEY6210 *ATG16-GFP::KAN*	[79]

PSY101	SEY6210 *ATG11-GFP::HIS3*	[65]
PSY143	SEY6210 *ATG1-GFP::HIS3*	[62]
SEY6210	*MATa ura3-52 leu2-3,112 his3-Δ200 trp1-Δ901 lys2-801 suc2-Δ9 mel GAL*	[147]
TN124	*MATa leu2-3,112 trp1 ura3-52 pho8::pho8Δ60 pho13::LEU2*	[148]
YZX246	TN124 *atg8Δ::KAN* $P_{VPS30\text{-}ATG18}$*GFP-ATG8::URA3 TRP1*	[79]
YZX247	TN124 *atg8Δ::KAN* P_{ATG8}*GFP-ATG8::URA3 TRP1*	[79]
YZX251	TN124 *atg8Δ::KAN* P_{ATG27}*GFP-ATG8::URA3 TRP1*	[79]
YZX254	TN124 *atg8Δ::KAN* P_{ATG8}*GFP-ATG8::URA3 pep4Δ::TRP1*	[79]
YZX257	TN124 *atg8Δ::KAN* P_{ATG3}*GFP-ATG8::URA3 TRP1*	[79]

P, promoter

Addendum: Quantitative regulation of vesicle formation in yeast nonspecific autophagy

Abstract

In eukaryotic cells, autophagy is a degradative pathway necessary for the turnover of different macromolecules. In yeast, this pathway also mediates the specific transport of a vacuolar hydrolase zymogen, precursor aminopeptidase (prApe1), from the cytoplasm to the vacuole. Autophagy is under precise regulation, not only qualitatively but also quantitatively, especially in the steps involved in the vesicle formation process. We have recently used a fluorescence microscopy-based method to study the stoichiometry of autophagy-related (Atg) proteins during different conditions. This analysis shows that increased expression of Atg11 in the cytoplasm-to-vacuole targeting (Cvt) pathway increases the amount of this protein localized at the phagophore assembly site (PAS). In turn, under nutrient-rich conditions, the increased level of Atg11 causes the recruitment of higher than normal levels of Atg8 and Atg9 to the PAS, resulting in the formation of more Cvt vesicles, whereas the vesicle size is not affected. Combined with results from previous studies in starvation conditions, in this addendum we discuss the possible role of Atg8 and Atg9 in quantitatively regulating the vesicle formation process.

In biological science, what can stoichiometry tell us? The best example to answer this question may be seen with Chargaff's rules "A=T/G=C" which was known many years before the identification of the structure of the DNA double helix. At that time, even without the help of modern physics, this formula gave scientists a useful hint to "imagine" the gorgeous structural model of DNA within their mind. As time goes by, the value of stoichiometry data has not diminished. Nowadays, it refers to not only structural information but also to the molecular level of biological processes, even in a real-time manner. Here we used quantitative fluorescence microscopy to study the stoichiometry of autophagy-related (Atg) proteins, which can help us understand the mechanism of quantitative regulation in autophagy.

Autophagosome formation is the key step of autophagy in eukaryotic organisms. It begins with a crescent-like membrane structure, called the phagophore, and this structure eventually expands into a double-membrane autophagosome. This process requires the concerted action of multiple Atg proteins in modulating what substrate or how much of it should be transported to the vacuole/lysosome. According to our current model in *Saccharomyces cerevisiae*, the phagophore assembly site (PAS) is the organization center for vesicle formation [54]. In the last ten years, the molecular components of this structure and the temporal order of their recruitment to the PAS have been elucidated [52,53,89]. However, what deserves more attention is the quantitative control of autophagosome formation, such as controlling the size or number of vesicles to be formed.

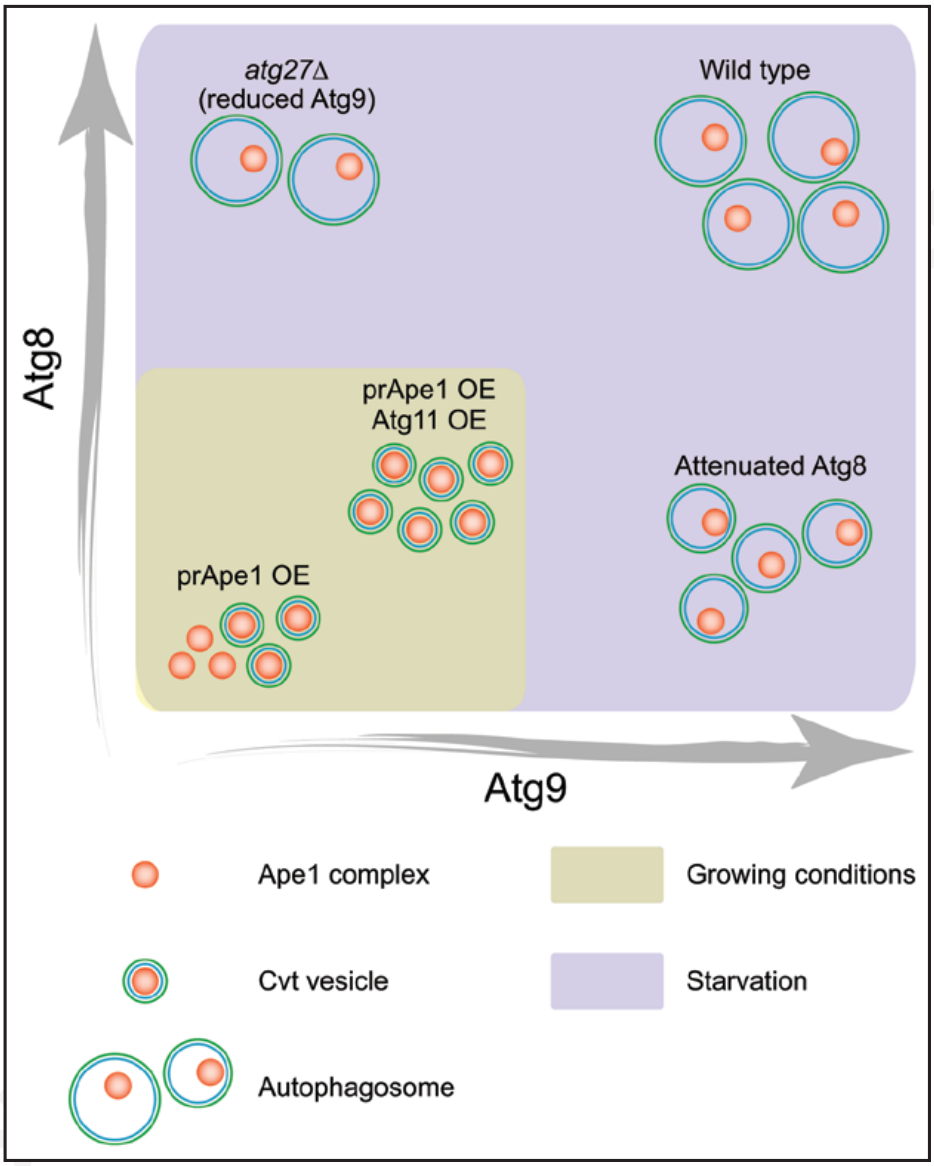

Figure 3.8 Schematic relationship between the Atg8 and Atg9 PAS population and vesicle formation. In growing conditions, the Cvt pathway can be saturated by overexpressing (OE) of prApe1. Overexpression of Atg11 enhances the PAS population of Atg8 and Atg9, resulting in the formation of more Cvt vesicles of the same size. In starved cells, the amount of Atg8 and Atg9 at the PAS increases substantially. The autophagosomes are bigger in volume than the Cvt vesicles and contain other cytosolic components besides prApe1. The absence of Atg27 diminishes Atg9 localization at the PAS, and fewer autophagosomes of the normal size are formed. On the other hand, attenuated Atg8 expression level in starvation conditions leads to the formation of smaller autophagosomes but has little effect on their number. Vesicle size and the amount of Atg8 and Atg9 are not in scale.

In nonspecific autophagy, several lines of evidence independently show the relationship between the amount of Atg8 and Atg9, and the size and/or number of autophagosomes. Atg9 is a trans-membrane protein, which shuttles between the PAS and several peripheral membrane structures [58,60]. Atg8 is a small protein that becomes membrane associated via a ubiquitination-like process that conjugates it to phosphatidylethanolamine; Atg8 is one of only two Atg proteins that remains associated with the completed autophagosome, and it is generally used as an autophagosome marker [56,80]. During starvation, the *atg27*Δ mutant shows diminished anterograde movement of Atg9 (from peripheral sites to the PAS) and fewer autophagosomes with normal size are formed [64]. On the other hand, an attenuated amount of Atg8 alone reduces the size of the autophagosomes but does not affect the number of vesicles [79]. We speculate that during bulk autophagy Atg8 probably functions as a component of a scaffold structure supporting the expansion of the phagophore membrane, and the level of Atg8 mainly decides the vesicle size. In contrast, the Atg9 cycle (i.e., movement between peripheral sites and the PAS) may represent the supply of potential membrane sources; so reduced Atg9 anterograde movement only limits the number of autophagosomes.

In specific types of autophagy, do Atg8 and Atg9 also contribute to vesicle formation in a quantitative manner? In yeast cells, the best-characterized example of specific autophagy is the Cvt pathway, which occurs in vegetative conditions [25,30]. Packaged within Cvt vesicles, prApe1 is delivered to the vacuole and processed into its mature form (mApe1). In a previous study, we reported that overexpressed prApe1 can overwhelm the Cvt pathway, resulting in the accumulation of prApe1 [30]. This observation indicates a limited capacity for the Cvt pathway. Interestingly, we found a

relationship between the amount of Atg11 and Cvt pathway capacity. Atg11 is a critical factor in specific autophagy that directs other Atg proteins to the PAS, but it is not necessary for nonspecific autophagy [34,82]. An increase in Atg11 expression allows the complete maturation of overexpressed prApe1. To our knowledge, this is the first example that the amount of an Atg protein correlates with the capacity of specific autophagy.

To investigate the mechanism of this phenomenon, we utilized an approach relying on fluorescence microscopy to quantitatively measure protein amounts *in vivo* [134]. We then examined the protein concentrations of Atg11 and other proteins at the PAS under various conditions. This method shows that Atg8 and Atg9 are recruited to the PAS in an Atg11-dosage dependent manner. Overexpressed Atg11 results in a bigger population of Atg8 and Atg9 at the PAS. Therefore, the amount of Atg8 and Atg9 is also involved in determining the capacity of specific autophagy. To increase the magnitude of vesicle transport, there are two possibilities: increasing the size of vesicles or increasing the number of vesicles. Electron microscopy analysis shows that in prApe1 overexpression cells, enhanced Atg11 expression significantly increases the number of Cvt vesicles but has little effect on their size. Accordingly, we can dissect the different roles of Atg8 and Atg9 in quantitative regulation of vesicle formation. In both specific and nonspecific autophagy, Atg9 flux from peripheral membrane structures to the PAS may correspond to the supply of membrane to the vesicle formation site. A higher amount of Atg9 at the PAS may provide more membrane in total, but this may not necessarily correspond to a bigger vesicle. Atg8, on the other hand, may mediate the expansion of the phagophore membrane in both specific and nonspecific autophagy

[79,130]. The expansion of the phagophore is thought to occur by membrane addition. *In vitro* assays indicate the possible role of Atg8 in membrane tethering and hemifusion [130]. This means that with more Atg8 recruited to the PAS the phagophore may expand in a more efficient manner. But Atg8 function also varies in the two types of autophagy. In specific autophagy, the membrane sac expands exclusively along (i.e., tightly apposed to) the cargo, the Cvt complex composed primarily of prApe1 and its receptor Atg19 [32]. The size of the Cvt vesicle may be determined only by the size of the Cvt complex. This hypothesis is supported by the observation of bigger Cvt vesicles when prApe1 is expressed from a multi-copy (2μ) plasmid [29], but not in Atg11 overexpression cells. Thus, more Atg8 at the PAS leads to rapid expansion of the phagophore and the formation of more vesicles. In contrast, during nonspecific autophagy, the expanding phagophore is enwrapping a portion of cytosol randomly and there is not a "rigid" mechanism of support from the concave side. The distribution of Atg8 on both side of the phagophore may provide a scaffold-like structure and impose curvature upon the expanding membrane. In this case, the amount of Atg8 can affect the size of the autophagosomes [79].

We also investigated whether the Atg19 amount is critical to allow efficient transport of overexpressed prApe1. In addition to being a prApe1 receptor, Atg19 also interacts with Atg8 [34], acting as an adaptor protein to bridge the cargo and Atg8-embedded membrane structure. The Atg19-Atg8 complex is thought to be the anchor that forces the membrane to expand exclusively around the Cvt complex. In terms of stoichiometry, prApe1 overexpression (bigger Cvt vesicles) does not increase the amount of Atg19 at the PAS (unpublished data). Similarly, although Atg11 interacts with Atg19

and directs it to the PAS [34], Atg11 overexpression (more Cvt vesicles) has no clear effect on the Atg19 amount at the PAS. Therefore, it is possible that there is no defined ratio of Atg19 to prApe1 and a relatively small amount of Atg19 is enough to recognize and allow efficient import of the Ape1 complex over a fairly wide range of prApe1 levels. It may also be worth noting that a large increase in the amount of prApe1 has a relatively small affect on the surface area of the Ape1 complex (which increases by the square of the radius, versus the volume, which increases by the cube of the radius) so that a substantial change in the level of Atg19 may not be necessary to accommodate efficient import of a higher level of prApe1.

The application of this quantitative microscopy method could be huge, but the sensitivity and accuracy of the microscope is still a limiting factor. For some GFP-tagged Atg proteins such as Atg5-GFP, the fluorescence intensity is not high enough to be quantified. In terms of real-time quantification, the fastest camera still cannot catch the rapid movement of Atg9. On the other hand, although we can measure the molecular number of several Atg proteins at the PAS, the physiological meaning of these numbers is not fully understood without knowing more about the mechanistic function of these proteins. In the near future, continuing functional analysis of Atg proteins will improve our understanding of the stoichiometry data and vise versa.

Chapter IV. Post-Golgi Sec proteins are required for autophagy in *Saccharomyces cerevisiae*

Abstract

In eukaryotic cells, autophagy mediates the degradation of cytosolic contents in response to environmental change. Genetic analyses in fungi have identified over 30 autophagy-related (*ATG*) genes and provide substantial insight into the molecular mechanism of this process. However, one essential issue that has not been resolved is the origin of the lipids that form the autophagosome, the sequestering vesicle that is critical for autophagy. Here, we report that two post-Golgi proteins, Sec2 and Sec4, are required for autophagy. Sec4 is a Rab family GTPase, and Sec2 is its guanine nucleotide exchange factor. In *sec2* and *sec4* conditional mutant yeast, the anterograde movement of Atg9, a proposed membrane carrier, is impaired during starvation conditions. Similarly, in the *sec2* mutant, Atg8 is inefficiently recruited to the phagophore assembly site, which is involved in autophagosome biogenesis, resulting in the generation of fewer autophagosomes. We propose that following autophagy induction the function of Sec2 and Sec4 are diverted to direct membrane flow to autophagosome formation.

Introduction

In eukaryotic cells, dynamic vesicle trafficking between the membrane-bounded organelles of the secretory pathway makes it possible for them to carry out their function, while a high degree of regulation allows these compartments to maintain their normal and discrete morphology. In contrast to membrane trafficking in the secretory pathway where the cargo-containing vesicle is formed from a preexisting organelle by budding, vesicle formation in autophagy is considered to be *de novo*; this is critical to autophagic function, which necessitates the use of sequestering vesicles of varying size to accommodate a wide range of cargo. Autophagy is a ubiquitous process conserved in eukaryotes that mediates an adaptive response to environmental change by degrading cytoplasm, including entire organelles, in the lysosome, or the fungal equivalent, the vacuole. Beyond its role as a degradative pathway, recent studies have elucidated the role of autophagy in human pathophysiology [110]. Based on the cargo sequestration process, autophagy can be divided into several types. The best-characterized type so far is macroautophagy, which we refer to as autophagy hereafter.

Genetic analyses in yeast have significantly enhanced our understanding of the molecular basis of autophagy. For example, many of yeast Atg proteins have homologues in higher eukaryotic cells [54]. In *Saccharomyces cerevisiae*, the autophagy pathway can be induced by starvation. In response to nutrient depletion, cytosolic components are enwrapped in a double-membrane compartment termed a phagophore. This structure expands to form a double-membrane vesicle, an autophagosome. The completed autophagosome fuses with the vacuole, releasing the inner vesicle, termed an autophagic body, into the vacuolar lumen. The autophagic body and its contents are then degraded by

vacuolar hydrolases. A perivacuolar locus called the phagophore assembly site (PAS) is proposed to be the vesicle formation site during autophagy [52,53]. As detected by fluorescence microscopy, most Atg proteins converge at this locus as a single dot, and the non-PAS population is diffuse in the cytosol.

In yeast, autophagy also mediates the cytoplasm-to-vacuole targeting (Cvt) pathway [25,26,30]. Unlike the nonspecific autophagy induced by starvation, the Cvt pathway operates exclusively as a biosynthetic process, specifically transporting certain vacuolar hydrolases, such as the precursor form of aminopeptidase I (prApe1), into the vacuole; this pathway is constitutively active in growing cells. The Cvt pathway has similar morphological features to starvation-induced autophagy and uses much of the same protein machinery [29,31]. Therefore, the Cvt pathway can be regarded as a specific form of autophagy. Besides the Cvt pathway, other types of specific autophagy that mediate the removal of excess organelles or invasive bacteria have also been reported in fungi as well as higher eukaryotes [41,45,128,132].

Ever since the initial observation of autophagy, a central question that remains to be answered is the origin of the membrane used for autophagosome formation. The biggest obstacle in investigating this question is that the autophagosome is almost totally lacking in transmembrane proteins [149-151]. As a result, proteomic analyses have failed to reliably identify organelle-specific markers, suggesting that resident proteins are excluded from the source membrane(s) used to generate the autophagosome. Data from yeast indicate that the secretory pathway contributes to the vesicle formation step during autophagy. Sec12, a guanine nucleotide exchange factor (GEF) involved in vesicle budding from the endoplasmic reticulum (ER), and some components of the COPII

complex are essential for autophagosome formation [152]. Similarly, strains that are defective in Golgi complex function, such as those with mutations in Sec7 or subunits of the COG complex, also show a block in autophagy [153-155]. In these studies, however, it is difficult to determine whether the autophagic block is due to a defect in a particular component of the secretory pathway or just reflects an indirect effect when membrane flow through the early secretory pathway is impaired. Along these lines, the defective autophagic phenotype observed in early *sec* mutants may indicate the involvement of a particular cargo protein that is transported via the secretory pathway. In addition, an impaired secretory pathway leads to cellular dysfunction in processes such as ribosome synthesis, endocytosis, and organization of the nucleus [156-158], which makes it difficult to differentiate which defect directly causes the block in autophagy. Thus, there has been considerable speculation and confusion regarding the role of the secretory pathway in autophagy.

In this report, we analyzed the function of two proteins involved in the late stage of the secretory pathway, Sec2 and Sec4, and show that both play important roles in autophagy. Sec2 is a GEF protein that acts on the yeast Rab protein Sec4, and both participate in the polarized transport of secretory vesicles toward the sites of active growth (bud and mother/daughter neck) [159,160]. As a Rab protein, Sec4 oscillates between the inactive GDP-bound form and the active GTP-bound form and thus functions as a molecular switch to regulate vesicle delivery [161]. Activated by Sec2, Sec4, together with Sec2, reversibly associates with secretory vesicles and the exocyst complex on the plasma membrane and thus directs the vesicles toward the secretion site. We propose that during autophagy the secretion machinery at the *trans*-Golgi network,

including Sec2 and Sec4, is diverted to direct membrane flow to the process of autophagosome formation.

Materials and Methods

Media and growth conditions

Yeast cells were grown in rich (YPD; 1% yeast extract, 2% peptone, 2% glucose) or synthetic minimal (SMD; 0.67% yeast nitrogen base, 2% glucose, and auxotrophic amino acids and vitamins as needed) media. For starvation conditions, SD-N medium (0.17% yeast nitrogen base without ammonium sulfate or amino acids, and 2% glucose) was used. For experiments with temperature-sensitive mutants, cells were grown at 24˚C to midlog phase and shifted to a nonpermissive temperature (34 or 37°C) for 30 min to inactivate the mutants. If not otherwise indicated, cells were grown at 30˚C.

Plasmids and strains

pGFP-Atg8(316), pCu416, and pRS413 have been reported previously [52,145,162]. To clone pSec2(413) and pSec4(413), the open reading frames (ORFs) as well as 500 base pairs of the 5' promoter regions were amplified by PCR from yeast genomic DNA and cloned into the XmaI/ClaI sites of pRS413. pCuSec2(416) and pCuSec4(416) were generated by amplifying the ORFs from pSec2(413) and pSec4(413) and then cloning them into the EcoRI/ClaI sites of pCu416. To generate pCuHASec2(416), pCuHASec2(1-450)(416) and pCuHASec2(1-508)(416), a forward primer with additional sequence encoding a single hemagglutinin (HA) epitope at the 5' end was used to introduce the HA tag at the N terminus. Corresponding reverse primers were designed depending on the truncation site. PCR fragments amplified from pCuSec2(416) were inserted into the EcoRI/ClaI sites of pCu416. To make pGFP-Atg8(405), the GFP-Atg8 coding sequence from pGFP-AUT7(316) [52] was moved as a PvuI fragment to pRS405.

pCuYpt31(416) was made by inserting the sequence corresponding to the Ypt31 ORF into the Xma/ClaI sites of pCu416. pVAM3^{ts}(404) was a generous gift from Dr. Zhiping Xie (Nankai University, China).

Yeast strains used in this article are listed in Table 4.1. Gene deletion, truncation, and C-terminal tagging were carried out using a PCR-based method as described previously [142,163]. For integration of Atg9-3xGFP, the pAtg9-3xGFP(306) plasmid [164] was linearized with BglII and integrated into the *ATG9* genomic locus. Red fluorescent protein (RFP)-Ape1 was incorporated into the chromosome by integrating AvrII-digested pRFP-Ape1(305) [74] into the *APE1* locus. To integrate green fluorescent protein (GFP)-Atg8, pGFP-Atg8(405) was linearized with AflII and integrated into the *LEU2* locus.

To generate the *sec2-78* and *sec2(Δ451-508)* strains, the endogenous copy of *SEC2* was replaced with mutated alleles by homologous recombination. First pCuSec2^{C483Y}(416) was made by PCR-based site-directed mutagenesis using pCuSec2(416) as the template. To construct pCuSec2(Δ451-508)(416), DNA fragments encoding Sec2(1-450) and Sec2(509-759) were amplified from pCuSec2(416) and annealed together as the template for the second round PCR that amplified the Sec2(Δ451-508) fragment. The resulting fragment was cloned into the EcoRI/ClaI sites of pCu416 to generate pCuSec2(Δ451-508)(416). Next, from these two plasmids and pCuSec2(416), the Sec2, Sec2^{C483Y} and Sec2(Δ451-508) sequences plus the *CYC1* terminator were amplified by PCR and inserted into the PstI/BglII sites of pFA6a-TRP1, which are upstream of the *TRP1* gene [142]. Then, the 700 bp genomic region downstream of the *SEC2* ORF including its terminator was cloned and ligated into the

EcoRI/SpeI sites of pFA6a-TRP1, which are downstream of *TRP1*, to complete the pSec2-TRP1, pSec2^{C483Y}-TRP1 and pSec2(Δ451-508)-TRP1 plasmids. These three plasmids were then digested with PstI/Spe1, and the resulting fragments were transformed into yeast cells to replace the endogenous copy of *SEC2*. PCR and DNA sequencing were used to confirm incorporation of the mutations.

EM analysis

Cells were cultured to midlog phase in YPD medium at 24˚C and shifted to 37˚C for 30 min to inactivate the temperature-sensitive mutants. After 2 h starvation at 37˚C, samples were harvested and analyzed by transmission electron microscopy as described previously [75]. Images of cells with intact morphology and clear vacuoles were collected. To measure the size of autophagic bodies, vesicles were outlined manually using Adobe Photoshop (San Joes, CA) and the area values of outlined regions were measure by ImageJ (http://rsb.info.nih.gov/ ij/). The area value (S) was then converted into diameter by the formula: $d = 2(S/\pi)^{1/2}$.

Fluorescence microscopy

Cells were grown in YPD or SMD without auxotrophic amino acids to midlog phase. For starvation experiments, cells were incubated in SD-N medium as indicated in the corresponding figure legends, and 1 OD_{600} unit of cells (equivalent to 1 ml culture at A_{600} = 1.0) were collected by centrifugation and resuspended in 20 µl of SMD without vitamins to reflect growing conditions or in SD-N for starvation conditions. When indicated in the figure legend, fixation was carried out as described previously [61];

otherwise, living cells were used for microscopy. The samples were then examined by microscopy (DeltaVision Spectris; Applied Precision, LLC) and pictures were captured with a CCD camera (CoolSnap HQ; Photometrics). For each microscopy picture, 12 Z-section images were captured. The distance between two neighboring sections was 0.5 μm and the total depth of each stack was 5.5 μm, which was the approximate diameter of a normal yeast cell. To show the fluorescence signal of the whole cell in one picture, the stack of Z-section images were projected into a 2-D image by sum projection and quantified using softWoRx software (Applied Precision, Issaquah, WA). To label vacuolar membrane, FM 4-64 ((Molecular Probes, Eugene, OR) staining was performed as described previously [88].

Radioactive pulse-chase

To study the kinetics of prApe1 maturation we used a pulse-chase analysis as described previously [64]. To quantify protein secretion, wild-type cells were grown in SMD to midlog phase at 30˚C, and 30 OD_{600} units of cells (equivalent to a 30 ml culture at A_{600} = 1.0) were harvested. The cells were labeled in 1 ml SMD with 200 μCi [^{35}S]methionine cysteine for 15 min. After washing, the cells were subjected to a nonradioactive chase in 4 ml SMD containing 0.2% yeast extract and 2 mM cysteine and methionine with or without 10 ng/ml cycloheximide or 0.8 μg/ml rapamycin, or in SD-N. At the indicated time points, 400 μl samples were collected and precipitated with 10% trichloroacetic acid. Protein samples were analyzed with a scintillation counter or SDS-PAGE. For the *sec2-59* mutant, cells were grown at 24˚C and incubated at 37˚C for 30 min before

labeling. The subsequent labeling and chase were done similar to the wild-type, but were carried out at 37˚C.

Autophagy assays

GFP-Atg8 processing and Pho8Δ60 assays were performed as described previously [138,165]

Results

Sec2 is required for both autophagy and the Cvt pathway

To identify new essential genes involved in autophagy, we screened a collection of *S. cerevisiae* temperature-sensitive mutants for an autophagic defect, using the GFP-Atg8 processing assay to monitor autophagy. After induction of autophagy, GFP-Atg8 is transported into the vacuole; the GFP moiety is released by proteolysis and it is relatively stable so that free GFP reflects the level of autophagy [138]. Using this method, we found a clear defect in autophagy in the *sec2-41* mutant and subsequently confirmed the phenotype in a second allele, *sec2-59* (Figure 4.1 A). At permissive temperature (PT), the appearance of free GFP in both *sec2-59* and *sec2-41* after starvation was comparable to that in wild-type cells. However, at nonpermissive temperature (NPT), no free GFP was detected in either *sec2* mutant after starvation (Figure 4.1 A). To confirm that the autophagic defect was due to the dysfunction of Sec2, we cloned the *SEC2* gene on a centromeric plasmid. Exogenous expression of Sec2 restored the induction of free GFP at the NPT in both *sec2-59* (Figure 4.1 B) and *sec2-41* (our unpublished data). To address the possibility that the autophagic defect was due to *sec2* mutant cell death at the NPT, we tested the viability of the *sec2* mutants at the conditions used in the previous experiments. After 2 h starvation at the NPT, the cell culture was diluted and spotted onto agar plates. Both *sec2* alleles showed normal growth similar to the wild-type cells (Figure 4.1 C). In addition, in the GFP-Atg8 processing assay after 2 h starvation at the NPT we shifted the cells back to the PT for another 2 h starvation (recovery period); under these conditions free GFP could be clearly detected (Figure 4.1 A) showing that autophagy

induction was recovered. These results suggested that the defect in autophagy in the *sec2* mutants was not due to loss of viability at the NPT.

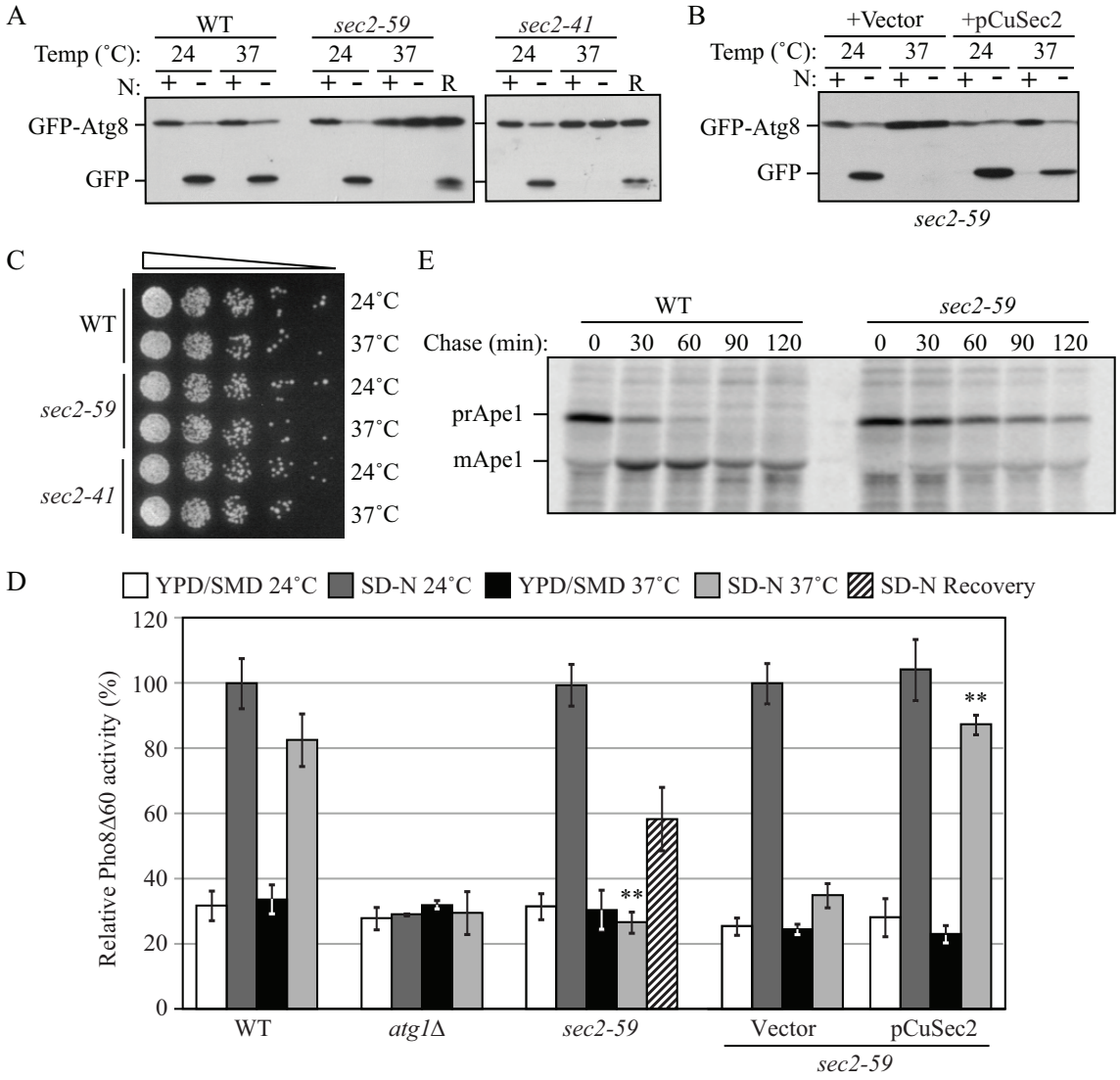

Figure 4.1 Sec2 is involved in both autophagy and the Cvt pathway. (A) GFP-Atg8 processing is blocked in *sec2* mutants. GFP-Atg8 was expressed by chromosomal integration in wild-type (JGY146), *sec2-59* (JGY183), and *sec2-41* (JGY184) strains. Cells were cultured in YPD at 24˚C to midlog phase. For each strain, the culture was divided into two parts. One-half was incubated at 37˚C for 30 min to inactivate the *sec2* mutant, whereas the other one remained at 24˚C. Then cells were shifted to SD-N and incubated for 2 h at the same temperature. Samples were taken before and after starvation. For recovery (R), cells starved at 37˚C for 2 h were shifted back to 24˚C and starved for another 2 h. Immunoblotting was done with anti-YFP antibody (that recognizes GFP) and the positions of full-length GFP-Atg8 and free GFP are indicated. (B) Exogenous expression of Sec2 restores autophagy in the *sec2-59* mutant. *sec2-59* GFP-Atg8 cells

(JGY183) harboring an empty vector or pCuSec2(416) were cultured in SMD medium and examined as described in A. (C) *sec2* mutants are viable after 2 h starvation at 37˚C. The same amount of starved cells from A were diluted and plated on a YPD plate, followed by 2 d incubation at room temperature. Cells were diluted 1:5 in each step from left to right. (D) Pho8Δ60 activity in the *sec2-59* mutant. Wild-type (TN124), *atg1*Δ (HAY572), and *sec2-59* (JGY112) cells as well as *sec2-59* cells expressing an empty vector or pCuSec2(416) were cultured as in A. The Pho8Δ60 assay was performed as described in *Materials and Methods*. Error bar, SD of three independent repeats. Significant difference compared to wild-type or vector alone, **p < 0.01. (E) The Cvt pathway is defective in the *sec2-59* mutant. Wild-type (SEY6210) and *sec2-59* (JGY113) cells were grown in SMD at 24˚C. After a 30 min inactivation at 37˚C, cells were subjected to pulse-chase labeling as described in *Materials and Methods*.

To extend our analysis, we used a more quantitative method, the Pho8Δ60 assay, to confirm the defect in autophagy in the *sec2* mutants. *PHO8* encodes an alkaline phosphatase that is transported to the vacuole via the ALP pathway; removal of a propeptide activates the zymogen in the vacuole lumen [166,167]. In contrast, Pho8Δ60, a mutated version without its transmembrane domain, can only be delivered to the vacuole via autophagy [148]. Thus, in a strain with a deletion of *PHO13*, which encodes the other yeast alkaline phosphatase, and where *pho8*Δ*60* replaces *PHO8*, the activity of alkaline phosphatase represents the magnitude of autophagy. At both the PT and NPT, wild-type cells showed a strong increase in Pho8Δ60 activity after incubation in starvation medium, whereas the activity did not increase in *atg1*Δ cells in which autophagy is completely blocked (Figure 4.1 D). In *sec2-59*, although the induction of Pho8Δ60-dependent alkaline phosphatase activity was normal at the PT, there was no significant increase when the cells were starved at the NPT. Similar to the GFP-Atg8 processing results, the Pho8Δ60 activity of *sec2-59* was partially recovered when the cells were shifted back to the PT (recovery period) or in the presence of plasmid-expressed *SEC2* (Figure 4.1 D).

In yeast, the majority of molecular components are shared between the Cvt pathway and nonspecific autophagy. The precursor form of Ape1 is transported to the vacuole through the Cvt pathway in nutrient-rich conditions and via autophagy in starvation conditions [29]. On delivery to the vacuole, the N-terminal propeptide is removed to generate the mature form of the enzyme (mApe1) [30]. The molecular-weight difference between mApe1 and prApe1 make it a useful marker to monitor protein sorting through the Cvt pathway. Therefore, we further tested the kinetics of prApe1 maturation in the *sec2* mutant using pulse-chase experiments. Wild-type and *sec2-59* cells were shifted from 24 to 37˚C for 30 min to inactivate Sec2 function. The cells were then subjected to a radioactive pulse-chase; samples at each time point were analyzed by immunoprecipitation. In wild-type cells, most prApe1 was converted to mApe1 after a 60 min chase, and no precursor was detected after 90 min (Figure 4.1 E). In contrast, in *sec2-59* cells only a small portion of prApe1 was processed into mApe1 even after a 120 min chase (Figure 4.1 E), suggesting the Cvt pathway was severely blocked in the *sec2* mutant. As a control, we examined the CPY pathway to confirm that the *sec2* mutation does not generally affect vacuolar protein sorting. As reported previously, in the *sec2-59* mutant most carboxypeptidase Y was processed into its mature form, although the kinetics were slightly slower than seen in the wild type (our unpublished data) [168]. Therefore, *sec2* mutants specifically affected autophagy and the Cvt pathway in starvation and growing conditions, respectively.

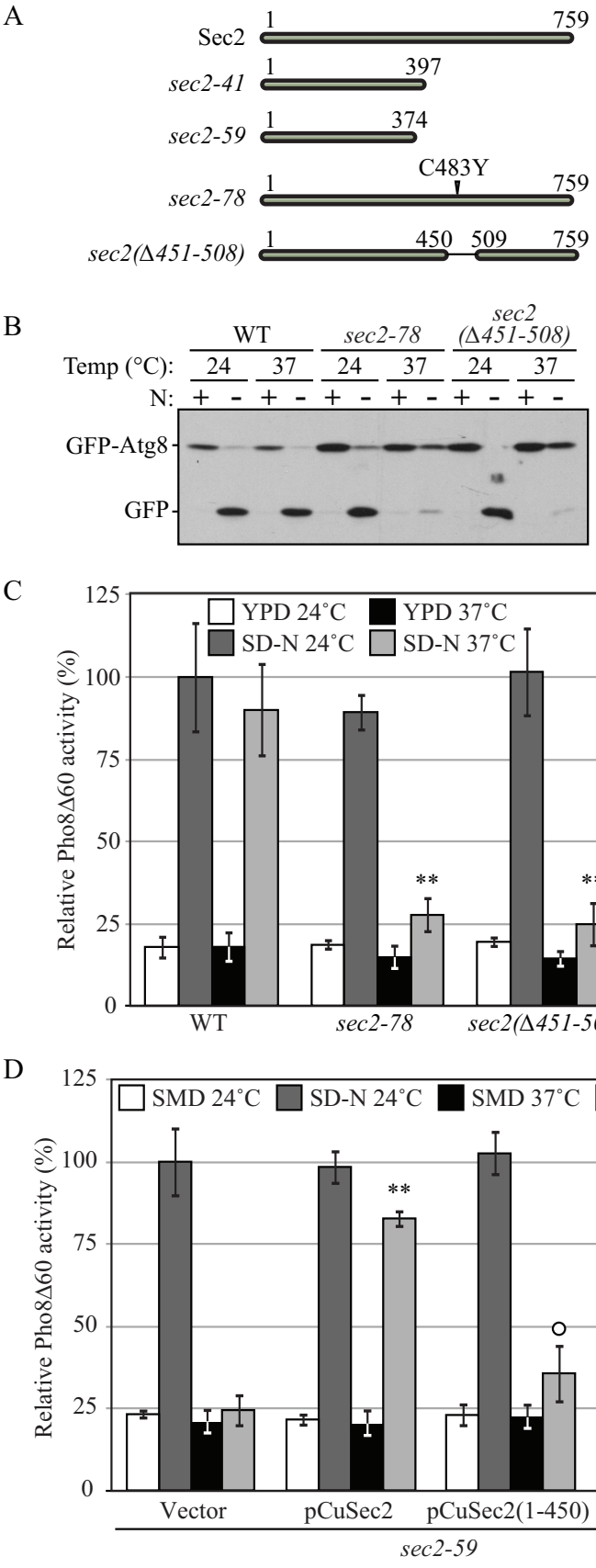
A
Sec2
1
759
sec2-41
1
397
sec2-59
1
374
C483Y
sec2-78
1
759
sec2(Δ451-508)
1
450
509
759
B
WT
sec2-78
sec2 (Δ451-508)
Temp (°C):
24
37
24
37
24
37
N:
+ - + - + - + - + - + -
GFP-Atg8
GFP
C
YPD 24˚C
YPD 37˚C
SD-N 24˚C
SD-N 37˚C
Relative Pho8Δ60 activity (%)
125
100
75
50
25
0
**
**
WT
sec2-78
sec2(Δ451-508)
D
SMD 24˚C
SD-N 24˚C
SMD 37˚C
SD-N 37˚C
Relative Pho8Δ60 activity (%)
125
100
75
50
25
0
**
**
Vector
pCuSec2
pCuSec2(1-450)
pCuSec2(1-508)
sec2-59

Figure 4.2 A 58-amino acid domain on Sec2 is essential for its role in autophagy. (A) Schematic representation of Sec2 alleles. (B) Mutations within the 58-amino acid domain result in defective GFP-Atg8 processing. Wild-type (JGY124), *sec2-78* (JGY125) and *sec2(Δ451-508)* (JGY126) cells were transformed with the pGFP-Atg8(316) plasmid and examined as in Figure 4.1 A. (C) An autophagic defect in *sec2-78* and *sec2(Δ451-508)* is confirmed by the Pho8Δ60 assay. The corresponding Pho8Δ60 strains (JGY127, JGY128, and JGY129) to those used in B were examined by the Pho8Δ60 assay. Error bar, SD of three independent repeats. Significant difference compared to wild-type, $^{**}p < 0.01$. (D) The extreme C terminus of Sec2 is dispensable to complement the *sec2-59* mutant. *sec2-59* (JGY112) cells were transformed with plasmids expressing various truncated forms of Sec2 and examined by the Pho8Δ60 assay. Error bar, SD of three independent repeats. Significant difference compared to vector along, $^{**}p < 0.01$; not significant difference, ○$p > 0.1$.

Mutations in amino acids 451-508 of Sec2 result in a temperature-sensitive phenotype in autophagy

Comprehensive studies have been performed on the role of Sec2 in the secretory pathway. The N-terminal half of Sec2 is required and sufficient for Sec2-Sec4 interaction and its GEF activity [160]. In contrast, the C-terminal half of Sec2 is dispensable for exchange activity, but truncation mutants display a temperature-sensitive phenotype [169]. As reported previously, *sec2-59* (which contains amino acids 1-374) and *sec2-41* are truncated alleles [160]. Sequencing data show that a TGG-to-TGA mutation in *sec2-41* results in a premature protein product with 397 amino acids (Figure 4.2 A). Within the C-terminal half of Sec2, a stretch of 58 amino acids (451-508) are critical for its proper localization and function. A point mutation within this domain (*sec2-78*, C483Y) results in a temperature-sensitive phenotype [169,170]. To investigate whether this domain is also involved in autophagy, we next examined the induction of autophagy in strains expressing Sec2 proteins lacking this 58-amino acid domain or carrying the C483Y mutation.

Sec2 mutant alleles with amino acids 451-508 deleted (*sec2(Δ451-508)*) or containing the C483Y point mutation (*sec2-78*) were used to replace the wild-type *SEC2* gene in the chromosome. Autophagy activity was examined by the GFP-Atg8 processing and Pho8Δ60 assays. Both the *sec2(Δ451-508)* and *sec2-78* strains showed a clear temperature-sensitive phenotype for autophagy. After 2 h starvation at 37˚C, there was severely reduced cleavage of GFP-Atg8 with either *sec2(Δ451-508)* or *sec2-78* (Figure 4.2 B), and this result was confirmed with the Pho8Δ60 assay. The increase of Pho8Δ60-dependent alkaline phosphatase activity after starvation was normal at the PT in both mutant strains, whereas it was barely above the background level at the NPT (Figure 4.2 C). Therefore, at the NPT, amino acids 451-508 of Sec2 were required for autophagy. In contrast to the previously published temperature-sensitive phenotype of the *sec2-78* mutant [170], cell growth was not completely blocked in the *sec2-78* allele that we constructed, although the growth rate was slower than in the corresponding wild-type cells (our unpublished data). This result meant that in this mutant the late stage of the secretory pathway necessary for cell growth was not completely blocked at 37˚C, even though autophagy under this condition was substantially diminished. Therefore, these findings suggested that it was not protein secretion per se that was required for autophagy, but rather Sec2 itself.

Next, we examined whether the amino acids at the extreme C terminus (downstream of amino acids 451-508) played a role in autophagy. Plasmids expressing full-length or truncated Sec2 were transformed into the *sec2-59* strain and the Pho8Δ60 activity was measured. As expected, full-length Sec2 complemented the autophagic defect at 37˚C. The expression of Sec2(1-508) also restored the Pho8Δ60 activity to ~69% the level of

full-length Sec2 (Figure 4.2 D). A similar result was observed in *sec2-59* cells expressing Sec2(1-541) (data no shown). As negative controls, when empty vector or Sec2(1-450) lacking the 58-amino acid domain were expressed, the Pho8Δ60 activity was barely rescued. Thus, the C-terminal 509-759 amino acids of Sec2 were not required to complement the autophagic defect seen in *sec2-59* cells.

Fewer autophagic bodies are formed in sec2-59 at the nonpermissive temperature

To further understand how autophagy is affected in the *sec2-59* mutant, we performed a morphological analysis using transmission electron microscopy. After being delivered into the vacuole, autophagic bodies are degraded in a Pep4-dependent manner [2]. To visualize intact autophagic bodies, the *PEP4* gene was deleted, which allows the accumulation of autophagic bodies inside the vacuole. In addition to *PEP4*, the *VPS4* gene was also knocked out to avoid the presence of small vesicles derived from the Mvb pathway [137]. Wild-type and *sec2-59* cells (both harboring *pep4*Δ *vps4*Δ double mutations) cultured in YPD medium were shifted from 24 to 37˚C and incubated for 30 min. The cells were then shifted to SD-N medium and starved at 37˚C for another 2 h, and samples were examined by electron microscopy as described in *Materials and Methods*.

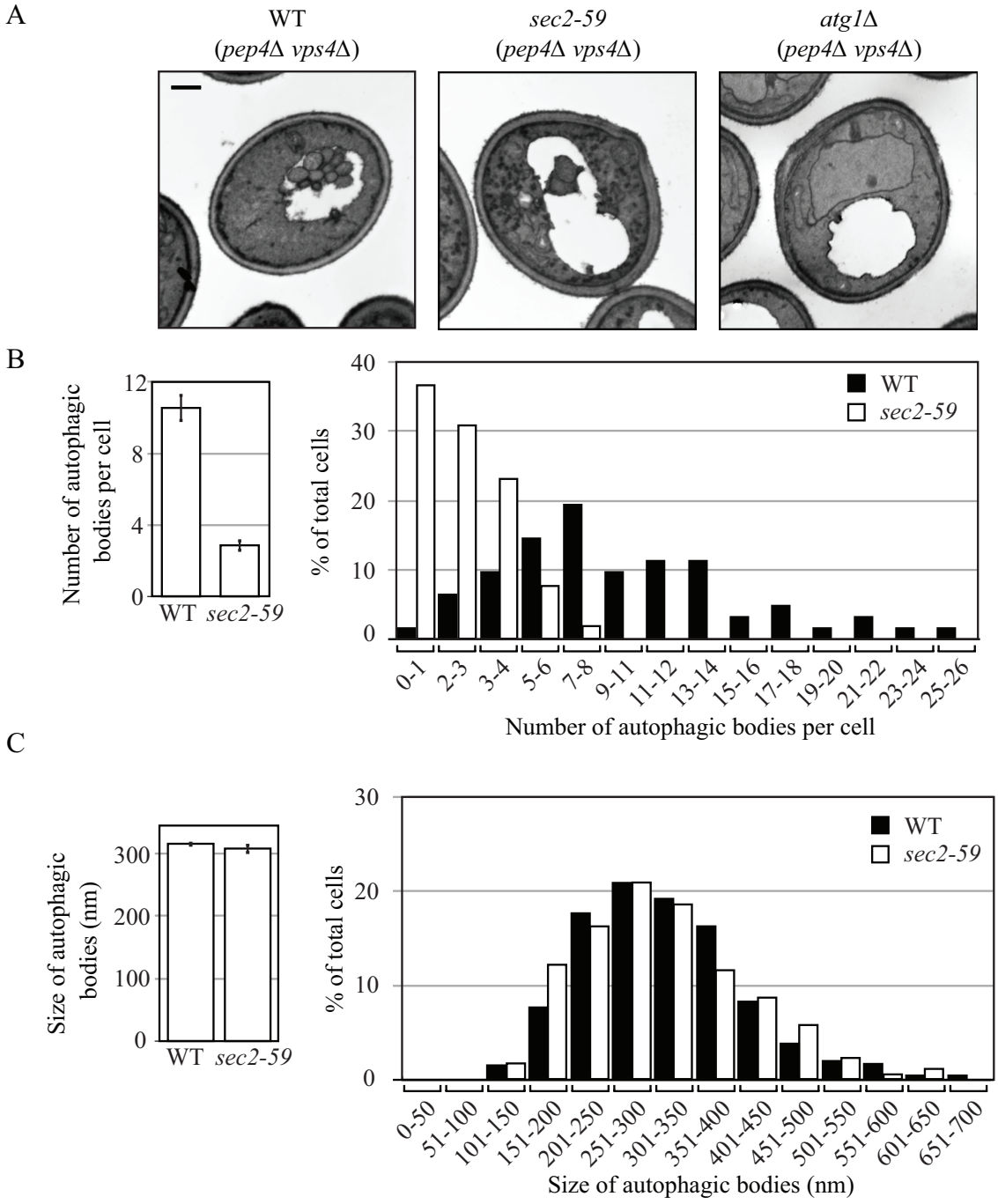

Figure 4.3 Sec2 mutation results in a reduced number of autophagic bodies, but has no effect on their size. After inactivation, the wild-type (*pep4*Δ *vps4*Δ, FRY143), *atg1*Δ (*atg1*Δ *pep4*Δ *vps4*Δ, HCY76), and *sec2-59* (*sec2-59 pep4*Δ *vps4*Δ, JGY180) strains were starved for 2 h at 37˚C and then analyzed by EM as described in *Materials and Methods*. (A) Representative images of wild-type, *atg1*Δ, and *sec2-59* strains. Scale bar, 500 nm. (B and C) Number and size of autophagic bodies. Quantification was done as described in *Materials and Methods*. Error bar represented SEM.

In wild-type cells, a large number of autophagic bodies (AB) accumulated in the vacuole after 2 h starvation (Figure 4.3 A). The average number was 10.55 ± 0.73 ABs per vacuole (mean ± SEM, n = 62 vacuoles; Figure 4.3 B). Under the same conditions, however, in *sec2-59* cells fewer ABs were observed (Figure 4.3 A); the average number was 2.88 ± 0.31 ABs per vacuole (mean ± SEM, n = 56 vacuoles; Figure 4.3 B), substantially lower than the number in wild-type cells. As a negative control, in *atg1*Δ cell there was no ABs visible in the vacuole (Figure 4.3 A). A histogram showed that more than 65% of the *sec2-59* vacuoles had fewer than four ABs, whereas in wild-type cells <10% fell into that category (Figure 4.3 B). Statistical analysis using a *t* test showed that the difference of AB number between wild-type and *sec2-59* cells was significant ($p < 0.01$). Although the disruption of Sec2 function at the NPT resulted in the formation of fewer autophagic bodies, it had little effect on their size. In wild-type cells, the average diameter of ABs was 315.42 ± 3.78 nm (mean ± SEM, n = 651 ABs) and that of *sec2-59* cells was 307.77 ± 7.73 nm (mean ± SEM, n = 172 ABs) (Figure 4.3 C); this difference between wild-type and *sec2-59* cells was not statistically significant ($p = 0.36$). Therefore, fewer autophagic bodies with normal size were formed in the *sec2* mutant.

Atg8 recruitment to the PAS is affected in sec2 mutants

EM analysis showed that fewer autophagic bodies accumulated in a *sec2* mutant. However, this analysis could not differentiate the step at which autophagy was affected. In particular, the substantially reduced number of ABs could be due to a defect in autophagosome formation or a block in autophagosome fusion with the vacuole. The apparent absence of accumulated autophagosomes in the cytosol (Figure 4.3 A) favored

the former explanation. However, to further address this question, we took advantage of a unique property of Atg8: Unlike most Atg proteins that dissociate from the completed autophagosome, a portion of Atg8 remains conjugated to the inner membrane of the autophagosome and is then delivered into the vacuole lumen following fusion [171]. Completed autophagosomes fuse with the vacuole in a Vam3-dependent manner [172]. In *vam3*^{ts} (temperature sensitive) mutant, completed autophagosomes cannot fuse with the vacuole and accumulate in the cytosol [172]; Atg8 is associated with completed autophagosomes and serves as a marker for these compartments [80]. We observed multiple GFP-Atg8 puncta in starved *vam3*^{ts} cells at the NPT (Figure 4.4 A), whereas most starved wild-type cells only displayed on GFP-Atg8 dot per cell (Figure 4.4 C). Therefore, examining the accumulation of GFP-Atg8 puncta in the *vam3* mutant background allows us to trace the formation of autophagosomes. Based on this strategy, we expressed GFP-Atg8 in either a *vam3*^{ts} mutant or a *sec2 vam3*^{ts} double mutant by genomic integration and measured the accumulation of GFP-Atg8 puncta after starvation at the NPT. Instead of the 2 h starvation used in previous experiments, in this assay we used a relatively short period of incubation in SD-N to avoid the appearance of too many GFP-Atg8 dots in the cytosol, which would make quantification more difficult.

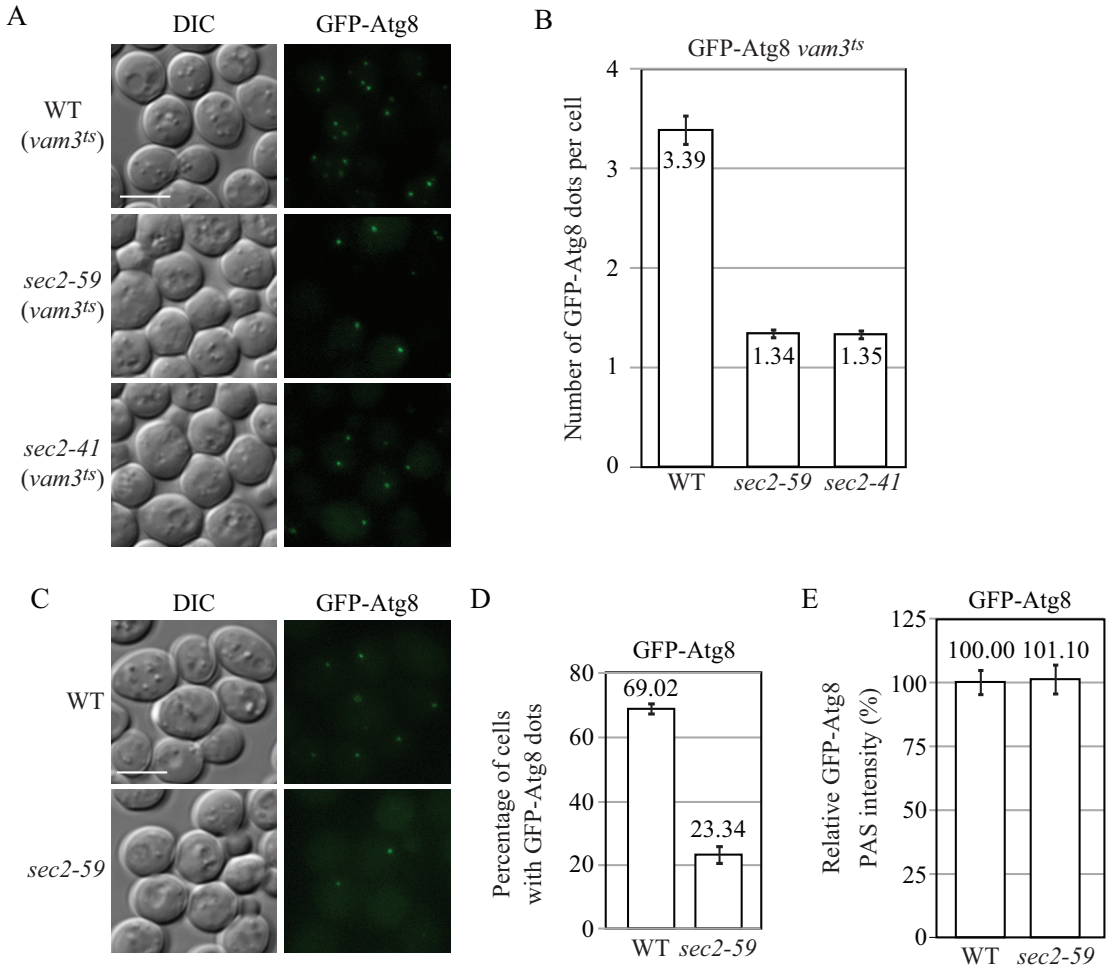

Figure 4.4 Recruitment of Atg8 to the PAS is affected in the *sec2-59* mutant. (A and B) In the *vam3*^{ts} background, *sec2-59* cells accumulate fewer GFP-Atg8 dots in the cytosol. After preinactivation, *vam3*^{ts} (JGY169) and *vam3*^{ts} *sec2* mutants (JGY171, JGY172) expressing chromosomally integrated GFP-Atg8 were starved for 20 min at 37˚C. Cells were fixed to avoid any movement of GFP-Atg8, and fluorescence microscopy was performed as described in *Materials and Methods*. Twelve Z-section images were projected to visualize all dots present throughout the entire cell. Representative images are shown in A, and quantification of the number of GFP-Atg8 puncta is shown in B. Error bar, SEM; n = 100. (C-E) PAS intensity of GFP-Atg8 is not affected in the *sec2-59* mutant although fewer cells have GFP-Atg8 dots. The wild-type (JGY146) and *sec2-59* (JGY183) GFP-Atg8 strains were incubated in SD-N for 20 min at 37˚C, and cells were examined by microscopy. (C) Representative images after projection of 12 Z-section pictures. (D) The percentage of cells that had at least one GFP-Atg8 dot was determined. Error bar, SD from 3 independent experiments; n = 300. (E) Relative PAS intensity of GFP-Atg8. The intensity in wild-type cells was set to 100%, and the other value was normalized. Error bar, SEM; n = 50. Scale bar, 5 μm.

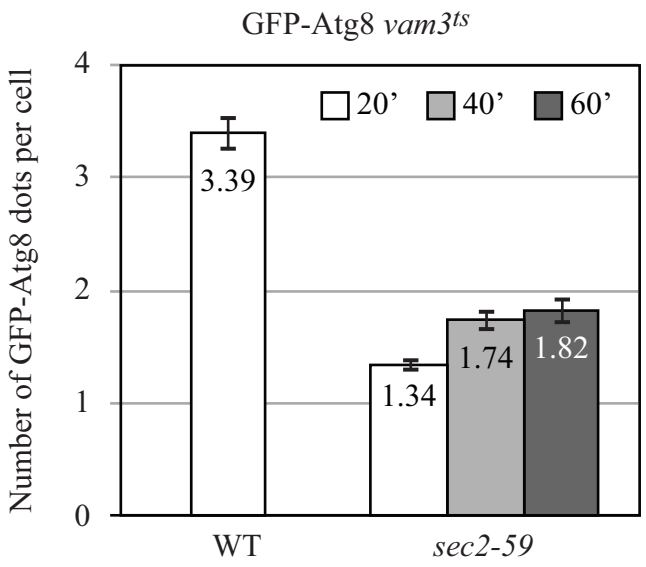

Figure 4.S1 In the *vam3*^{ts} background *sec2-59* cells accumulate fewer GFP-Atg8 dots in the cytosol even after longer starvation. *vam3*^{ts} (JGY169) and *vam3*^{ts} *sec2-59* (JGY172) cells were starved at 37˚C and fixed samples at indicated time points were checked by microscopy. In the control cells, only 20 min sample was quantified because after longer starvation there were too many overlapping GFP-Atg8 dots to allow accurate counting. Error bar, SEM; n = 100.

After 20 min starvation at the NPT, 98% of control cells (*vam3*^{ts}; WT) showed GFP-Atg8 dots, whereas only 48 and 46% of *sec2-59 vam3*^{ts} and *sec2-41 vam3*^{ts} cells, respectively, had at least one GFP-Atg8 dot (Figure 4.4 A). To normalize for the different percentages of punctate cells, we quantified the number of GFP-Atg8 puncta per cell, counting only those cells with at least one GFP-Atg8 dot. In wild-type (*vam3*^{ts}) cells, there were 3.39 ± 0.16 (mean ± SEM, n = 100 cells) GFP-Atg8 puncta per cell (Figure 4.4 B); with a long incubation time in starvation conditions, the number of GFP-Atg8 puncta elevated significantly and became impossible to count due to overlapping dots. In contrast, the *sec2-59 vam3*^{ts} and *sec2-41 vam3*^{ts} cells had only 1.34 ± 0.06 and 1.35 ± 0.06 (mean ± SEM, n = 100 cells) GFP-Atg8 puncta per cell, respectively (Figure 4.4 B). At longer time points of starvation, the number of GFP-Atg8 puncta in these mutants

barely increased (Figure 4.S1), suggesting that the reduced number of GFP-Atg8 dots in the *sec2* mutants was not due to a minor kinetic delay but rather reflected a severe reduction in autophagosome formation.

Recently, it has been shown that the amount of Atg8 at the PAS controls the level of autophagy by regulating the size of autophagosomes [79]. On the basis of this result, we examined whether the amount of Atg8 at the PAS was affected in the *sec2* mutant. Similar to the results in the *vam3*^{ts} background, fewer *sec2-59* cells harbored at least one GFP-Atg8 punctum in an otherwise wild-type background (Figure 4.4 C). After a 20 min incubation in SD-N at the NPT, 69% of the wild-type cells had at least one GFP-Atg8 dot. In contrast, only 23% of *sec2-59* cells had GFP-Atg8 puncta (Figure 4.4 D). To measure the amount of Atg8 at the PAS, we took advantage of a recent finding that within a certain range the fluorescence signal intensity correlates with the protein amount [127,134], which means we can measure the PAS fluorescence intensity of GFP-Atg8, and the corresponding value indicates the level of GFP-Atg8 at this site. Quantification of the data showed that after 20 min starvation at the NPT, the PAS intensity of GFP-Atg8 was the same in wild-type and *sec2-59* cells (Figure 4.4 E). This result suggested that although fewer *sec2-59* cells have Atg8 puncta corresponding to the PAS, once Atg8 is recruited to this site it is ultimately recruited at a level similar to that in wild-type cells. Combined with the EM data indicating that the reduced number of autophagosomes that were generated in the *sec2-59* mutant attained the normal size, this finding further supports the model that Atg8 plays a role in the regulation of autophagosome size during nonspecific autophagy [173,174].

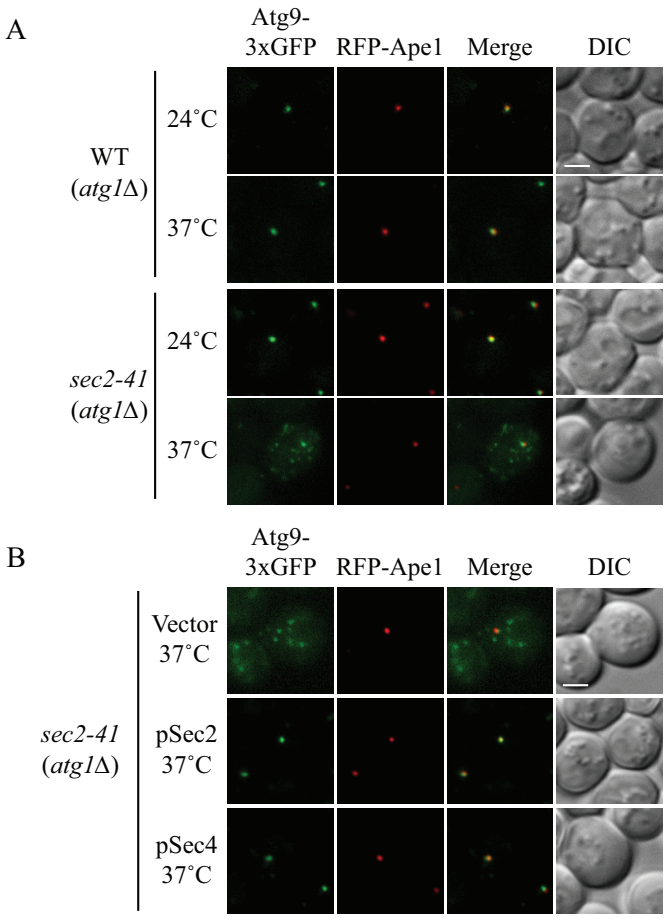

Figure 4.5 Atg9 anterograde movement is less efficient in the *sec2* mutant. (A) In the TAKA assay, Atg9 is localized to multiple dots in the *sec2-41* mutant at the NPT. Wild-type (Atg9-3xGFP RFP-Ape1 *atg1*Δ, JGY197) and *sec2-41* mutant (Atg9-3xGFP RFP-Ape1 *atg1*Δ, JGY107) cells were starved at the indicated temperature for 2 h. Cells were fixed and then analyzed by microscopy. 12 Z-section images were stacked, and representative images are shown. (B) Exogenous expression of Sec4 can restore the Atg9 anterograde movement defect in *sec2-41* cells as shown by the TAKA assay. *sec2-41* (Atg9-3xGFP RFP-Ape1 *atg1*Δ, JGY107) cells were transformed with empty vector, pSec2(413) and pSec4(413). Microscopy samples were prepared, and pictures were taken as described in A. Scale bar, 2 μm.

Sec2 affects Atg9 anterograde movement

Recently, it was reported that Atg8 localization to the PAS is dependent on the presence of Atg9 [89]. Of the core machinery required for autophagosome formation, Atg9 is the only transmembrane protein, and it shuttles between the PAS and other peripheral membrane structures [58,60]. The anterograde movement of Atg9, from peripheral sites

to the PAS, requires the presence of Atg27 [64]. In an *atg27*Δ mutant the number of autophagosomes is reduced compared to wild-type cells upon the induction of autophagy, but the size of the autophagosomes is not affected. This phenotype is similar to what we observed in the *sec2* mutant at the NPT. Therefore, we examined whether the anterograde transport of Atg9 was affected in the absence of functional Sec2.

To examine the cycling of Atg9 between the PAS and peripheral sites, we used the TAKA assay (Transport of Atg9 after Knocking out *ATG1*) [138]. This epistasis analysis is based on a previous finding that the retrieval of Atg9 from the PAS to peripheral sites is dependent on the Atg1-Atg13 complex [62]. In an *atg1*Δ mutant, Atg9 is restricted at the PAS as a single dot in contrast to the multiple dots detected in wild-type cells. If the introduction of a second mutation in the *atg1*Δ background results in multiple Atg9 puncta, the second mutation is epistatic to *atg1*Δ, suggesting that the corresponding protein is required for the anterograde movement of Atg9. Using this strategy, we looked at Atg9 localization in an *atg1*Δ *sec2-41* double mutant in starvation conditions. Atg9 was tagged with triple GFP at the C terminus, which does not affect the normal localization and functionality of Atg9 [59,164], and the chimera appears to be stable based on the absence of a detectable free GFP band when examined by Western blot analysis; furthermore, GFP expressed by itself does not display the type of punctate distribution pattern seen with Atg9-3xGFP (our unpublished data). As expected, in the *atg1*Δ mutant, essentially 100% of the Atg9-3xGFP accumulated at the PAS (marked by RFP-Ape1) at both 24 and 37˚C (Figure 4.5 A). At the PT, the Atg9-3xGFP signal in the *atg1*Δ *sec2-41* cells was localized to a single dot that colocalized with RFP-Ape1. However, when the cells were starved at the NPT, Atg9-3xGFP was localized to multiple

dots (Figure 4.5 A). In some cells, one of these dots colocalized with RFP-Ape1. These results suggested that in the *sec2-41* mutant the anterograde transport of Atg9 was reduced, but not completely blocked. To extend our analysis, we analyzed that localization of Atg9 in the *sec2-41* mutant in the presence of Atg1. After 2 h starvation at both 24 and 37˚C, we observed the localization of Atg9 as multiple punctate structures in *sec2-41* cells. Among all the cells at 24˚C, 49% had one of the Atg9 dots colocalized with RFP-Ape1. In contrast, at 37˚C only 26% of the cells showed any Atg9 colocalization at the PAS. This result was in agreement with the TAKA assay that Atg9 trafficking toward the PAS is partially defective in the *sec2* mutant.

It was reported that a second copy of *SEC4* suppresses the secretion defect in the *sec2-41* and *sec2-59* mutants [160]. There are other examples where overexpression of a GTPase complements, to some extent, the absence of the corresponding GEF. For instance, the autophagic activity in the *sec12* mutant can be restored by the overproduction of Sar1 [152], and the expression of the constitutively active form of Ypt1 suppresses the Cvt pathway defect resulting from the absence of Trs85 [175]. Accordingly, we examined whether an extra copy of Sec4 could restore the proper localization of Atg9 based on the TAKA assay. When empty vector was expressed in *atg1*Δ *sec2-41* cells, there was no effect on Atg9 localization; Atg9-3xGFP was still detected in multiple dots (Figure 4.5 B). As expected, plasmid-based Sec2 restored the Atg9 localization to a single dot at the PAS. When Sec4 was expressed on a plasmid under the control of its native promoter, the Atg9 signal again accumulated at the PAS. Therefore, the defect in anterograde Atg9 transport in *sec2* cells could be rescued by the overexpression of Sec4.

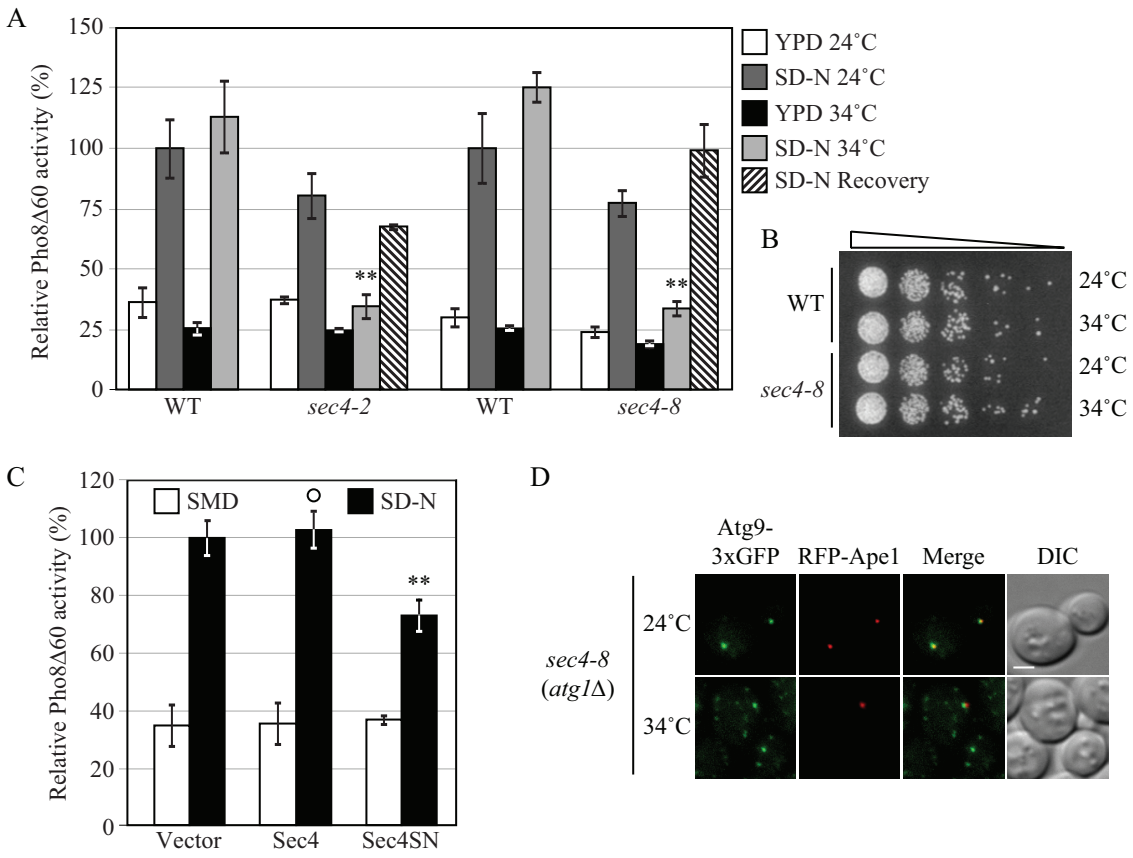

Figure 4.6 The *sec4* mutant displays an autophagic defect. (A) Two *sec4* alleles show a defect in Pho8Δ60 activity. The *sec4-2* (JGY168) and *sec4-8* (JGY159) mutants and the corresponding wild-type (JGY166, YTS158) strains were cultured in YPD medium at 24˚C to midlog phase. Half of the culture was inactivated for Sec4 function at 34˚C for 30 min, whereas the other half was kept growing at 24˚C. Then cells were shifted to SD-N, and the temperature was maintained. Samples were collected before and after 2 h starvation. For recovery, cells starved at 34˚C were shifted back to 24˚C and incubated for another 2 h. Error bar, SD from three independent assays. Significant difference compared to corresponding wild-type cells, **$p < 0.01$. (B) The *sec4* mutant is viable after 2 h starvation at 34˚C. The same amount of wild-type (YTS158) and *sec4-8* (JGY159) cells after 2 h starvation at the indicated temperature were diluted and spotted on a YPD plate. Cells were diluted 1:5 in each step from left to right. The plate was incubated at room temperature for 2 d. (C) $Sec4^{S34N}$ has a dominant-negative effect on autophagy. Wild-type cells (TN124) were transformed with an empty vector or a plasmid expressing either Sec4 or $Sec4^{S34N}$ under the control of the *CUP1* promoter. Transformants were cultured in SMD medium at 30˚C and shifted to SD-N for 2 h. Before and after starvation, samples were collected and tested by the Pho8Δ60 assay. Error bar, SD from three independent assays. Significant difference compared to vector alone, **$p < 0.01$; no significant difference, ○$p > 0.1$. (D) Atg9 movement to the PAS is defective in the *sec4-8* mutant. *sec4-8* (Atg9-3xGFP RFP-Ape1 *atg1*Δ, JGY198) cells were used for microscopy and the procedure was similar to that described in Figure 4.5 A. Scale bar, 2 μm.

Autophagy is severely compromised in sec4 mutants

So far, Sec4 is the only Rab protein for which Sec2 has exchange activity. Because Sec4 overexpression complemented the *sec2* phenotype in the TAKA assay, we hypothesized that Sec2 functions through Sec4 during autophagosome formation. To test this hypothesis, we studied the occurrence of autophagy in *sec4* mutants. Previously it was published that *sec4-2* shows a block in Pho8Δ60 activity when starved at 37˚C, but the alkaline phosphatase activity could not be recovered when the cells were shifted back to 24˚C. At a restrictive temperature of 34˚C, *sec4-2* shows both secretion and growth defects; however, at this temperature, autophagy was not affected [152]. To examine this result, we constructed Pho8Δ60 strains bearing two *sec4* alleles, *sec4-2* and *sec4-8*. Both *sec4* alleles were defective for autophagy induction based on the level of Pho8Δ60-dependent alkaline phosphatase activity at 34˚C, and the defect could be mostly recovered when the cells were starved again at permissive temperature, indicating that the cells were not dead (Figure 4.6 A and B). To confirm that Sec4 participates in autophagy as a GTPase, we examined the function of $Sec4^{S34N}$, a GDP-bound mutant of Sec4, in autophagy. When $Sec4^{S34N}$ was expressed in *sec4-8* cells, it could not restore the Pho8Δ60 activity (our unpublished data). Furthermore, when $Sec4^{S34N}$ was overexpressed in wild-type cells, it showed a dominant-negative effect on the magnitude of autophagy. In $Sec4^{S34N}$-overexpressing cells, the Pho8Δ60 activity was reduced to 73% compared to cells expressing an empty vector, whereas overexpression of wild-type Sec4 did not have a clear effect (Figure 4.6 C). Thus, the activation of Sec4 is necessary for autophagy and

the constitutively inactive mutant of Sec4 has a dominant-negative effect on the magnitude of autophagy.

Next, we examined Atg9 trafficking in the *sec4* mutant by the TAKA assay. At the PT, starved *atg1*Δ *sec4-8* cells showed one single dot of Atg9-3xGFP, which was localized at the PAS. In contrast, when *atg1*Δ *sec4-8* cells were starved at 34˚C, Atg9-3xGFP was localized to multiple dots, although in some cells one of the dots colocalized with RFP-Ape1 at the PAS (Figure 4.6 D). This phenotype was very similar to what was observed in *sec2*. Considering the complementation experiment using Sec4 overexpression (Figure 4.5 B), this result suggested that Sec2 and Sec4 function as a GTPase-GEF complex in Atg9 anterograde movement. We further tested whether the overexpression of Sec4 can restore the autophagy activity in *sec2* mutants. However, the overexpression of neither wild-type Sec4 nor a constitutively active mutant of Sec4 [161] had a substantial effect on Pho8Δ60 activity in the *sec2* mutant (our unpublished data). These results suggested that although a higher dosage of Sec4 could complement Atg9 movement in the *sec2* mutant, there is another defect(s) in *sec2* mutants that could not be suppressed by Sec4 overexpression.

Regulation between protein secretion and autophagy

We have identified several genes involved in the late-stage secretory pathway that also play a role in autophagy. One hypothesis is that there is a regulatory mechanism between exocytosis and autophagy when the nutrient condition is changed. If so, similar post-Golgi machinery being used by two different pathways makes it possible to quickly switch the membrane flow from one pathway to the other in response to environmental

changes. To investigate this hypothesis, we tested whether the level of protein secretion is down-regulated under starvation conditions. To measure the quantity of secreted proteins in either nutrient rich or starvation conditions, wild-type cells were labeled with [^{35}S]methionine cysteine and chased in either SMD or SD-N medium (Figure 4.7 A). At each time point, the extracellular media was harvested and the secreted proteins were collected by TCA precipitation. The pellet was then analyzed for radioactivity to determine the magnitude of protein secretion within a certain period of time.

When wild-type cells were chased in nutrient-rich medium, the amount of secreted proteins increased dramatically over time, and radioactivity was elevated by 8-fold after a 60 min chase (Figure 4.7 B). As a negative control, *sec2-41* cells chased at the NPT showed much less of an increase in the amount of secreted protein. When wild-type cells were chased in starvation medium, a very small amount of protein was secreted into the medium, and the secretion kinetics was comparable to that of *sec2-59* at the NPT (Figure 4.7 B). Protein synthesis is generally halted in starved cells. To exclude the possibility that the loss of protein secretion is because any newly synthesized proteins are necessary for exocytosis, we chased the wild-type cells in nutrient-rich medium in the presence of cycloheximide. Cycloheximide efficiently blocked protein synthesis (Figure 4.S2). In nutrient-rich medium with cycloheximide, the protein secretion kinetics was not affected (Figure 4.7 B) suggesting newly synthesized proteins were not required for exocytosis over the time course we utilized. To further confirm this result, we examined the protein pellet from the extracellular media by SDS-PAGE. After autoradiography, secreted proteins with molecular mass of ~50 and 140 kDa were visible in wild-type cells chased in nutrient-rich medium (Figure 4.7 C). In cells chased in starvation conditions, however,

these bands were completely absent, indicating a block in protein secretion. Accordingly, these results demonstrated that protein secretion was down-regulated when cells encountered a shortage of nutrient.

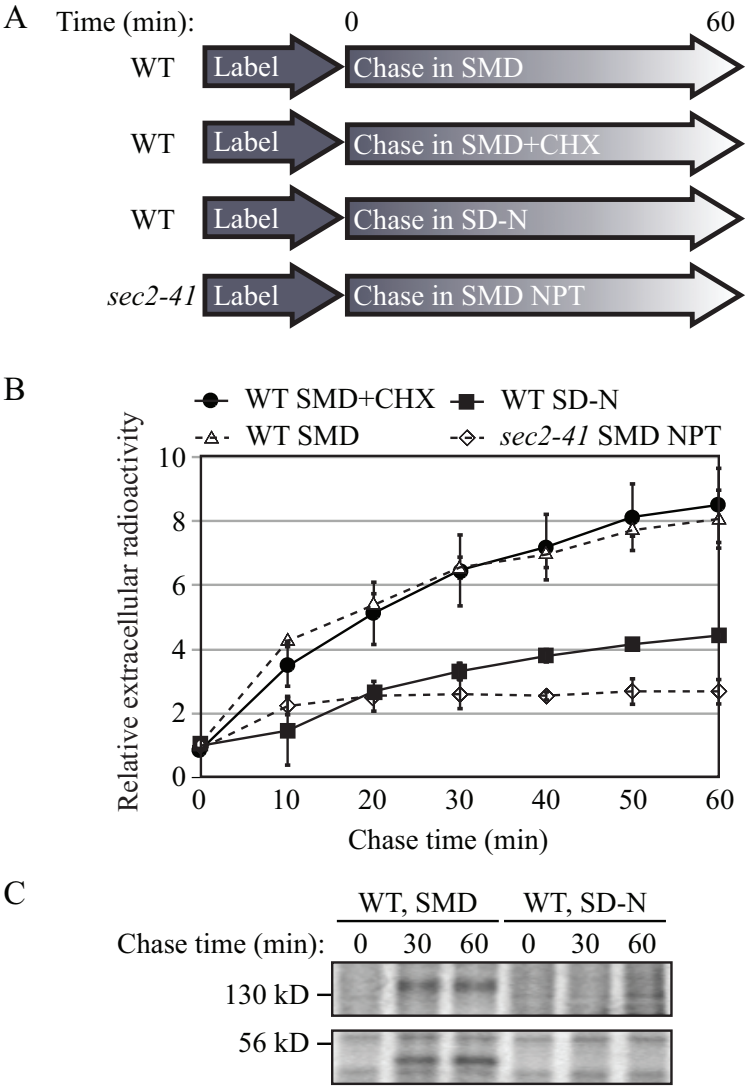

Figure 4.7 Protein secretion is down-regulated during starvation conditions. (A) Schematic representation of the procedure used for the pulse-chase experiments. (B) Relative radioactivity of the extracellular media. Cells were chased in the indicated media at 30˚C except for the *sec2-41* cells, which were chased at 37˚C. Samples were collected at the indicated time points. Extracellular proteins were precipitated and the amount of radioactivity was quantified using a scintillation counter. The values at time zero were set to 1.0, and other values were normalized. Error bar, SD from three independent experiments. (C) Secretion of extracellular protein was examined by SDS-PAGE. Samples collected at 0, 30, and 60 min from B were separated by SDS-PAGE and visualized by autoradiography.

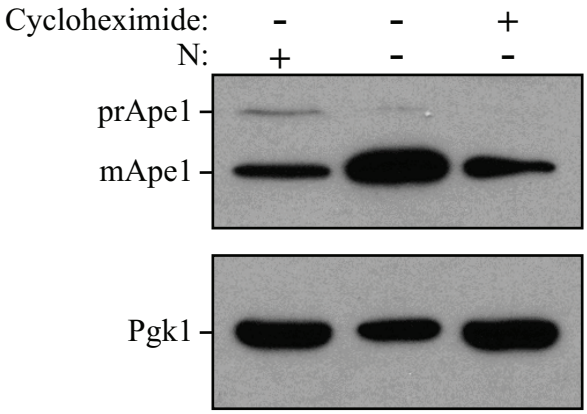

Figure 4.S2 Cycloheximide blocked protein synthesis. During starvation, the protein level of Ape1 is upregulated, but in the presence of cycloheximide the level of Ape1 remained unchanged. Wild-type (SEY6210) cells were cultured in YPD to midlog phase and shifted to SD-N with or without 10 ng/ml cycloheximide. Samples were collected before and after 2 h starvation and examined by western blot. Pgk1 was used as a loading control.

Exit from the trans-Golgi is essential for autophagy

To further test the hypothesis that membrane flow from the Golgi complex is diverted into the autophagy pathway during starvation, we investigated whether vesicle exit from the Golgi complex is required for autophagy. Studies show that Ypt31/32 are required for the exit of secretory vesicles from the *trans*-Golgi and that these proteins are involved in the recruitment of Sec2-Sec4 to secretory vesicles [176,177]. Ypt32 also interacts with Sec2, although Sec2 does not have exchange activity for Ypt32 [176]. Ypt32 shares a very similar amino acid sequence with Ypt31, and deletion of both genes is lethal [178]. Thus, we investigated whether there was an autophagic defect in cells with *ypt31*Δ and a conditional *ypt32* mutation (*ypt31/32*^{ts}) and whether the phenotype was similar to that of *sec2* and *sec4* cells, based on the GFP-Atg8 processing assay. The *ypt31/32*^{ts} mutant displayed a clear temperature-sensitive autophagy phenotype. At the NPT, the absence of free GFP after 2 h starvation indicated a defect of autophagy induction, and this defect

was reversible when the cells were shifted back to the PT (Figure 4.8 A). The failure of autophagy induction in *ypt31/32*^{ts} was also observed by the Pho8Δ60 assay (Figure 4.8 B). In addition, morphological analysis also confirmed the autophagic defect when the function of Ypt31/32 was disrupted. In the *ypt31/32*^{ts} mutant, ABs could hardly been seen by transmission electron microscopy after 2 h starvation at the NPT (Figure 4.8 C); the average number of ABs was 0.40 ± 0.12 (mean ± SEM, n = 75 vacuoles; Figure 4.8 D). When plasmid-based Ypt31 was overexpressed in this mutant, the accumulation of ABs within the vacuole was restored; under the same conditions, there were 8.22 ± 0.46 ABs per vacuole (mean ± SEM, n = 79 vacuoles; Figure 4.8 C and 8D). The complementation of autophagy activity by exogenous Ypt31 was further demonstrated by GFP-Atg8 processing (Figure 4.S3 A), suggesting the autophagic defect was a result of Ypt31/32 dysfunction.

Next we examined the localization of Atg8 in the *ypt31/32*^{ts} mutant. In both wild-type and *ypt31/32*^{ts} cells, GFP-Atg8 was mostly diffuse in the cytosol with a PAS punctum in nutrient-rich conditions. After starvation at the NPT, in addition to a prominent PAS dot, wild-type cells had GFP signal accumulated within the vacuolar lumen. However, when *yp31/32*^{ts} cells were starved at the NPT the vacuole was relatively empty of GFP signal, suggesting a block of autophagic flux. Furthermore, there were multiple GFP-Atg8 puncta in the cytosol of *ypt31/32*^{ts} cells under starvation conditions (Figure 4.8 E). Overexpression of Ypt31 in *ypt31/32*^{ts} restored the distribution of GFP-Atg8 as a single PAS dot and also allowed vacuolar accumulation (Figure 4.S3 B). There are two possibilities to explain why Atg8 was localized to multiple dots in the *ypt31/32*^{ts} strain: 1) Ypt31/32 is required for the fusion between formed autophagosomes and the

vacuole. Thus, the multiple GFP-Atg8 dots in the *ypt31/32*^{ts} mutant indicate the accumulation of autophagosomes in the cytosol; 2) Ypt31/32 is involved in double-membrane vesicle formation, and in the *ypt31/32*^{ts} mutant Atg8 is mislocalized to aberrant membrane structures. To further characterize the property of the multiple GFP-Atg8 puncta in the *ypt31/32*^{ts} mutant, cells were recovered in YPD medium at the PT. In this nutrient-rich condition no more autophagosomes would be formed. If there are completed autophagosomes accumulated in the cytosol, once cells are shifted back to the PT, even in nutrient-rich conditions, GFP-Atg8 dots will be delivered to the vacuole, resulting in a GFP signal within the vacuole. For example, in *vam3*^{ts} cells GFP-Atg8 dots were accumulated in the cytosol after starvation at the NPT. When cells were recovered in YPD medium at the PT, the GFP signal was mostly enriched in the vacuolar lumen (Figure 4.8 E), indicating that the completed autophagosomes rapidly fused with the vacuole (Figure 4.S3 C). In contrast, in *ypt31/32*^{ts} mutant cells, after the recovery period GFP-Atg8 regained its localization of one PAS dot, but there was no vacuolar GFP signal (Figure 4.8 E, 4.S3 C), suggesting that the GFP-Atg8 puncta detected at the NPT did not correspond to completed autophagosomes, but rather were incomplete/aberrant structures that were able to coalesce into a PAS at the PT. The presence or absence of the vacuolar GFP signal was confirmed by the analysis of GFP-Atg8 processing by immunoblot. After recovery in YPD, free GFP was detected in *vam3*^{ts} but not in *ypt31/32*^{ts} cells; when the recovery was carried out in starvation conditions, both *vam3*^{ts} and *ypt31/32*^{ts} cells showed cleavage of GFP-Atg8, but the intensity of the GFP band in the *vam3*^{ts} cells was stronger than that in the *ypt31/32*^{ts} mutant cells (Figure 4.8 F). Therefore, the *ypt31/32*^{ts} mutation may result in disruption of autophagosome formation.

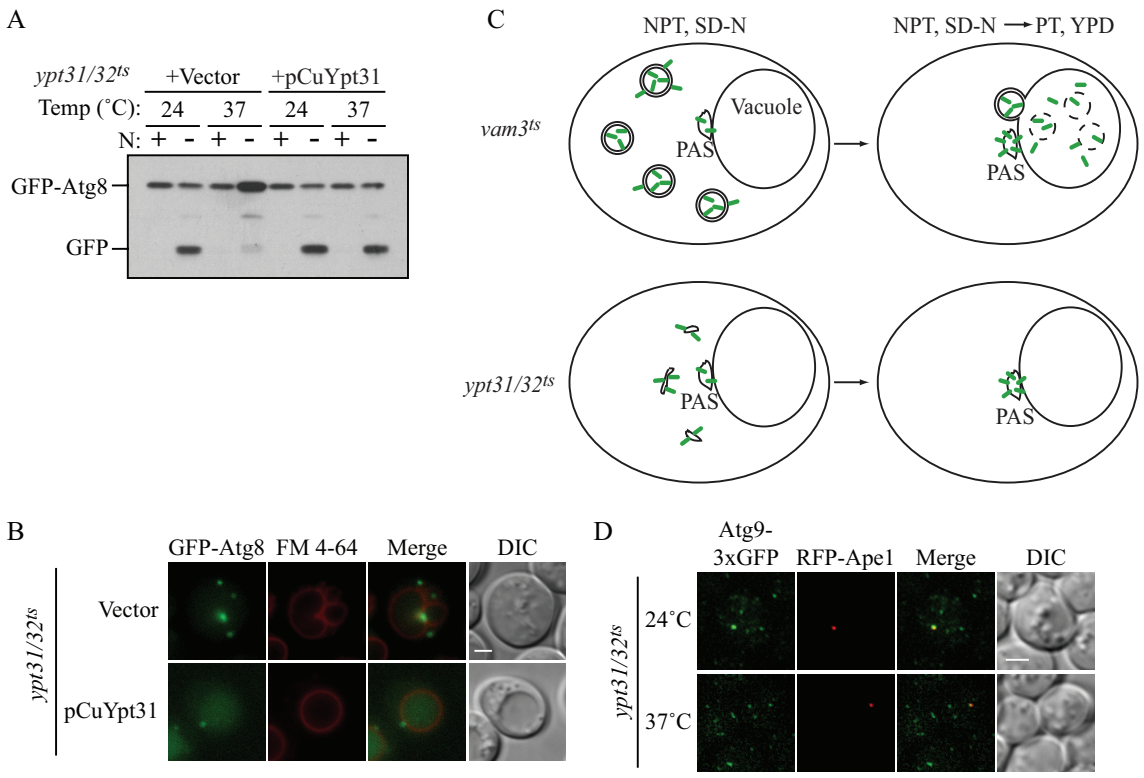

Figure 4.S3 *ypt31/32*^{ts} mutant affects Atg8 localization. (A) Expression of Ypt31 rescues the autophagic defect in *ypt31/32*^{ts} mutant. *ypt31/32*^{ts} GFP-Atg8 (JGY210) cells expressing empty vector or pCuYpt31(416) were examined as in Figure 4.1 A. (B) Exogenous expression of Ypt31 restores Atg8 localization in *ypt31/32*^{ts} cells at the NPT. *ypt31/32*^{ts} GFP-Atg8 (JGY210) cells expressing empty vector or pCuYpt31(416) were inactivated at 37˚C for 30 min and then starved at 37˚C for 2 h. Cell samples were then checked by microscopy. Vacuolar membrane was stained by FM 4-64. For each strain, only one Z-section with clear vacuole was shown. Scale bar, 2μm. (C) Schematic diagram illustrating the interpreted phenotypes for the *vam3*^{ts} and *ypt32/ypt32*^{ts} strains after shifting from NPT in SD-N to PT in YPD. (D) Ypt31/32 are not required for the localization of Atg9 to its peripheral sites. *ypt31/32*^{ts} Atg9-3xGFP RFP-Ape1(JGY207) cells were grown at 24˚C. Half of the culture was incubated at 37˚C for 30 min and the other half remained at 24˚C. Cells were shifted to SD-N for 2 h and samples were collected after starvation. After fixation, cells were examined by microscopy as described in *Materials and Methods*. Scale bar, 2 μm.

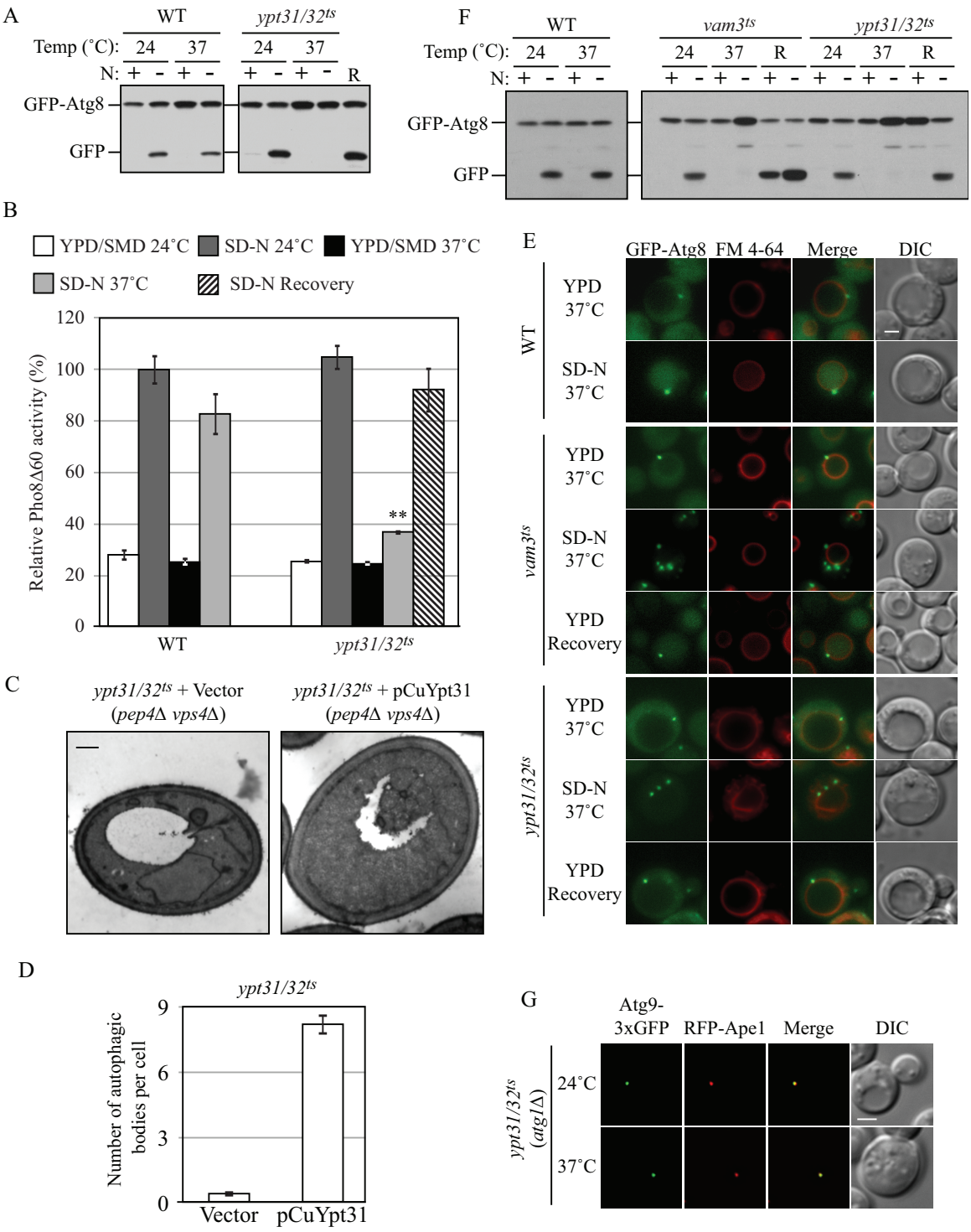

Figure 4.8 Autophagy defect and abnormal Atg8 localization in the *ypt31/32*^{ts} mutant. (A) GFP-Atg8 processing is blocked in the *ypt31/32*^{ts} mutant. Wild-type (NSY128) and *ypt31/32*^{ts} (NSY340) cells transformed with the pGFP-Atg8(316) plasmid were grown in SMD at 24˚C. Samples were collected after incubation at 24 or 37°C and examined as described in Figure 4.1 A. Recovery (R) refers to cells shifted back to 24°C after the 37°C incubation. (B) Pho8Δ60 assay in *ypt31/32*^{ts} mutant. Wild-type (JGY220) and

ypt31/32^{ts} (JGY209) cells were examined by the Pho8Δ60 assay. Error bar, SD of three independent experiments. Significant difference compared to wild-type, **p < 0.01. (C and D) On starvation, no autophagic bodies were accumulated in *ypt31/32*^{ts} cells. *ypt31/32*^{ts} *pep4*Δ *vps4*Δ (JGY222) cells harboring pCu416 or pCuYpt31(416) were cultured in SMD at 24˚C. After inactivation for 30 min, cells were starved for 2 h at the NPT. EM samples were prepared, and EM data were analyzed as described in Figure 4.3. (C) Representative EM images. Scale bar, 500 nm. The number of autophagic bodies was quantified and shown in D. Error bars represent SEM. (E and F) *ypt31/32*^{ts} is defective in Atg8 localization. Wild-type (JGY217), *vam3*^{ts} (JGY227), and *ypt31/32*^{ts} (JGY210) cells were cultured in YPD at 24°C, shifted to 37°C for 30 min, and subsequently starved at 37˚C. To recover the temperature-sensitive phenotype, *vam3*^{ts} and *ypt31/32*^{ts} cells were shifted back to 24°C and incubated in YPD or SD-N medium for another 2 h. (E) Representative fluorescence microscopy images. The vacuolar membrane was stained with FM 4-64 as described in *Materials and Methods*. For each condition, only one Z-section with a clearly defined vacuole was shown. Scale bar, 2 μm. (F) Samples taken at the indicated conditions were examined by immunoblotting using anti-YFP antibody. (G) Ypt31/32 are not involved in movement of Atg9 toward the PAS. *ypt31/32*^{ts} (Atg9-3xGFP RFP-Ape1 *atg1*Δ, JGY192) mutant cells were examined using the TAKA assay and the procedure was similar to that described in Figure 4.5 A. Scale bar, 2 μm.

In contrast to the *sec2* or *sec4* mutants, the *ypt31/32*^{ts} mutant appeared similar to the wild-type with regard to Atg9 localization. In the TAKA assay, at both the PT and NPT, *ypt31/32*^{ts} *atg1*Δ showed a single Atg9-3xGFP punctum colocalized with the PAS marker RFP-Ape1 (Figure 4.8 G). This result indicates that in the *ypt31/32*^{ts} mutant the Atg9 movement from peripheral sites to the PAS was not affected. In addition, we tested whether Atg9 was properly localized to its peripheral sites in *ypt31/32*^{ts} mutant cells. In starvation conditions, Atg9 was localized to multiple dots in the *ypt31/32*^{ts} mutant, and there was no clear difference between the localization patterns at the PT and NPT (Figure 4.S3 D). Therefore, the transport of Atg9 to its peripheral site does not require Ypt31/32-dependent vesicle exit from the *trans*-Golgi complex.

Discussion

In vesicle trafficking, Rab proteins and their downstream effectors coordinate consecutive steps of transport. In this paper we reported that a post-Golgi Rab protein (Sec4) and its GEF (Sec2) both participate in the autophagy pathway. Our data suggest that the Sec2-mediated nucleotide exchange on Sec4 (from the GDP- to GTP-bound form) is essential for autophagy. Dysfunction of either protein resulted in a substantial reduction in autophagy. In addition, the GDP-bound mutant of Sec4 shows a dominant-negative effect on autophagy, which further confirms its involvement in autophagy as a GTPase.

Sec4 and Sec2 as well as their downstream effectors during exocytosis have been studied extensively. By interacting with one of the exocyst complex components, Sec15, Sec2 and Sec4 direct the polarized transport of secretory vesicles toward the plasma membrane [179]. In addition to Sec15, another effector protein of Sec4, Sro7, has also been identified [180]. However, it remains unknown whether there is an autophagy-specific effector of Sec4. Sec15 can be excluded since it is dispensable for autophagy [152], and we also confirmed this result. The effector-binding domain on Sec4, which is essential for Sec4-Sec15 interaction, is required for autophagy (a *sec4* allele harboring a mutation in this domain could not complement the autophagy defect in *sec4-8*; our unpublished data). On the basis of this finding, we speculate that an autophagy-specific effector can compete with Sec15 by binding the same region on Sec4 and switch the function of Sec2-Sec4 to the autophagy pathway. *sec2-59* and *sec2-78* show a stronger interaction with Sec15 compared to the wild-type form of Sec2 [181]; thus, it is possible

that the secretion and autophagy defect in these two mutants is due to an insufficient pool of free Sec2.

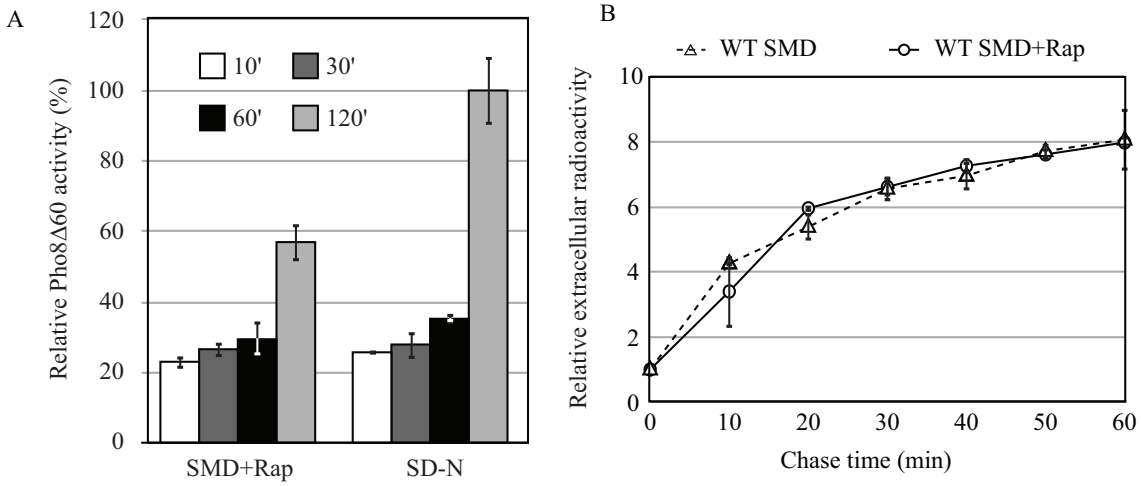

Figure 4.S4 Protein secretion is not regulated by rapamycin treatment. (A) Induction of autophagy by rapamycin treatment. A Pho8Δ60 strain (TN124) were treated with 0.8μg/ml rapamycin or incubated in SD-N medium. Pho8Δ60-dependent alkaline phosphatase activity was measured as described in *Materials and Methods*. Error bar, SD from three independent experiments. (B) Rapamycin treatment has no effect on the kinetics of protein secretion. After [^{35}S] labeling, cells were chased in SMD medium with or without 0.8 μg/ml rapamycin. Protein secretion was quantified as described in Figure 4.7 B. Error bar, SD from three independent experiments.

We observed a down-regulation of protein secretion during starvation conditions. Because there are several molecular factors shared between secretion and autophagy, one simple explanation is that starvation-induced autophagy competes for machinery that it uses in common with the secretory pathway. If the "competition" model is correct, it can be predicted that protein secretion will also be reduced when autophagy is triggered by other stimuli besides starvation. The Tor inhibitor rapamycin can clearly activate the autophagy pathway, although its magnitude is lower than starvation-induced autophagy (Figure 4.S4 A). According to the "competition" model, the level of protein secretion in rapamycin-treated cells will be lower than control cells, but higher than starved cells.

However, when cells were treated with rapamycin, the kinetics of protein secretion was not affected (Figure 4.S4 B). Therefore, the inhibition of protein secretion during starvation is not due to simple competition between two parallel pathways. In mammalian cells secretion is also inhibited under conditions of amino acid depletion [182], suggesting a conserved mechanism in various species that turns off secretion in response to nutrient shortage.

Atg9 movement to the PAS is speculated to represent the membrane flow from potential membrane sources toward the autophagosome formation site [62], and the amount of Atg9 affects the number of autophagosomes. On the other hand, the amount of Atg8 at the PAS is proposed to regulate membrane extension and determine the size of autophagosomes [79]. In *sec2* cells, Atg9 trafficking toward the PAS is defective, whereas the Atg8 protein level at the PAS ultimately attains that of the wild type (although the total number of cells with Atg8 puncta is substantially reduced). The combination of these two phenotypes results in the formation of fewer autophagosomes with normal size, as indicated by our EM analysis. During PAS assembly, Atg8 recruitment occurs at a relatively late stage [89]. Thus, the lower percentage of Atg8 puncta-positive cells in the *sec2* mutant may be a consequence of the defect in Atg9 transport to the PAS. Although the overexpression of Sec4 rescues Atg9 movement in the TAKA assay, it only increases the percentage of Atg8 puncta-positive cells slightly (our unpublished data). Because the TAKA assay mainly examines the anterograde movement of Atg9, it is possible that the proper cycling of Atg9 is not fully restored by Sec4 overexpression. This may explain why autophagy activity in *sec2* mutants is not restored by Sec4 overexpression.

A surprising result in our analysis was the finding that the *ypt31/32*^{ts} double mutant does not show an Atg9 localization defect. This result suggests that Atg9 may not exit from the post-Golgi en route to the PAS (Figure 4.8 D). Although the transport of Atg9 to the PAS is less efficient in *sec2* and *sec4* mutants, we still observed part of the Atg9 population colocalizing with, or in proximity to, mitochondria based on fluorescence microscopy. In contrast, in the *sec2* and *sec4* mutants there was no clear colocalization between Atg9 and Vrg4, a marker protein of the early Golgi. These results suggest that Sec2-Sec4 function is only required for Atg9 movement from peripheral sites toward the PAS during autophagy, but is not necessary for its transport through the late secretory pathway and localization to the peripheral sites. Nonetheless, it is not clear how Sec2 and Sec4 facilitate Atg9 movement.

During autophagosome formation, a continuous supply of lipid is necessary, and multiple membrane sources may be used. In this study, our results suggest that the Golgi apparatus may be, at least one of, the membrane source(s) for autophagosome formation through the action of Sec2-Sec4. Ypt31/32, involved in exit from the post-Golgi, were also required for autophagy, and other independent lines of evidence strengthen this hypothesis. For example, the COG complex and Sec7, which are essential for Golgi function, both participate in autophagy [153-155]. In mammalian cells, a Golgi Rab protein, Rab33B, interacts with Atg16L and shows some colocalization with Atg16L and LC3 (the mammalian homolog of Atg8) [183]. All these data suggest membrane flow from the Golgi to the PAS. There are at least two possibilities as to how the Golgi provides lipid flow to the PAS: 1) The Golgi-derived membrane first reaches an Atg9-positive structure and then is delivered to the PAS in an Atg9-dependent manner, or 2)

the Golgi directly supplies membrane to the PAS. In any case, the emergence of vesicles from the post-Golgi may occur in a Ypt31/32-dependent manner, with the movement of membrane containing Atg9 dependent upon Sec2-Sec4. It is possible that multiple membrane sources are required for different stages of autophagy and/or that the various sites of membrane mobilization involve distinct sets of proteins. Further analysis needs to be carried out to elucidate the contributions of each organelle to autophagosome formation.

Acknowledgements

The authors thank Dr. Lucy C. Robinson (Louisiana State University Health Sciences Center) and Dr. Charlie Boone (University of Toronto) for providing strains and Dr. Zhiping Xie (Nankai University, China) for constructing the *vam3*^{ts} integrating plasmid. This work was supported by National Institutes of Health Public Health Service grant GM53396 to D.J.K.

Table 4.1 Yeast strains used in this study

Name	Genotype	Reference
BY4742	*MATa his3Δ leu2Δ lys2Δ ura3Δ*	Invitrogen
FRY143	SEY6210 *vps4Δ::TRP1 pep4Δ::LEU2*	[88]
HAY572	TN124 *atg1Δ::URA3*	[165]
HCY76	*SEY6210 vps4ΔTRP1 pep4Δ::Kan atg1Δ::URA3*	[75]
JGY107	*sec2-41 ATG9-3xGFP::URA3 RFP-APE1::LEU2 atg1Δ::ble*	This study
JGY112	TN124 *sec2-59-PA::Kan*	This study
JGY113	SEY6210 *sec2-59-3HA::Kan*	This study
JGY124	SEY6210 *SEC2::TRP1*	This study
JGY125	SEY6210 *sec2-78::TRP1*	This study
JGY126	SEY6210 *sec2(Δ451-508)::TRP1*	This study
JGY127	TN124 *SEC2::TRP1*	This study
JGY128	TN124 *sec2-78::TRP1*	This study
JGY129	TN124 *sec2(Δ451-508)::TRP1*	This study
JGY146	SEY6210 *GFP-ATG8::LEU2*	This study
JGY159	*sec4-8 pho8Δ60::URA3 pho13Δ::ble*	This study
JGY166	LRB939 *pho8Δ60::URA3 pho13Δ::ble*	This study
JGY168	LRB932 *pho8Δ60::URA3 pho13Δ::ble*	This study
JGY169	SEY6210 *GFP-ATG8::LEU2 vam3^{ts}::TRP1*	This study
JGY171	SEY6210 *GFP-ATG8::LEU2 vam3^{ts}::TRP1 sec2-41-3HA::HIS3*	This study

JGY172	SEY6210 *GFP-ATG8::LEU2 vam3^{ts}::TRP1 sec2-59-3HA::HIS3*	This study
JGY180	SEY6210 *vps4Δ::TRP1 pep4Δ::LEU2 sec2-59-3HA::Kan*	This study
JGY183	SEY6210 *GFP-ATG8::LEU2 sec2-59-3HA::Kan*	This study
JGY184	SEY6210 *GFP-ATG8::LEU2 sec2-41-3HA::Kan*	This study
JGY192	NSY340 *ATG9-3xGFP::URA3 RFP-APE1::LEU2 atg1Δ::ble*	This study
JGY197	BY4742 *ATG9-3xGFP::URA3 RFP-APE1::LEU2 atg1Δ::Kan*	This study
JGY198	*sec4-8 ATG9-3xGFP::URA3 RFP-APE1::LEU2 atg1Δ::ble*	This study
JGY207	NSY340 *ATG9-3xGFP::URA3 RFP-APE1::LEU2*	This study
JGY209	NSY340 *pho8Δ60::URA3 pho13Δ::ble*	This study
JGY210	NSY340 *GFP-ATG8::LEU2*	This study
JGY217	NSY128 *GFP-ATG8::LEU2*	This study
JGY220	NSY128 *pho8Δ60::URA3 pho13Δ::ble*	This study
JGY222	NSY340 *pep4Δ::LEU2 vps4Δ::ble*	This study
JGY227	NSY128 *trp1Δ::Kan vam3^{ts}::TRP1 GFP-ATG8::LEU2*	This study
LRB932	LRB939 *sec4-2*	[184]
LRB939	*MATa his3 leu2 ura3-52*	[184]
NSY128	*MATa ade2 his3Δ200 leu2-3,112 lys2-801 ura3-52*	[177]
NSY340	*MATa leu2-3,112 lys2-801 ura3-52 ypt31Δ::HIS3 ypt32^{A141D}*	[185]
sec2-41	BY4742 *sec2-41*	This study
sec4-8	BY4742 *sec4-8*	This study
SEY6210	*MATa ura3-52 leu2-3,112 his3-Δ200 trp1-Δ901 lys2-801 suc2-Δ9 mel GAL*	[147]

TN124	*MATa leu2-3,112 trp1 ura3-52 pho8::pho8Δ60 pho13Δ::LEU2*	[148]
YTS158	BY4742 *pho8::pho8Δ60 pho13Δ::Kan*	[65]

Chapter V. Conclusion

Autophagy is a ubiquitous degradative pathway that mediates the vacuole/lysosome-dependent turnover of cytosolic components in various eukaryotes. Autophagy occurs in a step-wise manner: 1) Induction of autophagy, usually by stress conditions; 2) formation of the double-membrane autophagosome; 3) docking and fusion between the autophagosomes and vacuole/lysosome; and 4) degradation of autophagic bodies together with their contents followed by releasing of the degradation products back to the cytoplasm for reuse [10]. Substantial progress has been made in elucidating the mechanism of autophagosome formation [54]. A well-accepted model of this process can be described as involving a small crescent-shaped phagophore that expands gradually, probably by addition of small vesicles, and eventually matures into a completed autophagosome that sequesters cytoplasm. My research has been focusing on two questions in this process: 1) How is autophagosome formation quantitatively regulated? Our results provided some new insight to answer this question and established a quantification method, which has many prospective applications in other related work; 2) What is the membrane source in the autophagy pathway? We identified the Golgi as a possible membrane source in autophagy and showed that the post-Golgi membrane flow can be redirected to autophagy during starvation conditions.

Quantitative regulation of vesicle formation during specific and nonspecific autophagy

In Chapter III, we tried to study the autophagosome formation process from an unconventional angle. While most previous research on autophagy provided information such as the function of a particular protein, the physiological role of protein-protein interactions or the composition of a protein complex, we used a fluorescence microscopy-based method to study to the quantitative property of Atg proteins during autophagy. In both specific and nonspecific autophagy, the vesicle formation process is under precise control. With our quantitative method, we brought some new insight into understanding how the size and number of autophagic vesicles are quantitatively regulated.

In nonspecific autophagy, the number and the size of autophagosomes must coordinate to ensure the appropriate level of autophagy. If the autophagosome is too small, the cells have to produce more autophagosomes at this size to achieve the same autophagy magnitude, which is an energy-inefficient and unfavorable process, especially when the cells are facing nutrient limitation. If the cells are generating oversized autophagosomes, excessive autophagy activity may disrupt the intracellular homeostasis and eventually damage the cells [186]. On the other hand, in specific autophagy, the vesicle size is also accurately controlled to accommodate efficient and exclusive packing of various cargoes. For instance, compared to starvation-induced autophagosomes, *Saccharomyces cerevisiae* cells make smaller Cvt vesicles during nutrient-rich conditions [29], whereas mammalian cells can produce bigger autophagosomes in response to group A *Streptococcus* invasion [128]. What is the adaptive mechanism behind all these interesting phenomena? Taking advantage of our method to quantitatively analyze the

fluorescence microscopy data, we showed that Atg8 and Atg9 are two critical factors for the regulation of vesicle formation. Atg8 is a ubiquitin-like protein that is covalently conjugated to phosphatidylethanolamine [56]. Atg9 is an integral membrane protein that shuttles between the PAS and peripheral membrane structures [60]. When the autophagy machinery is switched from the Cvt pathway to nonspecific autophagy, we observed that the amount of Atg8 and Atg9 at the PAS increases substantially while that of other Atg proteins remains relatively unchanged during this switch. Corresponding to this change, bigger autophagosomes are formed rather than smaller Cvt vesicles. In addition, a reduced Atg8 level at the PAS leads to the formation of smaller autophagosomes [79]. Accordingly, we speculate that Atg8 may function as a scaffold factor supporting phagophore expansion during nonspecific autophagy. Atg9, on the other hand, may bring lipid to the PAS, and enhanced Atg9 anterograde movement represents a higher level of membrane supply to autophagosome formation. Consequently, reduced Atg9 anterograde movement in *atg27*Δ and *sec2-41* mutants limits the membrane supply so that fewer autophagosomes are formed (see Chapter IV) [64]. In the Cvt pathway, moderate overexpression of Atg11 recruits more Atg8 and Atg9 to the PAS and as a result more Cvt vesicles are formed. In this condition, the size of the Cvt vesicles is mainly determined only by the size of the cargo, the Cvt complex.

Using this method, for the first time we can visualize the autophagosome formation process in a real-time manner. Among the core machinery for autophagosome formation, Atg8 is the only one that associates with both the phagophore and the formed autophagosome. In a time-lapse experiment, we recorded a periodical change of Atg8 amount at the PAS. After the factors required for Atg8 PAS localization arrive at the

PAS, the Atg8 punctum emerges at the PAS and its fluorescence intensity increases corresponding to the expansion of an Atg8-containing phagophore. After reaching the maximal level, the Atg8 signal gradually decreases and eventually fades out with the degradation of the autophagic body within the vacuolar lumen. One cycle of Atg8 recruitment/dissociation represents the formation of one autophagosome. Besides our intensity-based method, another fluorescence microscopy method has also been established by Dr. Jennifer Lippincott-Schwartz's laboratory to pulse-label autophagosomes and monitor their turnover in mammalian cells [187].

There were many arguments concerning which protein or protein complex is the coat protein that imposes curvature upon the expanding phagophore. The Atg12–Atg5-Atg16 complex is associated with the expanding phagophore but dissociates from the completed autophagosome [5,111], which makes it a possible candidate as the coat protein. Nevertheless, our quantification analysis showed that the amount of the Atg12–Atg5-Atg16 complex at the PAS is extremely low. Among all the examined Atg proteins, Atg8 has the highest fluorescence intensity at the PAS. Given its function in regulating phagophore expansion, Atg8 may be a better candidate coat protein. Further analysis is needed to figure out how Atg8 supports membrane expansion and even prevents premature closure of the phagophore.

The Golgi as potential membrane source for autophagosome formation

An important missing piece in the autophagosome formation puzzle is where the membrane comes from. The induction of autophagy is robust and rapid in response to environmental changes. Local lipid synthesis may not be sufficient to generate enough

lipids. Thus, the lipids for autophagosome formation probably come from some pre-existing membrane structure(s) that continuously supply lipids to support phagophore expansion. Nevertheless, the major difficulty to solve is that autophagosomes are almost depleted of any organelle-specific protein markers [149,151]. For this reason, there has been a long-standing debate between two alternative models: 1) A maturation model in which the autophagosome membrane is directly derived from membrane-bound organelles; or 2) An assembly model in which the autophagosome is *de novo* assembled at its formation site, although its constituents may still originate from existing organelles.

The membrane source in mammalian autophagy

In mammalian cells, the early autophagic structure that corresponds to the phagophore is also called the isolation membrane. The ER has been proposed as a membrane source of the phagophore by the maturation model. This hypothesis is supported by the identification of ER proteins on the forming autophagosomes [188]. In epithelial cells, the phagophores are frequently observed between cisterns of rough ER [189]. Recently, electron tomography showed that the ER is interconnected with phagophores, and a subdomain of the ER forms a cradle-like structure to encircle the forming autophagosome [190,191]. However, some studies showed conflicting observations in that the phagophore lacks ER-resident proteins [151,192]. Moreover, real-time analysis showed that the phagophores continue to expand until the final completion of autophagosomes, which supports the assembly model rather than maturation model [5]. Besides the ER, other organelles have been speculated to serve as a membrane source, but there is still a lot of discrepancy. For example, in some cases Golgi markers were present on forming

autophagosomes, but other studies failed to detect them [188,193]. Lipid transfer from mitochondria to the forming autophagosome has also been shown, which suggests the implication of mitochondria in mammalian autophagy [194].

The membrane source in yeast autophagy

Similar to the situation in mammalian cells, in *S. cerevisiae* there is no clear answer to the question of the membrane source in autophagy. The assembly model is preferred in yeast autophagy, because the identification of Atg9 cycling between the PAS and peripheral membrane structures suggests the vesicular transport of lipids to the expanding phagophore [60,62]. Again, various membrane-bound organelles have been proposed to provide membrane in the autophagy pathway. Atg9 partially localizes on/adjacent to mitochondria under fluorescence microscopy [60]. Ultrastructural analysis showed that the Atg9-possitive structures are clusters of vesicles and tubules adjacent to mitochondria. These clusters may translocate to the PAS during starvation conditions (personal communication with Dr. Fulvio Reggiori). Therefore, these mitochondria-related structures may contribute to autophagosome formation.

In addition, autophagy is defective in some mutants of the early stage of the secretory pathway that is essential for ER-to-Golgi transport, suggesting the ER may contribute to autophagosome formation as a membrane source [152,153,175]. Subsequent studies, however, cast some arguments against this proposition, suggesting that it may be just an indirect effect if an autophagy-essential protein is transported through the secretory pathway. Thus, researchers will have to differentiate whether the membrane flow or the secretory pathway protein flow is required for autophagy. For instance, a

subset of the COPII complex (Sec16, Sec23, and Sec24), but not the rest (Sec13 and Sec31), is essential for autophagy [152]; correspondingly, secretory flow is normal in *sec13* or *sec31* during starvation conditions [195]. Overexpression of Sfb2 can restore secretory flow in *sec24* and also suppress the autophagy defect in this mutant [195]. So the COPII complex and Sec24 may not directly function in autophagy. Even so, some early secretory components may directly participate in autophagosome formation. For example, in *ypt1-1* mutant yeast, ER-to-Golgi transport is normal at permissive temperature but blocked only at nonpermissive temperature, while autophagy is defective at both permissive and nonpermissive temperatures, suggesting there may be an ER-derived membrane flow committed to autophagy in a Ypt1-dependent manner [175].

Yeast Golgi and autophagy

The Golgi apparatus is an intricate network of cisternae, tubules and associated vesicles. Golgi-derived vesicles are sorted toward the plasma membrane and other intracellular organelles. In our analysis, we identified two post-Golgi Sec proteins essential for autophagy and proposed that membrane flow from the Golgi can be redirected to the PAS for autophagosome formation (Figure 5.1). Compared to the early Sec proteins published previously, Sec2 and Sec4 may have a more direct function during autophagosome formation. Based on our current knowledge, Sec4, a Rab GTPase, and its GEF, Sec2, are only involved in the polarized sorting of secretory vesicles from the Golgi to the active growing site on the plasma membrane (PM) [160,161,170,196,197]. The Golgi-to-PM secretory flow is not required for autophagy, because protein secretion is downregulated to a very low level when autophagy is substantially induced by starvation conditions. For

this reason, the autophagy defect in *sec2* and *sec4* mutants is not due to a block of secretion, and the normal function of Sec2 and Sec4 is necessary for autophagy.

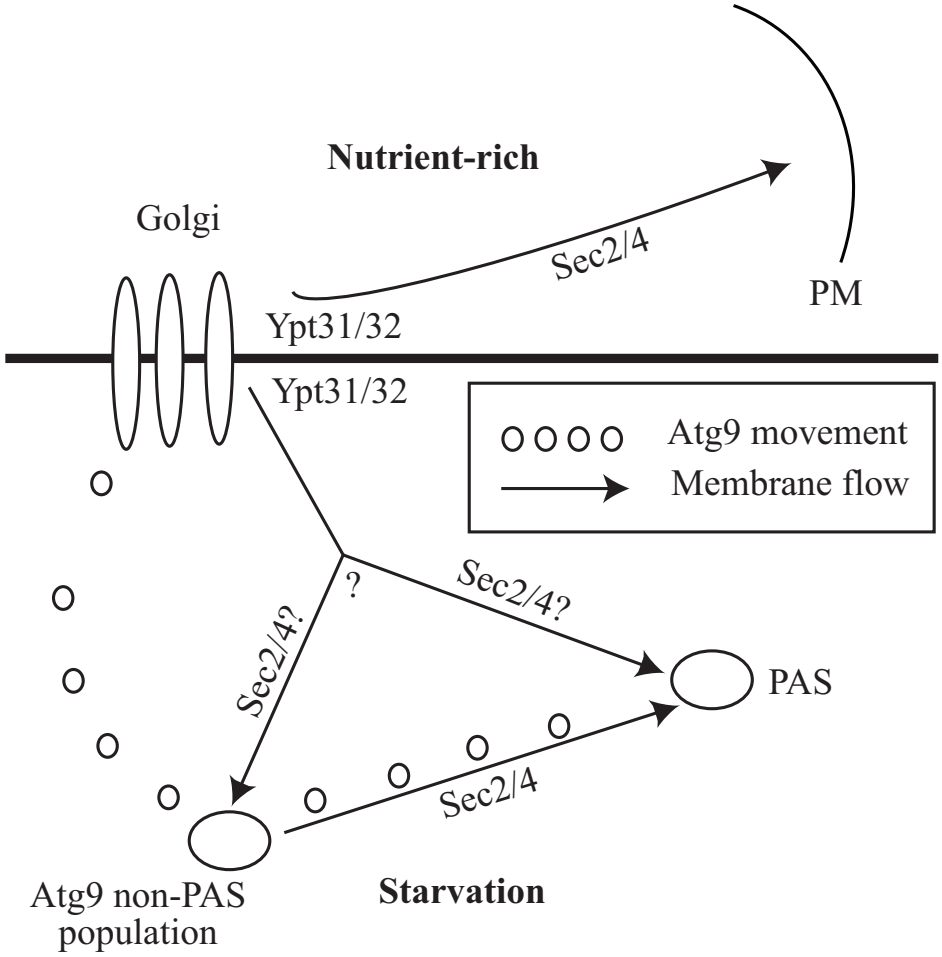

Figure 5.1 Working model of Sec2 and Sec4 in autophagy. In nutrient-rich conditions, Sec2 and Sec4 are associated with secretory vesicles and mediate transport to the plasma membrane. In starvation conditions, Sec2 and Sec4 facilitate the anterograde movement of Atg9 from peripheral sites to the PAS. Ypt31/32 are required for vesicle budding from the post-Golgi and autophagy, but not for the proper localization of Atg9. Golgi-derived membrane flow may be directed toward the PAS during starvation, but it is not clear whether it occurs independent of Atg9.

In the present model, Atg9 is speculated as a membrane carrier. Its movement to the PAS may represent membrane supply from a membrane source to participate in autophagosome formation. In both *sec2* and *sec4* mutants, Atg9 transport to the PAS is

less efficient, suggesting the membrane supply is limited in these mutants. Accordingly, autophagosome formation is severely diminished in the *sec2* mutant. Sec2 and Sec4 are associated with secretory vesicles during exocytosis [170,198]. They may be recruited to the Atg9-possitive vesicles and direct these vesicles to the PAS, which is still far from proven. Affinity isolation assay showed a weak interaction between Atg9 and Sec2 (unpublished data), but we failed to detect any Atg9-Sec2 colocalization under fluorescence microscopy, suggesting the possibility that the Sec2-Atg9 interaction may be weak and transient.

Besides the involvement of Sec2 and Sec4 in autophagy, additional evidence also implies the possible role of the Golgi apparatus in autophagosome formation. The conserved oligomeric Golgi (COG) complex is involved in retrograde intra-Golgi trafficking and probably in ER-to-Golgi transport [199-201]. Recently, it is reported that subunits of the COG complex are required for vesicle formation in both the Cvt and autophagy pathway [155]. Additionally, Sec7, a late Golgi GEF protein essential for the secretory pathway [202], is also indispensible for autophagy [153]. Further analysis showed that Sec7 participates in autophagy by acting on Arf GTPase, suggesting exit from the Golgi is necessary for phagophore expansion (personal communication with Dr. Fulvio Reggiori). Given our data on post-Golgi Sec proteins, it strongly indicates Golgi-derived membrane flow is switched from exocytosis to the autophagy pathway during starvation conditions.

As a conclusion, multiple membrane sources may be implicated in autophagosome formation. Blockage of membrane supply from any one of these sources leads to a failure in vesicle formation, suggesting the function of multiple membrane sources is not

redundant. It is possible that different membrane sources may participate in different stages of autophagosome formation. In addition, we found that at least four proteins, Sec2, Sec4, Ypt31 and Ypt32, are shared between exocytosis and autophagy. In biological systems, it is common that two distinct processes share some particular components, especially when these processes do not occur at the same time. The main function of Golgi-to-PM membrane flow is to support the growth of daughter cells, while this is not necessary when cell growth is halted in response to nutrient depletion. Therefore, late stage Sec proteins can be involved in different biological pathways as an adaptation to environmental changes.

There are still many unsolved questions regarding how Golgi-derived membrane participates in autophagy. For instance, there is no direct evidence showing lipid transport from the Golgi to the PAS. More advanced technologies in lipid labeling may be useful to monitor lipid redistribution when autophagy is induced. In addition, it is not clear how Sec4 recognize the PAS. What is the effector protein(s) of Sec4 at the PAS? Is there any downstream SNARE complex involved in the expansion or closure of the phagophore? Further analysis is needed to answer all these questions.

Appendix A. Determining Atg protein stoichiometry at the PAS by fluorescence microscopy

Summary

In eukaryotic cells, autophagy is a lysosomal/vacuolar degradative pathway necessary for the turnover of different macromolecules. Autophagy is under precise regulation, not only qualitatively but also quantitatively, and excess or reduced levels of autophagy may lead to various human diseases. In yeast, genetic screens led to the identification of more than 30 autophagy-related (*ATG*) genes, and most of them reside at the phagophore assembly site (PAS). However, our attempt to understand the quantitative properties of autophagy is usually hampered, because traditional methods of analysis cannot provide stoichiometric information. We have recently used a fluorescence microscopy-based method to study the stoichiometry of Atg proteins at the PAS, trying to explain the mechanism of how the vesicle formation process is precisely regulated. This article describes a practical guide on this method. Its application and further analysis will improve our understanding of the quantitative properties of autophagy.

1. Introduction

Ever since its initial discovery, the green fluorescent protein (GFP) has substantially changed the research methodology of modern biology. By fusing GFP and its various derivatives to other interesting, but otherwise invisible proteins, researchers can "watch" the positions, movements and interactions of tagged proteins in different conditions. The application of fluorescent protein methodologies is still expanding. Recently, Wu and Pollard reported that protein concentration can be directly measured by fluorescence microscopy in *Schizosaccharomyces pombe* [134]. Inspired by their results, we applied similar methods in *Saccharomyces cerevisiae* to study the stoichiometry of Atg proteins during the vesicle formation process [127].

This method is feasible and useful in the study of autophagy. First, most Atg proteins localize to a very restricted region, the phagophore assembly site (PAS, also known as pre-autophagosomal structure) [52,53]. This property makes the quantification process much easier. Second, it is also important to know the stoichiometry of Atg proteins at this locus. The PAS is thought to be the organization center for the formation of the Cvt vesicle and autophagosome. Multiple lines of evidence has pointed out that the amount of some Atg proteins (e.g., Atg8 and Atg9) at the PAS is under precise regulation and related to the quantitative property of the vesicle formation process, such as vesicle size or vesicle number [64,65,79]. However, traditional methods cannot provide information on the quantitative analysis of Atg proteins at a specific subcellular locus. In contrast, this fluorescence microscopy method can directly measure the protein amount in living cells and even in a time-course experiment.

In this protocol article, we described the method to quantify the amount of Atg

proteins at the PAS. Theoretically we can use this method to measure the protein amount at any subcellular localization. In our analysis of Atg proteins, the PAS is the clearest structure for fluorescence quantification. The method can be divided into two basic parts. The first part is to establish a standard curve showing the linear relationship between fluorescence intensity and protein amount; the second part is to use this standard curve to measure and calculate the protein amount at the PAS. In some cases, relative quantification provides sufficient information, for example, in asking how does the Atg8 concentration at the PAS change in different conditions, or what are the kinetics of Atg8 recruitment to the PAS? In this situation, after confirming the linear relationship between the protein amount and fluorescence intensity, it is possible to simply measure the relative intensity and convert it into relative protein amount without determining the absolute value.

2. Materials

2.1. Cells and culture

1. Cells: Choose a set of proteins with different expression levels and tag them to GFP, e.g., A-GFP, B-GFP, C-GFP, etc (*see* **Notes 1-3**), which will be used to set up the standard curve. For the proteins of interest, also fuse them to GFP.
2. Growth medium (YPD): 1% yeast extract, 2% peptone, and 2% glucose. This medium is stable for months at room temperature.
3. Synthetic minimal medium (SMD): 0.67% yeast nitrogen base, 2% glucose and auxotrophic amino acids and vitamins as needed. This medium is stable for months at room temperature.

4. Starvation medium (SD-N): 0.17% yeast nitrogen base without ammonium sulfate or amino acids, containing 2% glucose. This medium is stable for months at room temperature.

2.2. Standard protein: GST-GFP

1. Clone the ORF of GFP(S65T) into pGEX-4T-1 (GE Healthcare, 27-4580-01) and express it in *E. coli* strain BL-21. Follow a standard protein purification protocol to purify the fusion protein on glutathione-Sepharose beads (GE Healthcare, 17-0756-01).
2. Measure the concentration of purified protein (in ng/μl) using the bicinchoninic acid (BCA) assay (Pierce Chemical Co., 23223 and 23224) and convert the concentration to mol/μl ([mol/μl] = [ng/μl]*10^{-9}/$MW_{GST-GFP}$, $MW_{GST-GFP}$=54808.7).

2.3. Microscopy

1. Samples are examined with an inverted fluorescence microscope (DeltaVision Spectris; Applied Precision, LLC or equivalent equipments).
2. Microscopy images are analyzed and quantified using softWoRx (Applied Precision, LLC) or equivalent software.
3. Concavity slides (Fisher, S175201) for time-course experiments.

2.4. Antibody

1. Living colors A.v. monoclonal antibody JL-8 (Clontech, 632381).

3. Methods

3.1. Standard curve: linear relationship between protein amount and fluorescence intensity

3.1.1. Measure fluorescence intensity per cell

1. Yeast strains expressing GFP-tagged proteins (A-GFP, B-GFP, C-GFP, etc.) are cultured in 5 ml YPD medium at 30°C in test tubes. Cells are grown to log phase, then diluted, and cells are then regrown to early log-phase (A_{600} = 0.6-0.8). For experiments under starvation condition, cells are shifted to SD-N medium and cultured at 30°C for another 2 h.
2. Harvest 1 ml culture. Centrifuge at 3,000 rpm for 2 min to pellet the cells. If time permits, an additional aliquot of cells is collected to determine the amount of GFP-fusion protein per cell (*see* section 3.1.2).
3. The supernatant fraction is discarded. The cell pellet is washed with 1 ml SMD medium without vitamins (*see* **Notes 4 and 5**) and centrifuged again.
4. Discard the supernatant fraction and resuspend the pellet fraction in 30 µl SMD medium (*see* **Note 5**).
5. Mount 5 µl of sample on a microscope slide and cover it with a coverslip. Press the coverslip down gently.
6. Observe by fluorescence microscopy and take pictures. For each picture, take 12 Z-section images at a 0.5 µm interval (*see* **Note 6**).
7. Deconvolve the images.
8. In softWoRx software, go to "View → Quick Projection". Input 12 Z-section images and stack them into a 2-D image using "sum projection".

9. Open the projected image. Go to "Tool → Data Inspector". Draw a circle with the proper size to cover the whole yeast cell. Record the "Total" intensity within this region.
10. Quantify the fluorescence intensity of wild-type cells in which no GFP-fusion protein is expressed. Use this value as the autofluorescence background. Subtract the background from the "Total" value obtained in the previous step.
11. For each strain (A-GFP, B-GFP, C-GFP, etc.), quantify 200 cells. Calculate the mean value and SEM. (standard error of the mean: standard deviation divided by the square root of the sample size).

3.1.2. Measure amount of GFP-fusion protein per cell

1. Culture cells (A-GFP, B-GFP, C-GFP, etc.) under the same condition as used for the microscopy experiments. Harvest 1 OD_{600} unit of cells (equivalent to 1 ml of culture at A_{600} = 1.0). Ideally, these samples should be collected at the same time that the cells are prepared for the microscopy analysis, using the same culture (section 3.1.1).
2. Resuspend in 10% TCA. Keep on ice for 30 min (the samples can also be stored at 4°C or -20°C for later processing).
3. Centrifuge at 13,000 rpm for 5 min at 4°C. Discard the supernatant fraction.
4. Add 1 ml ice-cold acetone. Resuspend by sonication, using a water bath sonicator to disrupt the pellet fraction.
5. Centrifuge at 13,000 rpm for 5 min at 4°C. Discard the supernatant fraction. Dry the pellet fraction on ice.
6. Add 50 µl 1x SDS sample buffer (equivalent to 0.02 OD_{600} cell/µl) and 0.4-0.6 mm

acid washed soda lime glass beads. Glass beads are prepared as described previously [203].

7. Mix on a vortex at 4°C for 5 min. Incubate at 85˚C for 5 min (*see* **Note 7**). Centrifuge at 13,000 rpm for 1 min at 4°C.
8. Load an appropriate amount of the cell lysate sample for SDS-PAGE. On the same gel, also load a concentration gradient of standard protein, GST-GFP (*see* **Note 8**).
9. Follow a standard protocol to do western blotting. Use YFP antibody and overnight incubation. After development with appropriate exposure (*see* **Note 9**), scan the film.
10. Quantify the band intensity using NIHimage (*see* **Note 10**). Compare the band intensity of the GFP fusion protein with the GST-GFP standard protein to determine the protein concentration in mol/OD_{600} units of cells.
11. Repeat the western blot and quantification three times. Calculate the mean value and SEM.
12. Convert the protein concentration into molecules/cell by multiplying by Avogadro's number and dividing by the number of cells per OD_{600}.

3.1.3. Standard curve: fluorescence intensity vs. protein amount

1. For A-GFP, B-GFP, C-GFP, etc. plot the fluorescence intensity against the protein amount (X axis: molecules/cell; Y axis: intensity/cell).
2. Set intercept to 0 (*see* **Note 11**) and do linear regression. The slope corresponds to the ratio between fluorescence intensity and number of molecules.
3. Calculate R^2 to evaluate the fit of the line (*see* **Note 12**).

3.2. Use standard curve to calculate the concentration of Atg proteins at the PAS

1. Culture cells expressing the GFP fusion protein of interest. Choose the culture condition based on your specific aim.
2. Prepare microscopy sample and take pictures as described previously.
3. (Optional) In time-course experiments, prepare slides as follows: Add warm medium containing 1.8% agar into the concave region of a concavity slide. Cover it with a coverslip and wait until complete solidification of the agar. Remove the coverslip by "sliding" to get a smooth surface on the solidified agar. Mount your sample to this region and cover it with a new coverslip. Seal the edge of the coverslip with nail polish to avoid liquid evaporation. Take pictures at every time-point as described previously but with relatively short exposure times to minimize photobleaching. The effect of photobleaching can be determined empirically [127].
4. Deconvolve the images and make 2-D projections.
5. Draw a circle around the PAS dot. Record the intensity value.
6. Move the circle to an adjacent cytosolic region. Record the intensity as background.
7. Subtract the background value from the raw PAS intensity.
8. Use the slope obtained from the standard curve to convert the fluorescence intensity into number of molecules (*see* **Note 13**).
9. Repeat this quantification process. Calculate the mean and SEM.

Notes

1. It not necessary that A, B, C, etc. are different proteins as long as their expression level is different. For instance, in our initial study we used strains expressing GFP-

Atg8 driven by various promoters.

2. It is critical that the range of your standard curve is wide enough to cover the abundance of the protein you want to study. Large scale data on gene expression level [139] is available in the *Saccharomyces* Genome Database (www.yeastgenome.org), which can help you decide which protein to choose.
3. Chromosomal tagging is strongly suggested rather than using CEN plasmids because of the consistent expression level from cell to cell. If you tag the fluorophore to the C-terminus of your gene, the PCR-based method can be used as described by Longtine *el al* [142]. If C-terminal tagging is not feasible such as with Atg8, you should clone the N-terminal fusion protein into an integration plasmid and then integrate it into the yeast genome. In this case, the endogenous copy of the gene should be deleted to avoid changing the normal protein level. We found essentially identical results using either N- or C-terminal fusions; however, the function of the fusion protein should always be confirmed.
4. YPD medium produces a high autofluorescence background. For the same reason, do not add vitamin in SMD medium at this step.
5. Starved cells are washed and resuspended in SD-N medium to maintain the nutrient condition.
6. No more than three pictures should be taken on the same slide to minimize the effect of photobleaching. The total depth of each stack is 5.5 μm, which is the approximate diameter of a normal yeast cell. Focus to the middle plane of the cell.
7. For proteins such as Atg9, high temperature impairs its solubility. In such cases, incubate the protein samples at 55°C for 15 min.

8. It is critical to do pre-experiments in order to decide on the appropriate loading amount. To make sure the band intensity is in the linear range, use at least two concentrations of samples.
9. Prevent overexposure during development. Saturated bands significantly affect the quantification results.
10. Draw a rectangle big enough to cover one single western band. First, move the rectangle to a clear area on the film and measure the intensity, which is used for the background. Then move the rectangle to the band you want to quantify, measure the intensity and subtract the background. Other equivalent software such as ImageJ can also be used.
11. When the protein concentration is zero, we expect the fluorescence intensity to theoretically be zero as well.
12. The R^2 value varies from 0 to 1. An R^2 of 1.0 indicates that the regression line perfectly fits the data. There is no objective criteria to judge what value of R^2 is acceptable, although the R^2 values in similar studies showing the linearity between fluorescence intensity and protein amount are higher than 0.95 [127,134].
13. One obstacle for fluorescence quantification is that the measured intensity usually varies in repetitive experiments. Therefore, every time you want to quantify the absolute amount of a protein, it is important to include two proteins used in determining the standard curve (e.g., the two with the highest and lowest protein level) in the assay to calibrate the slope of the standard curve.

Acknowledgment

This work was supported by Public Health Service grant GM53396 to D.J.K. from the National Institutes of Health.

References

[1] de Duve, C. and Wattiaux, R. (1966). Functions of lysosomes. Annu Rev Physiol 28, 435-92.

[2] Takeshige, K., Baba, M., Tsuboi, S., Noda, T. and Ohsumi, Y. (1992). Autophagy in yeast demonstrated with proteinase-deficient mutants and conditions for its induction. J Cell Biol 119, 301-11.

[3] Klionsky, D.J., Cregg, J.M., Dunn, W.A., Jr., Emr, S.D., Sakai, Y., Sandoval, I.V., Sibirny, A.A., Subramani, S., Thumm, M., Veenhuis, M. and Ohsumi, Y. (2003). A unified nomenclature for yeast autophagy-related genes. Dev Cell 5, 539-45.

[4] Mizushima, N., Sugita, H., Yoshimori, T. and Ohsumi, Y. (1998). A new protein conjugation system in human. The counterpart of the yeast Apg12p conjugation system essential for autophagy. J Biol Chem 273, 33889-92.

[5] Mizushima, N., Yamamoto, A., Hatano, M., Kobayashi, Y., Kabeya, Y., Suzuki, K., Tokuhisa, T., Ohsumi, Y. and Yoshimori, T. (2001). Dissection of autophagosome formation using Apg5-deficient mouse embryonic stem cells. J Cell Biol 152, 657-68.

[6] Nishida, K., Kyoi, S., Yamaguchi, O., Sadoshima, J. and Otsu, K. (2009). The role of autophagy in the heart. Cell Death Differ 16, 31-8.

[7] Chen, N. and Debnath, J. (2010). Autophagy and tumorigenesis. FEBS Lett 584, 1427-35.

[8] Rubinsztein, D.C., DiFiglia, M., Heintz, N., Nixon, R.A., Qin, Z.H., Ravikumar, B., Stefanis, L. and Tolkovsky, A. (2005). Autophagy and its possible roles in nervous system diseases, damage and repair. Autophagy 1, 11-22.

[9] Yen, W.-L. and Klionsky, D.J. (2008). How to live long and prosper: autophagy, mitochondria, and aging. Physiology (Bethesda, Md) 23, 248-62.

[10] Reggiori, F. and Klionsky, D.J. (2005). Autophagosomes: biogenesis from scratch? Curr Opin Cell Biol 17, 415-22.

[11] Kunz, J., Henriquez, R., Schneider, U., Deuter-Reinhard, M., Movva, N.R. and Hall, M.N. (1993). Target of rapamycin in yeast, TOR2, is an essential phosphatidylinositol kinase homolog required for G1 progression. Cell 73, 585-96.

[12] Blommaart, E.F., Luiken, J.J., Blommaart, P.J., van Woerkom, G.M. and Meijer, A.J. (1995). Phosphorylation of ribosomal protein S6 is inhibitory for autophagy in isolated rat hepatocytes. J Biol Chem 270, 2320-6.

[13] Sattler, T. and Mayer, A. (2000). Cell-free reconstitution of microautophagic vacuole invagination and vesicle formation. J Cell Biol 151, 529-38.

[14] Kunz, J.B., Schwarz, H. and Mayer, A. (2004). Determination of four sequential stages during microautophagy in vitro. J Biol Chem 279, 9987-96.

[15] Muller, O., Sattler, T., Flotenmeyer, M., Schwarz, H., Plattner, H. and Mayer, A. (2000). Autophagic tubes: vacuolar invaginations involved in lateral membrane sorting and inverse vesicle budding. J Cell Biol 151, 519-28.

[16] Chiang, H.L., Terlecky, S.R., Plant, C.P. and Dice, J.F. (1989). A role for a 70-kilodalton heat shock protein in lysosomal degradation of intracellular proteins. Science 246, 382-5.

[17] Cuervo, A.M., Knecht, E., Terlecky, S.R. and Dice, J.F. (1995). Activation of a selective pathway of lysosomal proteolysis in rat liver by prolonged starvation. Am J Physiol 269, C1200-8.
[18] Massey, A.C., Kaushik, S., Sovak, G., Kiffin, R. and Cuervo, A.M. (2006). Consequences of the selective blockage of chaperone-mediated autophagy. Proc Natl Acad Sci USA 103, 5805-10.
[19] Kaushik, S., Massey, A.C., Mizushima, N. and Cuervo, A.M. (2008). Constitutive activation of chaperone-mediated autophagy in cells with impaired macroautophagy. Mol Biol Cell 19, 2179-92.
[20] Dice, J.F., Chiang, H.-L., Spencer, E.P. and Backer, J.M. (1986). Regulation of catabolism of microinjected ribonuclease A. Identification of residues 7-11 as the essential pentapeptide. J Biol Chem 261, 6853-9.
[21] Dice, J.F. (1990). Peptide sequences that target cytosolic proteins for lysosomal proteolysis. Trends Biochem Sci 15, 305-9.
[22] Agarraberes, F.A. and Dice, J.F. (2001). A molecular chaperone complex at the lysosomal membrane is required for protein translocation. J Cell Sci 114, 2491-9.
[23] Cuervo, A.M. and Dice, J.F. (1996). A receptor for the selective uptake and degradation of proteins by lysosomes. Science 273, 501-3.
[24] Bandyopadhyay, U., Kaushik, S., Varticovski, L. and Cuervo, A.M. (2008). The chaperone-mediated autophagy receptor organizes in dynamic protein complexes at the lysosomal membrane. Mol Cell Biol 28, 5747-63.
[25] Harding, T.M., Morano, K.A., Scott, S.V. and Klionsky, D.J. (1995). Isolation and characterization of yeast mutants in the cytoplasm to vacuole protein targeting pathway. J Cell Biol 131, 591-602.
[26] Hutchins, M.U. and Klionsky, D.J. (2001). Vacuolar localization of oligomeric α-mannosidase requires the cytoplasm to vacuole targeting and autophagy pathway components in *Saccharomyces cerevisiae*. J Biol Chem 276, 20491-8.
[27] Kim, J., Scott, S.V., Oda, M.N. and Klionsky, D.J. (1997). Transport of a large oligomeric protein by the cytoplasm to vacuole protein targeting pathway. J Cell Biol 137, 609-18.
[28] Scott, S.V., Baba, M., Ohsumi, Y. and Klionsky, D.J. (1997). Aminopeptidase I is targeted to the vacuole by a nonclassical vesicular mechanism. J Cell Biol 138, 37-44.
[29] Baba, M., Osumi, M., Scott, S.V., Klionsky, D.J. and Ohsumi, Y. (1997). Two distinct pathways for targeting proteins from the cytoplasm to the vacuole/lysosome. J Cell Biol 139, 1687-95.
[30] Klionsky, D.J., Cueva, R. and Yaver, D.S. (1992). Aminopeptidase I of *Saccharomyces cerevisiae* is localized to the vacuole independent of the secretory pathway. J Cell Biol 119, 287-99.
[31] Scott, S.V., Hefner-Gravink, A., Morano, K.A., Noda, T., Ohsumi, Y. and Klionsky, D.J. (1996). Cytoplasm-to-vacuole targeting and autophagy employ the same machinery to deliver proteins to the yeast vacuole. Proc Natl Acad Sci USA 93, 12304-8.
[32] Scott, S.V., Guan, J., Hutchins, M.U., Kim, J. and Klionsky, D.J. (2001). Cvt19 is a receptor for the cytoplasm-to-vacuole targeting pathway. Mol Cell 7, 1131-41.

[33] Leber, R., Silles, E., Sandoval, I.V. and Mazon, M.J. (2001). Yol082p, a novel CVT protein involved in the selective targeting of aminopeptidase I to the yeast vacuole. J Biol Chem 276, 29210-7.
[34] Shintani, T., Huang, W.-P., Stromhaug, P.E. and Klionsky, D.J. (2002). Mechanism of cargo selection in the cytoplasm to vacuole targeting pathway. Dev Cell 3, 825-37.
[35] Yorimitsu, T. and Klionsky, D.J. (2005). Atg11 links cargo to the vesicle-forming machinery in the cytoplasm to vacuole targeting pathway. Mol Biol Cell 16, 1593-605.
[36] Kim, I., Rodriguez-Enriquez, S. and Lemasters, J.J. (2007). Selective degradation of mitochondria by mitophagy. Arch Biochem Biophys 462, 245-53.
[37] Kanki, T. and Klionsky, D.J. (2008). Mitophagy in yeast occurs through a selective mechanism. J Biol Chem 283, 32386-93.
[38] Kanki, T., Kang, D. and Klionsky, D.J. (2009). Monitoring mitophagy in yeast: the Om45-GFP processing assay. Autophagy 5, 1186-9.
[39] Okamoto, K., Kondo-Okamoto, N. and Ohsumi, Y. (2009). Mitochondria-anchored receptor Atg32 mediates degradation of mitochondria via selective autophagy. Dev Cell 17, 87-97.
[40] Kanki, T. and Klionsky, D.J. (2010). The molecular mechanism of mitochondria autophagy in yeast. Molecular microbiology
[41] Kanki, T., Wang, K., Cao, Y., Baba, M. and Klionsky, D.J. (2009). Atg32 is a mitochondrial protein that confers selectivity during mitophagy. Dev Cell 17, 98-109.
[42] Kanki, T., Wang, K., Baba, M., Bartholomew, C.R., Lynch-Day, M.A., Du, Z., Geng, J., Mao, K., Yang, Z., Yen, W.-L. and Klionsky, D.J. (2009). A genomic screen for yeast mutants defective in selective mitochondria autophagy. Mol Biol Cell 20, 4730-8.
[43] Tuttle, D.L. and Dunn, W.A., Jr. (1995). Divergent modes of autophagy in the methylotrophic yeast *Pichia pastoris*. J Cell Sci 108, 25-35.
[44] Kiel, J.A.K.W., Komduur, J.A., van der Klei, I.J. and Veenhuis, M. (2003). Macropexophagy in *Hansenula polymorpha*: facts and views. FEBS Lett 549, 1-6.
[45] Dunn, W.A., Jr, Cregg, J.M., Kiel, J.A.K.W., van der Klei, I.J., Oku, M., Sakai, Y., Sibirny, A.A., Stasyk, O.V. and Veenhuis, M. (2005). Pexophagy: the selective autophagy of peroxisomes. Autophagy 1, 75-83.
[46] Roberts, P., Moshitch-Moshkovitz, S., Kvam, E., O'Toole, E., Winey, M. and Goldfarb, D.S. (2003). Piecemeal microautophagy of nucleus in *Saccharomyces cerevisiae*. Mol Biol Cell 14, 129-41.
[47] Pan, X., Roberts, P., Chen, Y., Kvam, E., Shulga, N., Huang, K., Lemmon, S. and Goldfarb, D.S. (2000). Nucleus-vacuole junctions in *Saccharomyces cerevisiae* are formed through the direct interaction of Vac8p with Nvj1p. Mol Biol Cell 11, 2445-57.
[48] Kvam, E. and Goldfarb, D.S. (2004). Nvj1p is the outer-nuclear-membrane receptor for oxysterol-binding protein homolog Osh1p in *Saccharomyces cerevisiae*. J Cell Sci 117, 4959-68.

[49] Levine, T.P. and Munro, S. (2001). Dual targeting of Osh1p, a yeast homologue of oxysterol-binding protein, to both the Golgi and the nucleus-vacuole junction. Mol Biol Cell 12, 1633-44.
[50] Millen, J.I., Krick, R., Prick, T., Thumm, M. and Goldfarb, D.S. (2009). Measuring piecemeal microautophagy of the nucleus in *Saccharomyces cerevisiae*. Autophagy 5, 75-81.
[51] Krick, R., Muehe, Y., Prick, T., Bremer, S., Schlotterhose, P., Eskelinen, E.-L., Millen, J., Goldfarb, D.S. and Thumm, M. (2008). Piecemeal microautophagy of the nucleus requires the core macroautophagy genes. Mol Biol Cell 19, 4492-505.
[52] Suzuki, K., Kirisako, T., Kamada, Y., Mizushima, N., Noda, T. and Ohsumi, Y. (2001). The pre-autophagosomal structure organized by concerted functions of APG genes is essential for autophagosome formation. EMBO J 20, 5971-81.
[53] Kim, J., Huang, W.-P., Stromhaug, P.E. and Klionsky, D.J. (2002). Convergence of multiple autophagy and cytoplasm to vacuole targeting components to a perivacuolar membrane compartment prior to *de novo* vesicle formation. J Biol Chem 277, 763-73.
[54] Xie, Z. and Klionsky, D.J. (2007). Autophagosome formation: core machinery and adaptations. Nat Cell Biol 9, 1102-9.
[55] Mizushima, N., Noda, T., Yoshimori, T., Tanaka, Y., Ishii, T., George, M.D., Klionsky, D.J., Ohsumi, M. and Ohsumi, Y. (1998). A protein conjugation system essential for autophagy. Nature 395, 395-8.
[56] Ichimura, Y., Kirisako, T., Takao, T., Satomi, Y., Shimonishi, Y., Ishihara, N., Mizushima, N., Tanida, I., Kominami, E., Ohsumi, M., Noda, T. and Ohsumi, Y. (2000). A ubiquitin-like system mediates protein lipidation. Nature 408, 488-92.
[57] Hanada, T., Noda, N.N., Satomi, Y., Ichimura, Y., Fujioka, Y., Takao, T., Inagaki, F. and Ohsumi, Y. (2007). The Atg12-Atg5 conjugate has a novel E3-like activity for protein lipidation in autophagy. J Biol Chem 282, 37298-302.
[58] Noda, T., Kim, J., Huang, W.-P., Baba, M., Tokunaga, C., Ohsumi, Y. and Klionsky, D.J. (2000). Apg9p/Cvt7p is an integral membrane protein required for transport vesicle formation in the Cvt and autophagy pathways. J Cell Biol 148, 465-80.
[59] He, C., Baba, M., Cao, Y. and Klionsky, D.J. (2008). Self-interaction is critical for Atg9 transport and function at the phagophore assembly site during autophagy. Mol Biol Cell 19, 5506-16.
[60] Reggiori, F., Shintani, T., Nair, U. and Klionsky, D.J. (2005). Atg9 cycles between mitochondria and the pre-autophagosomal structure in yeasts. Autophagy 1, 101-9.
[61] Legakis, J.E., Yen, W.-L. and Klionsky, D.J. (2007). A cycling protein complex required for selective autophagy. Autophagy 3, 422-32.
[62] Reggiori, F., Tucker, K.A., Stromhaug, P.E. and Klionsky, D.J. (2004). The Atg1-Atg13 complex regulates Atg9 and Atg23 retrieval transport from the pre-autophagosomal structure. Dev Cell 6, 79-90.
[63] Reggiori, F. and Klionsky, D.J. (2006). Atg9 sorting from mitochondria is impaired in early secretion and VFT-complex mutants in *Saccharomyces cerevisiae*. J Cell Sci 119, 2903-11.

[64] Yen, W.-L., Legakis, J.E., Nair, U. and Klionsky, D.J. (2007). Atg27 is required for autophagy-dependent cycling of Atg9. Mol Biol Cell 18, 581-93.

[65] He, C., Song, H., Yorimitsu, T., Monastyrska, I., Yen, W.-L., Legakis, J.E. and Klionsky, D.J. (2006). Recruitment of Atg9 to the preautophagosomal structure by Atg11 is essential for selective autophagy in budding yeast. J Cell Biol 175, 925-35.

[66] Sekito, T., Kawamata, T., Ichikawa, R., Suzuki, K. and Ohsumi, Y. (2009). Atg17 recruits Atg9 to organize the pre-autophagosomal structure. Genes Cells 14, 525-38.

[67] Matsuura, A., Tsukada, M., Wada, Y. and Ohsumi, Y. (1997). Apg1p, a novel protein kinase required for the autophagic process in *Saccharomyces cerevisiae*. Gene 192, 245-50.

[68] Kamada, Y., Funakoshi, T., Shintani, T., Nagano, K., Ohsumi, M. and Ohsumi, Y. (2000). Tor-mediated induction of autophagy via an Apg1 protein kinase complex. J Cell Biol 150, 1507-13.

[69] Young, A.R.J., Chan, E.Y.W., Hu, X.W., Köchl, R., Crawshaw, S.G., High, S., Hailey, D.W., Lippincott-Schwartz, J. and Tooze, S.A. (2006). Starvation and ULK1-dependent cycling of mammalian Atg9 between the TGN and endosomes. J Cell Sci 119, 3888-900.

[70] Kihara, A., Noda, T., Ishihara, N. and Ohsumi, Y. (2001). Two distinct Vps34 phosphatidylinositol 3-kinase complexes function in autophagy and carboxypeptidase Y sorting in *Saccharomyces cerevisiae*. J Cell Biol 152, 519-30.

[71] Liang, X.H., Jackson, S., Seaman, M., Brown, K., Kempkes, B., Hibshoosh, H. and Levine, B. (1999). Induction of autophagy and inhibition of tumorigenesis by *beclin 1*. Nature 402, 672-6.

[72] Nice, D.C., Sato, T.K., Stromhaug, P.E., Emr, S.D. and Klionsky, D.J. (2002). Cooperative binding of the cytoplasm to vacuole targeting pathway proteins, Cvt13 and Cvt20, to phosphatidylinositol 3-phosphate at the pre-autophagosomal structure is required for selective autophagy. J Biol Chem 277, 30198-207.

[73] Guan, J., Stromhaug, P.E., George, M.D., Habibzadegah-Tari, P., Bevan, A., Dunn, W.A., Jr. and Klionsky, D.J. (2001). Cvt18/Gsa12 is required for cytoplasm-to-vacuole transport, pexophagy, and autophagy in *Saccharomyces cerevisiae* and *Pichia pastoris*. Mol Biol Cell 12, 3821-38.

[74] Strømhaug, P.E., Reggiori, F., Guan, J., Wang, C.-W. and Klionsky, D.J. (2004). Atg21 is a phosphoinositide binding protein required for efficient lipidation and localization of Atg8 during uptake of aminopeptidase I by selective autophagy. Mol Biol Cell 15, 3553-66.

[75] Cheong, H., Nair, U., Geng, J. and Klionsky, D.J. (2007). The Atg1 kinase complex is involved in the regulation of protein recruitment to initiate sequestering vesicle formation for nonspecific autophagy in *Saccharomyces cerevisiae*. Mol Biol Cell 19, 668-81.

[76] Wang, C.-W., Kim, J., Huang, W.-P., Abeliovich, H., Stromhaug, P.E., Dunn, W.A., Jr. and Klionsky, D.J. (2001). Apg2 is a novel protein required for the cytoplasm to vacuole targeting, autophagy, and pexophagy pathways. J Biol Chem 276, 30442-51.

[77] Kirisako, T., Ichimura, Y., Okada, H., Kabeya, Y., Mizushima, N., Yoshimori, T., Ohsumi, M., Takao, T., Noda, T. and Ohsumi, Y. (2000). The reversible modification regulates the membrane-binding state of Apg8/Aut7 essential for autophagy and the cytoplasm to vacuole targeting pathway. J Cell Biol 151, 263-76.

[78] Kametaka, S., Okano, T., Ohsumi, M. and Ohsumi, Y. (1998). Apg14p and Apg6/Vps30p form a protein complex essential for autophagy in the yeast, *Saccharomyces cerevisiae*. J Biol Chem 273, 22284-91.

[79] Xie, Z., Nair, U. and Klionsky, D.J. (2008). Atg8 controls phagophore expansion during autophagosome formation. Mol Biol Cell 19, 3290-8.

[80] Kirisako, T., Baba, M., Ishihara, N., Miyazawa, K., Ohsumi, M., Yoshimori, T., Noda, T. and Ohsumi, Y. (1999). Formation process of autophagosome is traced with Apg8/Aut7p in yeast. J Cell Biol 147, 435-46.

[81] Shintani, T., Mizushima, N., Ogawa, Y., Matsuura, A., Noda, T. and Ohsumi, Y. (1999). Apg10p, a novel protein-conjugating enzyme essential for autophagy in yeast. EMBO J 18, 5234-41.

[82] Kim, J., Kamada, Y., Stromhaug, P.E., Guan, J., Hefner-Gravink, A., Baba, M., Scott, S.V., Ohsumi, Y., Dunn, W.A. and Klionsky, D.J. (2001). Cvt9/Gsa9 functions in sequestering selective cytosolic cargo destined for the vacuole. J Cell Biol 153, 381-96.

[83] Funakoshi, T., Matsuura, A., Noda, T. and Ohsumi, Y. (1997). Analyses of *APG13* gene involved in autophagy in yeast, *Saccharomyces cerevisiae*. Gene 192, 207-13.

[84] Scott, S.V., Nice, D.C., Nau, J.J., Weisman, L.S., Kamada, Y., Keizer-Gunnink, I., Funakoshi, T., Veenhuis, M., Ohsumi, Y. and Klionsky, D.J. (2000). Apg13p and Vac8p are part of a complex of phosphoproteins that are required for cytoplasm to vacuole targeting. J Biol Chem 275, 25840-9.

[85] Teter, S.A., Eggerton, K.P., Scott, S.V., Kim, J., Fischer, A.M. and Klionsky, D.J. (2001). Degradation of lipid vesicles in the yeast vacuole requires function of Cvt17, a putative lipase. J Biol Chem 276, 2083-7.

[86] Mizushima, N., Noda, T. and Ohsumi, Y. (1999). Apg16p is required for the function of the Apg12p-Apg5p conjugate in the yeast autophagy pathway. EMBO J 18, 3888-96.

[87] Fujita, N., Itoh, T., Omori, H., Fukuda, M., Noda, T. and Yoshimori, T. (2008). The Atg16L complex specifies the site of LC3 lipidation for membrane biogenesis in autophagy. Mol Biol Cell 19, 2092-100.

[88] Cheong, H., Yorimitsu, T., Reggiori, F., Legakis, J.E., Wang, C.-W. and Klionsky, D.J. (2005). Atg17 regulates the magnitude of the autophagic response. Mol Biol Cell 16, 3438-53.

[89] Suzuki, K., Kubota, Y., Sekito, T. and Ohsumi, Y. (2007). Hierarchy of Atg proteins in pre-autophagosomal structure organization. Genes Cells 12, 209-18.

[90] Kabeya, Y., Noda, N.N., Fujioka, Y., Suzuki, K., Inagaki, F. and Ohsumi, Y. (2009). Characterization of the Atg17-Atg29-Atg31 complex specifically required for starvation-induced autophagy in *Saccharomyces cerevisiae*. Biochem Biophys Res Commun 389, 612-5.

[91] Barth, H., Meiling-Wesse, K., Epple, U.D. and Thumm, M. (2001). Autophagy and the cytoplasm to vacuole targeting pathway both require Aut10p. FEBS Lett 508, 23-8.
[92] Nair, U., Cao, Y., Xie, Z. and Klionsky, D.J. (2010). The roles of the lipid-binding motifs of Atg18 and Atg21 in the cytoplasm to vacuole targeting pathway and autophagy. J Biol Chem 285, 11476-88.
[93] Barth, H., Meiling-Wesse, K., Epple, U.D. and Thumm, M. (2002). Mai1p is essential for maturation of proaminopeptidase I but not for autophagy. FEBS Lett 512, 173-9.
[94] Meiling-Wesse, K., Barth, H., Voss, C., Eskelinen, E.-L., Epple, U.D. and Thumm, M. (2004). Atg21 is required for effective recruitment of Atg8 to the preautophagosomal structure during the Cvt pathway. J Biol Chem 279, 37741-50.
[95] Yang, Z., Huang, J., Geng, J., Nair, U. and Klionsky, D.J. (2006). Atg22 recycles amino acids to link the degradative and recycling functions of autophagy. Mol Biol Cell 17, 5094-104.
[96] Tucker, K.A., Reggiori, F., Dunn, W.A., Jr. and Klionsky, D.J. (2003). Atg23 is essential for the cytoplasm to vacuole targeting pathway and efficient autophagy but not pexophagy. J Biol Chem 278, 48445-52.
[97] Monastyrska, I., Kiel, J.A.K.W., Krikken, A.M., Komduur, J.A., Veenhuis, M. and van der Klei, I.J. (2005). The *Hansenula polymorpha ATG25* gene encodes a novel coiled-coil protein that is required for macropexophagy. Autophagy 1, 92-100.
[98] Oku, M., Warnecke, D., Noda, T., Muller, F., Heinz, E., Mukaiyama, H., Kato, N. and Sakai, Y. (2003). Peroxisome degradation requires catalytically active sterol glucosyltransferase with a GRAM domain. EMBO J 22, 3231-41.
[99] Cao, Y. and Klionsky, D.J. (2007). Atg26 is not involved in autophagy-related pathways in *Saccharomyces cerevisiae*. Autophagy 3, 17-20.
[100] Farré, J.-C., Vidal, J. and Subramani, S. (2007). A cytoplasm to vacuole targeting pathway in *P. pastoris*. Autophagy 3, 230-4.
[101] Kawamata, T., Kamada, Y., Kabeya, Y., Sekito, T. and Ohsumi, Y. (2008). Organization of the pre-autophagosomal structure responsible for autophagosome formation. Mol Biol Cell 19, 2039-50.
[102] Kawamata, T., Kamada, Y., Suzuki, K., Kuboshima, N., Akimatsu, H., Ota, S., Ohsumi, M. and Ohsumi, Y. (2005). Characterization of a novel autophagy-specific gene, *ATG29*. Biochem Biophys Res Commun 338, 1884-9.
[103] Kabeya, Y., Kawamata, T., Suzuki, K. and Ohsumi, Y. (2007). Cis1/Atg31 is required for autophagosome formation in *Saccharomyces cerevisiae*. Biochem Biophys Res Commun 356, 405-10.
[104] Kerscher, O., Felberbaum, R. and Hochstrasser, M. (2006). Modification of proteins by ubiquitin and ubiquitin-like proteins. Annu Rev Cell Dev Biol 22, 159-80.
[105] Sugawara, K., Suzuki, N.N., Fujioka, Y., Mizushima, N., Ohsumi, Y. and Inagaki, F. (2004). The crystal structure of microtubule-associated protein light chain 3, a mammalian homologue of *Saccharomyces cerevisiae* Atg8. Genes Cells 9, 611-8.

[106] Suzuki, N.N., Yoshimoto, K., Fujioka, Y., Ohsumi, Y. and Inagaki, F. (2005). The crystal structure of plant ATG12 and its biological implication in autophagy. Autophagy 1, 119-26.
[107] Vijay-Kumar, S., Bugg, C.E. and Cook, W.J. (1987). Structure of ubiquitin refined at 1.8 A resolution. J Mol Biol 194, 531-44.
[108] Lupyan, D., Leo-Macias, A. and Ortiz, A.R. (2005). A new progressive-iterative algorithm for multiple structure alignment. Bioinformatics 21, 3255-63.
[109] Shintani, T. and Klionsky, D.J. (2004). Autophagy in health and disease: a double-edged sword. Science 306, 990-5.
[110] Huang, J. and Klionsky, D.J. (2007). Autophagy and human disease. Cell Cycle 6, 1837-49.
[111] Mizushima, N., Kuma, A., Kobayashi, Y., Yamamoto, A., Matsubae, M., Takao, T., Natsume, T., Ohsumi, Y. and Yoshimori, T. (2003). Mouse Apg16L, a novel WD-repeat protein, targets to the autophagic isolation membrane with the Apg12-Apg5 conjugate. J Cell Sci 116, 1679-88.
[112] Nair, U. and Klionsky, D.J. (2005). Molecular mechanisms and regulation of specific and nonspecific autophagy pathways in yeast. J Biol Chem 280, 41785-8.
[113] Sakai, Y., Oku, M., van der Klei, I.J. and Kiel, J.A.K.W. (2006). Pexophagy: autophagic degradation of peroxisomes. Biochim Biophys Acta 1763, 1767-75.
[114] Tanida, I., Mizushima, N., Kiyooka, M., Ohsumi, M., Ueno, T., Ohsumi, Y. and Kominami, E. (1999). Apg7p/Cvt2p: A novel protein-activating enzyme essential for autophagy. Mol Biol Cell 10, 1367-79.
[115] Kuma, A., Mizushima, N., Ishihara, N. and Ohsumi, Y. (2002). Formation of the approximately 350-kDa Apg12-Apg5.Apg16 multimeric complex, mediated by Apg16 oligomerization, is essential for autophagy in yeast. J Biol Chem 277, 18619-25.
[116] Komatsu, M., Tanida, I., Ueno, T., Ohsumi, M., Ohsumi, Y. and Kominami, E. (2001). The C-terminal region of an Apg7p/Cvt2p is required for homodimerization and is essential for its E1 activity and E1-E2 complex formation. J Biol Chem 276, 9846-54.
[117] Tanida, I., Tanida-Miyake, E., Ueno, T. and Kominami, E. (2001). The human homolog of *Saccharomyces cerevisiae* Apg7p is a protein-activating enzyme for multiple substrates including human Apg12p, GATE-16, GABARAP, and MAP-LC3. J Biol Chem 276, 1701-6.
[118] Mizushima, N., Yoshimori, T. and Ohsumi, Y. (2002). Mouse Apg10 as an Apg12-conjugating enzyme: analysis by the conjugation-mediated yeast two-hybrid method. FEBS Lett 532, 450-4.
[119] Yamada, Y., Suzuki, N.N., Hanada, T., Ichimura, Y., Kumeta, H., Fujioka, Y., Ohsumi, Y. and Inagaki, F. (2007). The crystal structure of Atg3, an autophagy-related ubiquitin carrier protein (E2) enzyme that mediates Atg8 lipidation. J Biol Chem 282, 8036-43.
[120] Huang, W.-P., Scott, S.V., Kim, J. and Klionsky, D.J. (2000). The itinerary of a vesicle component, Aut7p/Cvt5p, terminates in the yeast vacuole via the autophagy/Cvt pathways. J Biol Chem 275, 5845-51.
[121] Kabeya, Y., Mizushima, N., Yamamoto, A., Oshitani-Okamoto, S., Ohsumi, Y. and Yoshimori, T. (2004). LC3, GABARAP and GATE16 localize to

autophagosomal membrane depending on form-II formation. J Cell Sci 117, 2805-12.
[122] Tanida, I., Komatsu, M., Ueno, T. and Kominami, E. (2003). GATE-16 and GABARAP are authentic modifiers mediated by Apg7 and Apg3. Biochem Biophys Res Commun 300, 637-44.
[123] Tanida, I., Tanida-Miyake, E., Komatsu, M., Ueno, T. and Kominami, E. (2002). Human Apg3p/Aut1p homologue is an authentic E2 enzyme for multiple substrates, GATE-16, GABARAP, and MAP-LC3, and facilitates the conjugation of hApg12p to hApg5p. J Biol Chem 277, 13739-44.
[124] Tanida, I., Sou, Y.-S., Minematsu-Ikeguchi, N., Ueno, T. and Kominami, E. (2006). Atg8L/Apg8L is the fourth mammalian modifier of mammalian Atg8 conjugation mediated by human Atg4B, Atg7 and Atg3. FEBS J 273, 2553-62.
[125] Kabeya, Y., Mizushima, N., Ueno, T., Yamamoto, A., Kirisako, T., Noda, T., Kominami, E., Ohsumi, Y. and Yoshimori, T. (2000). LC3, a mammalian homologue of yeast Apg8p, is localized in autophagosome membranes after processing. EMBO J 19, 5720-8.
[126] Mizushima, N., Yamamoto, A., Matsui, M., Yoshimori, T. and Ohsumi, Y. (2004). In vivo analysis of autophagy in response to nutrient starvation using transgenic mice expressing a fluorescent autophagosome marker. Mol Biol Cell 15, 1101-11.
[127] Geng, J., Baba, M., Nair, U. and Klionsky, D.J. (2008). Quantitative analysis of autophagy-related protein stoichiometry by fluorescence microscopy. J Cell Biol 182, 129-40.
[128] Nakagawa, I., Amano, A., Mizushima, N., Yamamoto, A., Yamaguchi, H., Kamimoto, T., Nara, A., Funao, J., Nakata, M., Tsuda, K., Hamada, S. and Yoshimori, T. (2004). Autophagy defends cells against invading group A *Streptococcus*. Science 306, 1037-40.
[129] Pankiv, S., Clausen, T.H., Lamark, T., Brech, A., Bruun, J.A., Outzen, H., Øvervatn, A., Bjørkøy, G. and Johansen, T. (2007). p62/SQSTM1 binds directly to Atg8/LC3 to facilitate degradation of ubiquitinated protein aggregates by autophagy. J Biol Chem 282, 24131-45.
[130] Nakatogawa, H., Ichimura, Y. and Ohsumi, Y. (2007). Atg8, a ubiquitin-like protein required for autophagosome formation, mediates membrane tethering and hemifusion. Cell 130, 165-78.
[131] Yorimitsu, T. and Klionsky, D.J. (2005). Autophagy: molecular machinery for self-eating. Cell Death Differ 12, 1542-52.
[132] Iwata, J., Ezaki, J., Komatsu, M., Yokota, S., Ueno, T., Tanida, I., Chiba, T., Tanaka, K. and Kominami, E. (2006). Excess peroxisomes are degraded by autophagic machinery in mammals. J Biol Chem 281, 4035-41.
[133] Mizushima, N. (2005). The pleiotropic role of autophagy: from protein metabolism to bactericide. Cell Death Differ 12 Suppl 2, 1535-41.
[134] Wu, J.-Q. and Pollard, T.D. (2005). Counting cytokinesis proteins globally and locally in fission yeast. Science 310, 310-4.
[135] Ammerer, G., Hunter, C.P., Rothman, J.H., Saari, G.C., Valls, L.A. and Stevens, T.H. (1986). *PEP4* gene of *Saccharomyces cerevisiae* encodes proteinase A, a

vacuolar enzyme required for processing of vacuolar precursors. Mol Cell Biol 6, 2490-9.

[136] Babst, M., Katzmann, D.J., Estepa-Sabal, E.J., Meerloo, T. and Emr, S.D. (2002). ESCRT-III: an endosome-associated heterooligomeric protein complex required for MVB sorting. Dev Cell 3, 271-82.

[137] Babst, M., Wendland, B., Estepa, E.J. and Emr, S.D. (1998). The Vps4p AAA ATPase regulates membrane association of a Vps protein complex required for normal endosome function. EMBO J 17, 2982-93.

[138] Shintani, T. and Klionsky, D.J. (2004). Cargo proteins facilitate the formation of transport vesicles in the cytoplasm to vacuole targeting pathway. J Biol Chem 279, 29889-94.

[139] Ghaemmaghami, S., Huh, W.-K., Bower, K., Howson, R.W., Belle, A., Dephoure, N., O'Shea, E.K. and Weissman, J.S. (2003). Global analysis of protein expression in yeast. Nature 425, 737-41.

[140] Longtine, M.S., DeMarini, D.J., Valencik, M.L., Al-Awar, O.S., Fares, H., De Virgilio, C. and Pringle, J.R. (1996). The septins: roles in cytokinesis and other processes. Curr Opin Cell Biol 8, 106-19.

[141] Luo, J., Vallen, E.A., Dravis, C., Tcheperegine, S.E., Drees, B. and Bi, E. (2004). Identification and functional analysis of the essential and regulatory light chains of the only type II myosin Myo1p in *Saccharomyces cerevisiae*. J Cell Biol 165, 843-55.

[142] Longtine, M.S., McKenzie, A. III, Demarini, D.J., Shah, N.G., Wach, A., Brachat, A., Philippsen, P. and Pringle, J.R. (1998). Additional modules for versatile and economical PCR-based gene deletion and modification in *Saccharomyces cerevisiae*. Yeast 14, 953-61.

[143] Kim, J., Huang, W.-P. and Klionsky, D.J. (2001). Membrane recruitment of Aut7p in the autophagy and cytoplasm to vacuole targeting pathways requires Aut1p, Aut2p, and the autophagy conjugation complex. J Cell Biol 152, 51-64.

[144] Budovskaya, Y.V., Stephan, J.S., Reggiori, F., Klionsky, D.J. and Herman, P.K. (2004). The Ras/cAMP-dependent protein kinase signaling pathway regulates an early step of the autophagy process in *Saccharomyces cerevisiae*. J Biol Chem 279, 20663-71.

[145] Labbé, S. and Thiele, D.J. (1999). Copper ion inducible and repressible promoter systems in yeast. Meth Enzymol 306, 145-53.

[146] Sheff, M.A. and Thorn, K.S. (2004). Optimized cassettes for fluorescent protein tagging in *Saccharomyces cerevisiae*. Yeast 21, 661-70.

[147] Robinson, J.S., Klionsky, D.J., Banta, L.M. and Emr, S.D. (1988). Protein sorting in *Saccharomyces cerevisiae*: isolation of mutants defective in the delivery and processing of multiple vacuolar hydrolases. Mol Cell Biol 8, 4936-48.

[148] Noda, T., Matsuura, A., Wada, Y. and Ohsumi, Y. (1995). Novel system for monitoring autophagy in the yeast *Saccharomyces cerevisiae*. Biochem Biophys Res Commun 210, 126-32.

[149] Fengsrud, M., Erichsen, E.S., Berg, T.O., Raiborg, C. and Seglen, P.O. (2000). Ultrastructural characterization of the delimiting membranes of isolated autophagosomes and amphisomes by freeze-fracture electron microscopy. Eur J Cell Biol 79, 871-82.

[150] Hirsimaki, Y., Hirsimaki, P. and Lounatmaa, K. (1982). Vinblastine-induced autophagic vacuoles in mouse liver and Ehrlich ascites tumor cells as assessed by freeze-fracture electron microscopy. Eur J Cell Biol 27, 298-301.
[151] Strømhaug, P.E., Berg, T.O., Fengsrud, M. and Seglen, P.O. (1998). Purification and characterization of autophagosomes from rat hepatocytes. Biochem J 335 (Pt 2), 217-24.
[152] Ishihara, N., Hamasaki, M., Yokota, S., Suzuki, K., Kamada, Y., Kihara, A., Yoshimori, T., Noda, T. and Ohsumi, Y. (2001). Autophagosome requires specific early Sec proteins for its formation and NSF/SNARE for vacuolar fusion. Mol Biol Cell 12, 3690-702.
[153] Reggiori, F., Wang, C.-W., Nair, U., Shintani, T., Abeliovich, H. and Klionsky, D.J. (2004). Early stages of the secretory pathway, but not endosomes, are required for Cvt vesicle and autophagosome assembly in *Saccharomyces cerevisiae*. Mol Biol Cell 15, 2189-204.
[154] van der Vaart, A., Griffith, J. and Reggiori, F. (2010). Exit from the Golgi is required for the expansion of the autophagosomal phagophore in yeast *Saccharomyces cerevisiae*. Mol Biol Cell 21, 2270-84.
[155] Yen, W.-L., Shintani, T., Nair, U., Cao, Y., Richardson, B.C., Li, Z., Hughson, F.M., Baba, M. and Klionsky, D.J. (2010). The conserved oligomeric Golgi complex is involved in double-membrane vesicle formation during autophagy. J Cell Biol 188, 101-14.
[156] Mizuta, K. and Warner, J.R. (1994). Continued functioning of the secretory pathway is essential for ribosome synthesis. Mol Cell Biol 14, 2493-502.
[157] Hicke, L., Zanolari, B., Pypaert, M., Rohrer, J. and Riezman, H. (1997). Transport through the yeast endocytic pathway occurs through morphologically distinct compartments and requires an active secretory pathway and Sec18p/N-ethylmaleimide-sensitive fusion protein. Mol Biol Cell 8, 13-31.
[158] Nanduri, J., Mitra, S., Andrei, C., Liu, Y., Yu, Y., Hitomi, M. and Tartakoff, A.M. (1999). An unexpected link between the secretory path and the organization of the nucleus. J Biol Chem 274, 33785-9.
[159] Itzen, A., Rak, A. and Goody, R.S. (2007). Sec2 is a highly efficient exchange factor for the Rab protein Sec4. J Mol Biol 365, 1359-67.
[160] Nair, J., Müller, H., Peterson, M. and Novick, P.J. (1990). Sec2 protein contains a coiled-coil domain essential for vesicular transport and a dispensable carboxy terminal domain. J Cell Biol 110, 1897-909.
[161] Walworth, N.C., Brennwald, P., Kabcenell, A.K., Garrett, M. and Novick, P.J. (1992). Hydrolysis of GTP by Sec4 protein plays an important role in vesicular transport and is stimulated by a GTPase-activating protein in *Saccharomyces cerevisiae*. Mol Cell Biol 12, 2017-28.
[162] Christianson, T.W., Sikorski, R.S., Dante, M., Shero, J.H. and Hieter, P. (1992). Multifunctional yeast high-copy-number shuttle vectors. Gene 110, 119-22.
[163] Gueldener, U., Heinisch, J., Koehler, G.J., Voss, D. and Hegemann, J.H. (2002). A second set of loxP marker cassettes for Cre-mediated multiple gene knockouts in budding yeast. Nucleic Acids Res 30, e23.

[164] Monastyrska, I., He, C., Geng, J., Hoppe, A.D., Li, Z. and Klionsky, D.J. (2008). Arp2 links autophagic machinery with the actin cytoskeleton. Mol Biol Cell 19, 1962-75.
[165] Abeliovich, H., Zhang, C., Dunn, W.A., Jr., Shokat, K.M. and Klionsky, D.J. (2003). Chemical genetic analysis of Apg1 reveals a non-kinase role in the induction of autophagy. Mol Biol Cell 14, 477-90.
[166] Kaneko, Y., Hayashi, N., Toh-e, A., Banno, I. and Oshima, Y. (1987). Structural characteristics of the *PHO8* gene encoding repressible alkaline phosphatase in *Saccharomyces cerevisiae*. Gene 58, 137-48.
[167] Klionsky, D.J. and Emr, S.D. (1989). Membrane protein sorting: biosynthesis, transport and processing of yeast vacuolar alkaline phosphatase. EMBO J 8, 2241-50.
[168] Stevens, T., Esmon, B. and Schekman, R. (1982). Early stages in the yeast secretory pathway are required for transport of carboxypeptidase Y to the vacuole. Cell 30, 439-48.
[169] Elkind, N.B., Walch-Solimena, C. and Novick, P.J. (2000). The role of the COOH terminus of Sec2p in the transport of post-Golgi vesicles. J Cell Biol 149, 95-110.
[170] Walch-Solimena, C., Collins, R.N. and Novick, P.J. (1997). Sec2p mediates nucleotide exchange on Sec4p and is involved in polarized delivery of post-Golgi vesicles. J Cell Biol 137, 1495-509.
[171] Geng, J. and Klionsky, D.J. (2008). The Atg8 and Atg12 ubiquitin-like conjugation systems in macroautophagy. EMBO Rep 9, 859-64.
[172] Darsow, T., Rieder, S.E. and Emr, S.D. (1997). A multispecificity syntaxin homologue, Vam3p, essential for autophagic and biosynthetic protein transport to the vacuole. J Cell Biol 138, 517-29.
[173] Xie, Z., Nair, U., Geng, J., Szefler, M.B., Rothman, E.D. and Klionsky, D.J. (2009). Indirect estimation of the area density of Atg8 on the phagophore. Autophagy 5, 217-20.
[174] Geng, J. and Klionsky, D.J. (2008). Quantitative regulation of vesicle formation in yeast nonspecific autophagy. Autophagy 4, 955-7.
[175] Lynch-Day, M.A., Bhandari, D., Menon, S., Huang, J., Cai, H., Bartholomew, C.R., Brumell, J.H., Ferro-Novick, S. and Klionsky, D.J. (2010). Trs85 directs a Ypt1 GEF, TRAPPIII, to the phagophore to promote autophagy. Proc Natl Acad Sci USA 107, 7811-6.
[176] Ortiz, D., Medkova, M., Walch-Solimena, C. and Novick, P.J. (2002). Ypt32 recruits the Sec4p guanine nucleotide exchange factor, Sec2p, to secretory vesicles; evidence for a Rab cascade in yeast. J Cell Biol 157, 1005-15.
[177] Jedd, G., Mulholland, J. and Segev, N. (1997). Two new Ypt GTPases are required for exit from the yeast trans-Golgi compartment. J Cell Biol 137, 563-80.
[178] Benli, M., Doring, F., Robinson, D.G., Yang, X. and Gallwitz, D. (1996). Two GTPase isoforms, Ypt31p and Ypt32p, are essential for Golgi function in yeast. EMBO J 15, 6460-75.
[179] Guo, W., Roth, D., Walch-Solimena, C. and Novick, P.J. (1999). The exocyst is an effector for Sec4p, targeting secretory vesicles to sites of exocytosis. EMBO J 18, 1071-80.

[180] Grosshans, B.L., Andreeva, A., Gangar, A., Niessen, S., Yates, J.R., Brennwald, P. and Novick, P.J. (2006). The yeast lgl family member Sro7p is an effector of the secretory Rab GTPase Sec4p. J Cell Biol 172, 55-66.
[181] Medkova, M., France, Y.E., Coleman, J. and Novick, P.J. (2006). The rab exchange factor Sec2p reversibly associates with the exocyst. Mol Biol Cell 17, 2757-69.
[182] Shorer, H., Amar, N., Meerson, A. and Elazar, Z. (2005). Modulation of N-ethylmaleimide-sensitive factor activity upon amino acid deprivation. J Biol Chem 280, 16219-26.
[183] Itoh, T., Fujita, N., Kanno, E., Yamamoto, A., Yoshimori, T. and Fukuda, M. (2008). Golgi-resident small GTPase Rab33B interacts with Atg16L and modulates autophagosome formation. Mol Biol Cell 19, 2916-2925.
[184] Babu, P., Bryan, J.D., Panek, H.R., Jordan, S.L., Forbrich, B.M., Kelley, S.C., Colvin, R.T. and Robinson, L.C. (2002). Plasma membrane localization of the Yck2p yeast casein kinase 1 isoform requires the C-terminal extension and secretory pathway function. J Cell Sci 115, 4957-68.
[185] Liang, Y., Morozova, N., Tokarev, A.A., Mulholland, J.W. and Segev, N. (2007). The role of Trs65 in the Ypt/Rab guanine nucleotide exchange factor function of the TRAPP II complex. Mol Biol Cell 18, 2533-41.
[186] Kang, C., You, Y.J. and Avery, L. (2007). Dual roles of autophagy in the survival of *Caenorhabditis elegans* during starvation. Genes Dev 21, 2161-71.
[187] Hailey, D.W. and Lippincott-Schwartz, J. (2009). Using photoactivatable proteins to monitor autophagosome lifetime. Methods Enzymol 452, 25-45.
[188] Dunn, W.A., Jr. (1990). Studies on the mechanisms of autophagy: formation of the autophagic vacuole. J Cell Biol 110, 1923-33.
[189] Kovacs, A.L., Rez, G., Palfia, Z. and Kovacs, J. (2000). Autophagy in the epithelial cells of murine seminal vesicle in vitro. Formation of large sheets of nascent isolation membranes, sequestration of the nucleus and inhibition by wortmannin and 3-ethyladenine. Cell Tissue Res 302, 253-61.
[190] Hayashi-Nishino, M., Fujita, N., Noda, T., Yamaguchi, A., Yoshimori, T. and Yamamoto, A. (2009). A subdomain of the endoplasmic reticulum forms a cradle for autophagosome formation. Nat Cell Biol 11, 1433-7.
[191] Ylä-Anttila, P., Vihinen, H., Jokitalo, E. and Eskelinen, E.-L. (2009). 3D tomography reveals connections between the phagophore and endoplasmic reticulum. Autophagy 5, 1180-5.
[192] Furuno, K., Ishikawa, T., Akasaki, K., Lee, S., Nishimura, Y., Tsuji, H., Himeno, M. and Kato, K. (1990). Immunocytochemical study of the surrounding envelope of autophagic vacuoles in cultured rat hepatocytes. Exp Cell Res 189, 261-8.
[193] Yang, D.-M. and Chiang, A.-S. (1997). Formation of a whorl-like autophagosome by Golgi apparatus engulfing a ribosome-containing vacuole in corpora allata of the cockroach *Diploptera punctata*. Cell Tissue Res 287, 385-91.
[194] Hailey, D.W., Rambold, A.S., Satpute-Krishnan, P., Mitra, K., Sougrat, R., Kim, P.K. and Lippincott-Schwartz, J. (2010). Mitochondria supply membranes for autophagosome biogenesis during starvation. Cell 141, 656-67.
[195] Hamasaki, M., Noda, T. and Ohsumi, Y. (2003). The early secretory pathway contributes to autophagy in yeast. Cell Struct Funct 28, 49-54.

[196] Salminen, A. and Novick, P.J. (1987). A ras-like protein is required for a post-Golgi event in yeast secretion. Cell 49, 527-38.
[197] Walworth, N.C., Goud, B., Kabcenell, A.K. and Novick, P.J. (1989). Mutational analysis of *SEC4* suggests a cyclical mechanism for the regulation of vesicular traffic. EMBO J 8, 1685-93.
[198] Goud, B., Salminen, A., Walworth, N.C. and Novick, P.J. (1988). A GTP-binding protein required for secretion rapidly associates with secretory vesicles and the plasma membrane in yeast. Cell 53, 753-68.
[199] Bruinsma, P., Spelbrink, R.G. and Nothwehr, S.F. (2004). Retrograde transport of the mannosyltransferase Och1p to the early Golgi requires a component of the COG transport complex. J Biol Chem 279, 39814-23.
[200] Suvorova, E.S., Duden, R. and Lupashin, V.V. (2002). The Sec34/Sec35p complex, a Ypt1p effector required for retrograde intra-Golgi trafficking, interacts with Golgi SNAREs and COPI vesicle coat proteins. J Cell Biol 157, 631-43.
[201] VanRheenen, S.M., Cao, X., Lupashin, V.V., Barlowe, C. and Waters, M.G. (1998). Sec35p, a novel peripheral membrane protein, is required for ER to Golgi vesicle docking. J Cell Biol 141, 1107-19.
[202] Novick, P.J., Field, C. and Schekman, R. (1980). Identification of 23 complementation groups required for post-translational events in the yeast secretory pathway. Cell 21, 205-15.
[203] Cheong, H. and Klionsky, D.J. (2008). Biochemical methods to monitor autophagy-related processes in yeast. Meth Enzymol 451, 1-26.